NASA CR- 134177
ERIM 190900-10-T

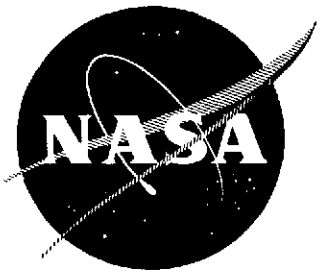

MICHIGAN EXPERIMENTAL MULTISPECTRAL MAPPING SYSTEM A DESCRIPTION OF THE M7 AIRBORNE SENSOR AND ITS PERFORMANCE

by

Philip G. Hasell, Jr., et al.
Infrared and Optics Division

JANUARY 1974
prepared for

NATIONAL AERONAUTICS AND SPACE ADMINISTRATION

Johnson Space Center, Houston, Texas 77058
Earth Observations Division
Contract NAS 9-9384

NOTICE

Sponsorship. The work reported herein was conducted by the Environmental Research Institute of Michigan for the National Aeronautics and Space Administration, Johnson Space Center, Houston, Texas 77058, under Contract NAS 9-9304. Mr. William Shaw/TC was Technical Monitor from December 1970 through June 1972; Mr. Charles Harlan/FC2 now serves in the same capacity. Contracts and grants to the Institute for the support of sponsored research are administered through the Office of Contracts Administration.

Availability Notice. Requests for copies of this report should be referred to:

National Aeronautics and Space Administration
Scientific and Technical Information Facility
P. O. Box 33
College Park, Maryland 20740

Final Disposition. After this document has served its purpose, it may be destroyed. Please do not return it to the Environmental Research Institute of Michigan.

TECHNICAL REPORT STANDARD TITLE PAGE

1. Report No.	2. Government Accession No.	3. Recipient's Catalog No.
NASA-CR-ERIM 190900-10-T		

4. Title and Subtitle	5. Report Date
MICHIGAN EXPERIMENTAL MAPPING SYSTEM — A DESCRIPTION OF THE M7 AIRBORNE SENSOR AND ITS PERFORMANCE	January 1974
	6. Performing Organization Code

7. Author(s)	8. Performing Organization Report No.
Philip G. Hasell, Jr., et al., Infrared and Optics Division	ERIM 190900-10-T

9. Performing Organization Name and Address	10. Work Unit No.
Environmental Research Institute of Michigan Infrared and Optics Division P.O. Box 618 Ann Arbor, MI 48107	11. Contract or Grant No. NAS 9-9304
	13. Type of Report and Period Covered Technical Report December 1970 through June 1972
12. Sponsoring Agency Name and Address National Aeronautics and Space Administration Johnson Space Center Earth Observations Division Houston, Texas 77058	14. Sponsoring Agency Code

15. Supplementary Notes

Mr. William Shaw/TC was Technical Monitor for the work reported here.
Mr. Charles Harlan/FC 2 now monitors the contract.

16. Abstract

Beginning in the mid-sixties with experimental hardware developments, Willow Run Laboratories (now ERIM) pioneered the application of multispectral mapping techniques to earth resource problems. Thus when, with NASA support, the Michigan M7 airborne scanner system became operational in June 1971, its introduction represented a significant milestone in a continuing effort. This report describes M7 scanner design, system characteristics, and various departures from a previous (M5) design.

The M7 scanner system can function in as many as 19 spectral bands covering the UV, visible, and IR (0.3- to 15-μm wavelength range). Any 12 of these bands may be selected for simultaneous, optically registered recording on a 14-track analog tape machine. Because terrain data is gathered along a single optical line-of-sight (rather than along several paths as with the older M5 system), the choice of bands for multispectral processing does not carry the severe restriction of the previous design. Five separate radiation reference sources are sequentially scanned and recorded along with the imagery.

Multispectral imagery recorded on magnetic tape in the aircraft can be laboratory-reproduced on film strips for visual analysis or optionally machine-processed in analog and/or digital computers before display. Such machine processing at ERIM can range from simple level-slicing to automatic identification of terrain cover or features.

17. Key Words	18. Distribution Statement
Airborne sensor Multispectral scanner Calibrated scanner Scanner performance Multispectral techniques	

19. Security Classif. (of this report)	20. Security Classif. (of this page)	21. No. of Pages	22. Price
UNCLASSIFIED	UNCLASSIFIED	ix + 147	

PREFACE

The M7 airborne multispectral scanner developed by the Willow Run Laboratories is described in this report. The work was performed under Contract NAS 9-9304 for the National Aeronautics and Space Administration, Earth Observations Division, L. B. Johnson Space Center, Houston, Texas. The period of development extended from December 1970 through June 1972.

Mr. Richard Legault, Director of the Infrared and Optics Division at WRL (now ERIM), is Project Director, and Mr. Philip G. Hasell, Jr., is Principal Investigator. NASA's Technical Monitor for this development was Mr. William Shaw/TC who functioned during this program period under the direction of Mr. Allen H. Watkins, Manager of the Earth Observations Aircraft Program.

The Principal Investigator acknowledges the assistance of Messrs. Leo M. Larsen, Edgar A. Work, Jr., Leo A. Levereault, Stephen R. Stewart, and Robert E. Marshall in report preparation. The ERIM number for this report is 190900-10-T.

The information presented herein is current as of July, 1972. Since that time, because experimental equipment tends to change continually, a number of minor changes and additions have been implemented—primarily to make the multispectral data easier to retrieve and to improve its quality. However, at the time of this report's publication, the basic configuration and performance of the system remain primarily as described herein.

While an effort of this magnitude depends upon the support of an entire organization, key personnel determined the success of this program. The instrumentation system described is the product primarily of the following persons:

R. R. Legault, Research Mathematician and Vice President of WRL/ERIM
P. G. Hasell, Jr., Research Engineer, System Design
J. G. Braithwaite, Research Physicist, Optical Design
L. M. Larsen, Research Engineer, Electrical Design
S. R. Lampert, Research Engineer, Electrical Design
E. A. Work, Jr., Assoc. Research Engineer, Mechanical Design
L. A. Levereault, Research Associate, Electrical Calibration
S. R. Stewart, Research Associate, Radiation Calibration
P. F. Lambeck, Research Assistant, System Error Analysis
J. K. Wiseman, Assistant in Research, Detector Performance
J. C. Ladd, Technical Associate, System Fabrication and Testing

W. J. Juodawlkis, Senior Technician, Electrical Fabrication
N. V. Griffin, Senior Technician, Mechanical Fabrication
E. L. Kraudelt, Instrument Maker, Mechanical Fabrication

Various inputs influencing this design were supplied by users of multispectral scanner data, but in particular the following persons at the Willow Run Laboratories (now ERIM) contributed greatly by interfacing this instrumentation to remote sensing applications and by working out optimal methods of data processing for ready interpretation:

F. C. Polcyn, Research Engineer - Earth Resources Problems
F. J. Thomson, Assoc. Research Engineer - Data Processing Techniques

Numerous companies and individuals outside of WRL/ERIM contributed to the M7 Scanner Program. To Barnes Engineering and Honeywell, Inc., goes much credit for the radiation detectors. Both companies have worked closely with us for several years on our ongoing requirements for ordinary and special-purpose detectors. Two other contributors also merit special mention: Speedring Systems* for their admirable performance in engineering and manufacture of the very difficult single-faceted scan mirror; and Mr. Howard Padgitt,** who from the onset of the program provided valuable consulting comments on design feasibility and supplied detailed optical component designs. To these and the other contributors named below we express our gratitude.

Contributor	Contribution
Exotic Materials, Inc., Costa Mesa, Calif.	coatings and dichroics
Optical Coating Labs., Inc., Santa Rosa, Calif.	coatings and dichroics
L. H. Sampson Co., Farmington, Michigan	mirror coatings
Broomer Research Corp., Plainview, N.Y.	lenses
A. D. Jones Optical Works, Burlington, Mass.	lenses
Perkin Elmer Corp., Costa Mesa, California	mirrors
Eastman Kodak Co., Rochester, N.Y.	dichroics

*Speedring Systems, Warren, Michigan
**Mr. Howard Padgitt, Park Ridge, Illinois

CONTENTS

ILLUSTRATIONS

TABLES

MICHIGAN EXPERIMENTAL MULTISPECTRAL MAPPING SYSTEM
A DESCRIPTION OF THE M7 AIRBORNE SENSOR
AND ITS PERFORMANCE

1
SUMMARY

Beginning in the mid-sixties with experimental hardware developments, the Willow Run Laboratories—then a unit of The University of Michigan's Institute of Science and Technology—pioneered in the application of multispectral mapping techniques to earth resource surveys. This experimental airborne hardware supplied for approximately six years (1966-72) all of the multispectral scanner data processed and analyzed by Michigan, Purdue, NASA/MSC, and others. Then, during FY71 under NASA/MSC support, WRL extensively modified its original multispectral airborne scanner system (which had been of multipath type) to provide the same spectral bands along a single optical line of sight. This modification removed a serious restriction on the choice of spectral bands for machine processing. In the previous M5 system only those few bands handled by the same scanner head and thus grouped in one of four separate optical paths could be processed together. After the modification, any multispectral bands recorded—whether in ultraviolet, visible, or infrared regions—could be selected and processed in combination with any other band.

The M7 system became operational in late June, 1971, only six months after contract go-ahead and just in time for use in the Corn Blight Watch experiment. Initially its principal difference from the M5 was the substitution of a single scanner assembly to replace the two doubled-ended (military surplus) scanners formerly used. Radiation detectors, radiation calibration sources, electronics, operator displays and controls, and the magnetic tape machine were at first the same as the older system. Later in FY72, because the system is intended to be sufficiently flexible in design to allow continual changes to improve performance, new detectors were acquired, different radiation reference sources were incorporated, and the electronics were repackaged to obtain better performance from newly developed components. All these improvements, as well as the performance characteristics of the system as configured at the close of FY72,are detailed in this report. Appendix A briefly describes points of compromise in the system's initial (interim) configuration—that of early FY72.

A relatively small organization but one with an excellent background, ERIM is well-versed in all aspects of remote sensing and has made many contributions to advance the state of the art. Moreover, the scientific and technical interests of current as well as potential users of remotely sensed data are ably represented in the various ERIM laboratories. In addition, the staff of The University of Michigan, particularly the School of Natural Resources, is also available to participate in investigative programs. ERIM's interest and expertise in investigating earth resource problems is supported by personnel experienced in the development

and operation of ground and airborne radiation measuring and recording instrumentation and also in designing, adapting, and using analog and digital computers to automatically process multispectral data. All of this diverse talent has influenced the design of the M7 scanner system described herein.

2
GENERAL DESCRIPTION OF MULTISPECTRAL DATA COLLECTING AND PROCESSING CAPABILITIES

ERIM capabilities for acquiring and processing remotely sensed multispectral imagery are outlined in broad perspective in this section. Also described is the form in which data outputs from the airborne scanner system are obtained.

2.1 AIRBORNE MULTISPECTRAL SCANNER SYSTEM, M7

During FY71 and FY72, WRL (now ERIM) developed its M7 multispectral scanner system for airborne use. This system offers the capability of operation in up to nineteen different spectral bands over a wavelength range of from 0.3 to 15.0 μm. At any one time, twelve of these bands can be selected for tape recording on a 14-track analog tape machine. The scanner includes provisions for using five separate radiation reference sources. Each radiation detector views these sources in sequence as part of each narrow line scan of the terrain passing beneath the aircraft.

For those not familiar with airborne scanners, a functional description of line scanning is presented below. As shown in the optical schematic at the top of Fig. 1, the airborne scanner consists of an optical telescope with its narrow field of view directed by a rotating flat mirror to scan in a plane at right angles to the longitudinal axis of the aircraft. In place of the usual eyeball at the receiving end of the telescope, we have radiation detectors that convert the incoming radiation to electrical signals. Again referring to Fig. 1, we see that the telescope field-of-view (or ground resolution element) scans laterally across the aircraft ground track through an opening in the bottom of the aircraft. Then, before making the next ground scan, it scans radiation references internal to the scanner. By the time the next ground scan begins, the aircraft has moved forward; thus successive line scans build upon one another to form a continuous strip image of the terrain over which the aircraft is flying.

An electrical voltage representation of a single line scan is shown in Fig. 2. Note that while the detectors for all wavelength bands view, in phase, each of the radiation references as well as the terrain, not all references apply to every wavelength band. Although the thermal ambient and dark level references may represent common radiation sources, the other sources are associated with either thermal or nonthermal bands. For indexing purposes, two synchronization references are generated by the scanner and recorded with the video signals: The marker pulse relates the scan position to internally mounted radiation references; the roll-stabilized pulse is referenced to ground scan nadir with aircraft roll motion removed.

The complete airborne scanner system is shown in block diagram form in Fig. 3. Terrain radiation enters the scanner at the bottom left and is registered, along with operator-controlled reference sources, by the radiation detectors. Electrical signals from the radiation detectors

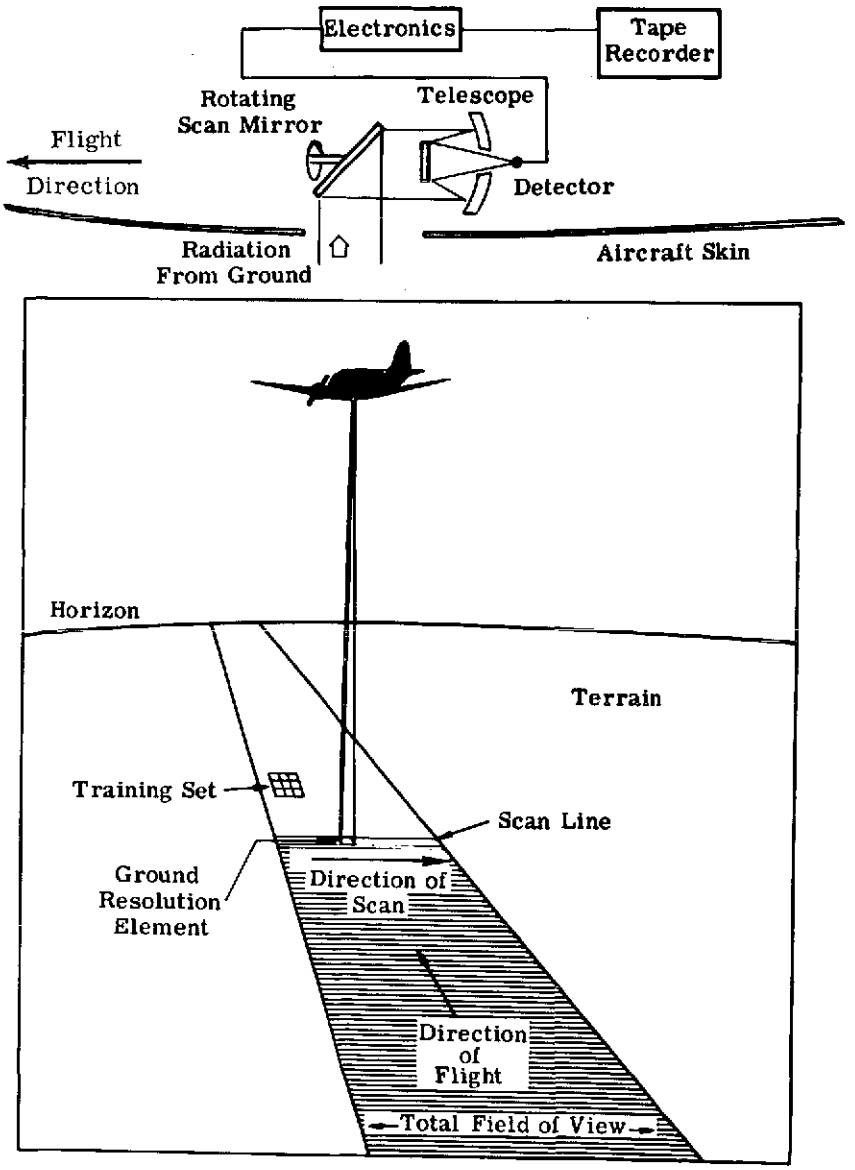

FIGURE 1. GEOMETRY OF AIRBORNE SCANNING

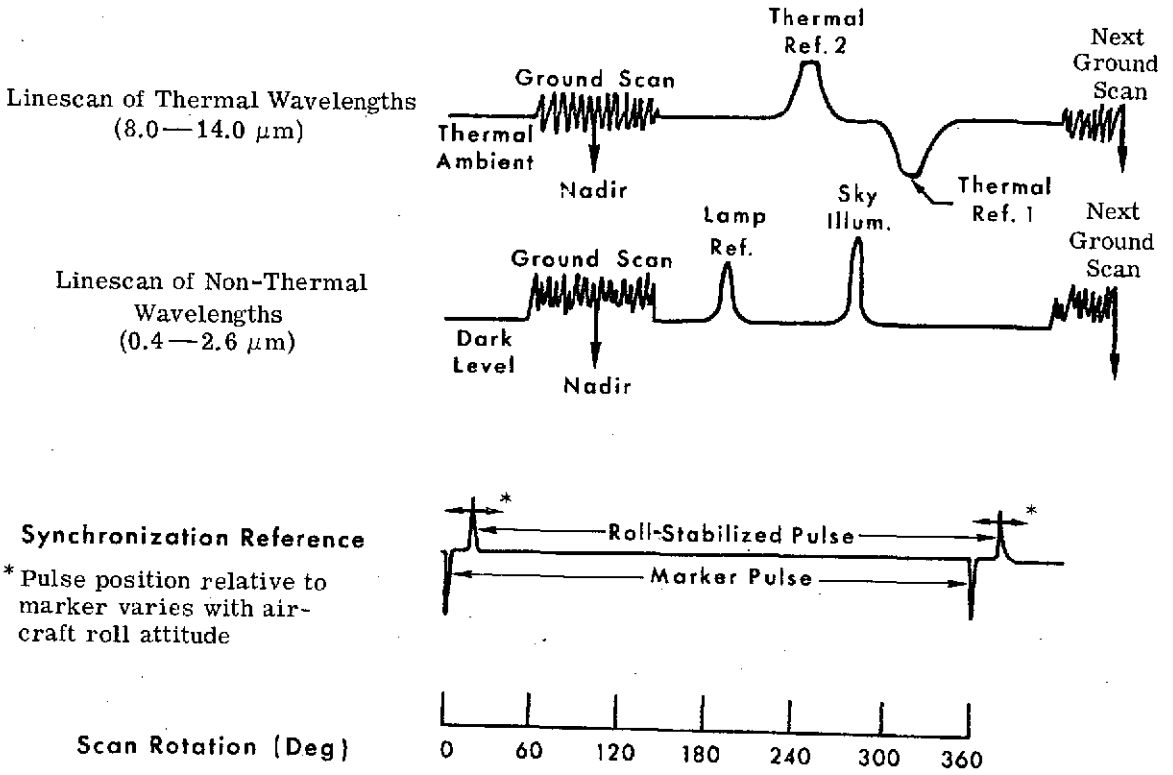

FIGURE 2. SCANNER VOLTAGE OUTPUT VERSUS TIME

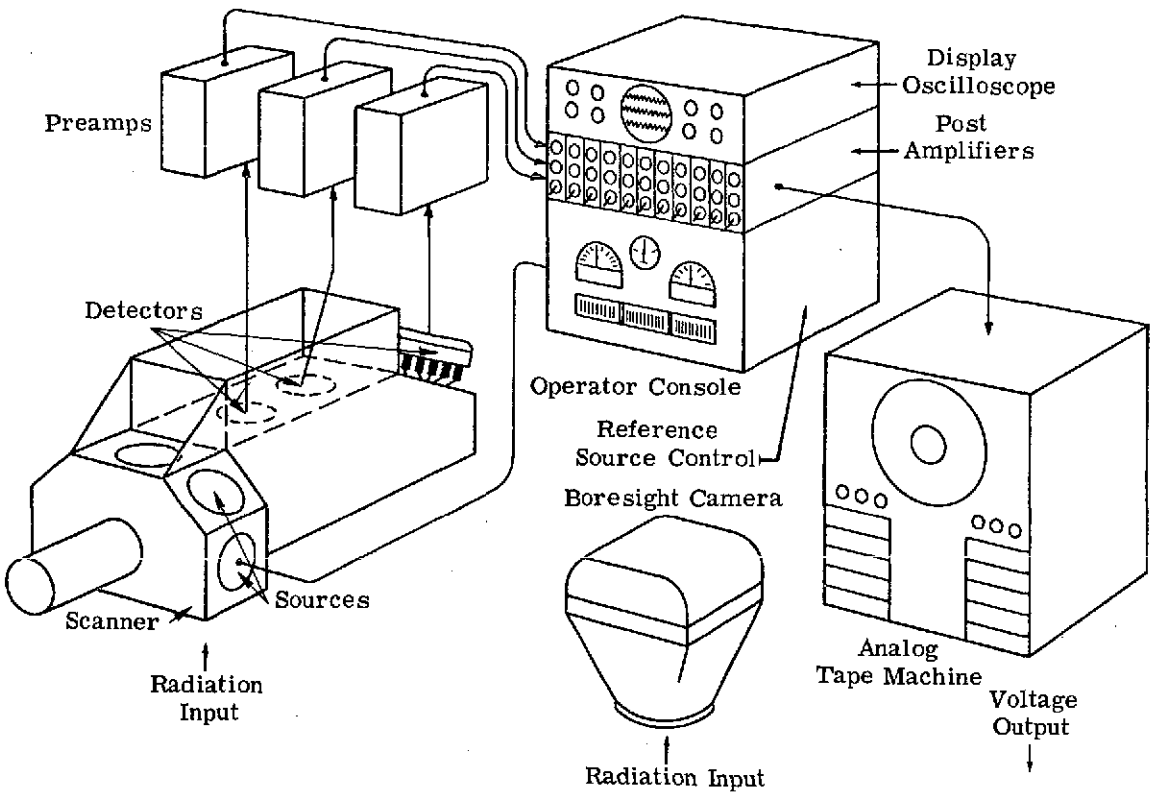

FIGURE 3. ERIM EXPERIMENTAL MULTISPECTRAL SCANNER SYSTEM

are amplified in preamplifiers before being routed to an operator console where further gain is supplied by postamplifiers. The operator first monitors the video signals and adjusts them to the proper level for tape recording; then, during actual recording, he monitors signals reproduced from the tape record to confirm that the recording is satisfactory. The system linearly transforms input radiation into a voltage which is recorded in analog form on magnetic tape. Table 1 enumerates significant parameters of M7 system performance. The boresight camera, which is part of the system, film-records visible radiation for use in later analysis of the scanner data.

Figure 4 shows the optical configuration of the M7 Michigan Experimental Multispectral scanner. Figure 5 affords a similar view of the actual scanner with inspection panels removed. A key feature of scanner design is the ease with which it can accept different radiation reference sources and new detector assemblies. This flexibility, for which weight and space savings were sacrificed, allowed the immediate use of references and detector assemblies from the original system; it also permitted the same assemblies to be later replaced as time and funds permitted. Also, the scan motor drive shaft was extended beyond the aft end of the motor housing so that illumination sources (such as lasers) might later be added to the system and registered with the scan mirror.

The radiation intercepted by the 5-in.-diameter collecting aperture is directed into the Dall-Kirkham telescope which has a nominal 3-in. diameter, broadband (0.3 to 15 μm), secondary mirror. The incoming radiation this secondary mirror blocks from the telescope is directed upward to Detector Positions 1A and 1B. Currently a focusing lens designed for 2.0 to 15.0 μm is used at Position 1A with a HgCdTe detector to provide thermal data. A dichroic mirror mounted ahead of this lens diverts UV and visible radiation onto a photomultiplier detector in Position 1B. Various other detector assemblies may be optionally substituted in either position.

The radiation collected by the effective 4-in. aperture of the telescope is folded into a dichroic mirror which reflects the radiation below a nominal 1.0 μm and which transmits the energy beyond this wavelength. The radiation beyond 1.0 μm is focused onto three separately filtered InAs detector elements in Position 2 by a lens optimized for transmission in the 1.0- to 2.6-μm region. This dichroic and lens can be changed relatively easily for different detector configurations. Planned flexibility for Detector Position 2 includes a multi-layered HgCdTe detector to provide 1.0 to 1.8 and 2.0 to 2.6 μm bands in registration and a new dichroic and lens which, if desired, will transmit radiation to a thermal detector in this position.

The radiation at wavelengths shorter than 1.0 μm is focused onto the entrance slit of a prism spectrometer at Detector Position 3. This spectrometer disperses visible and near-

TABLE 1. NOMINAL M7 SCANNER PERFORMANCE CHARACTERISTICS

- 12 Spectral Bands in UV, Visible, IR Regions
- 90° External FOV ($\pm 45^{\circ}$ from nadir)
- 2 mrad Max. Spatial Resolution, 3 mrad Nominal
- 0.1°C Nominal Thermal Resolution
- 1% Nominal Reflectance Resolution
- 5 Radiation Reference Ports
- 5-in.-Diameter Collector Optics
- 60 or 100 scans/sec
- DC to 90 kHz Electronic Bandwidth
- Roll-Stabilized Imagery

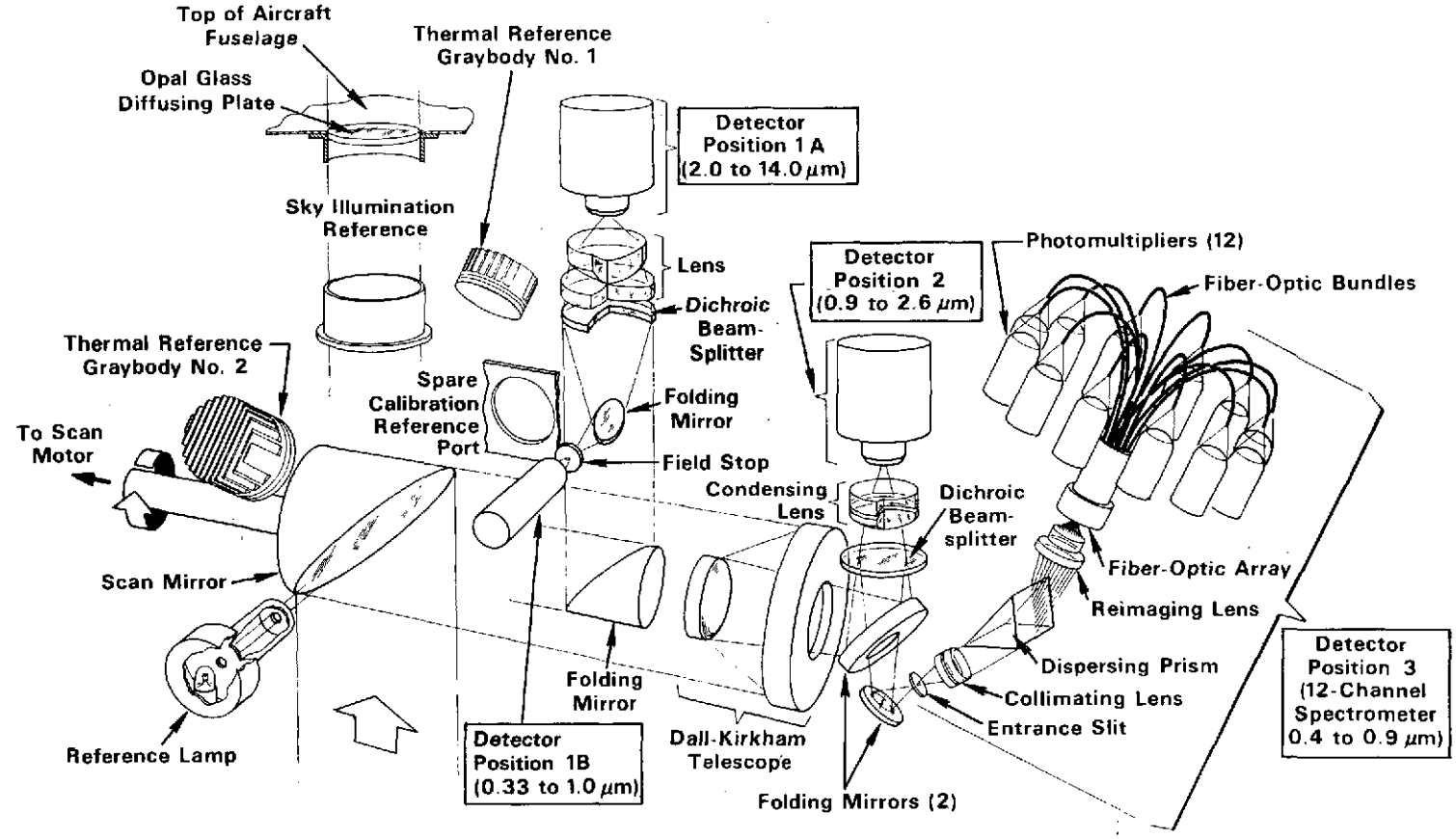

FIGURE 4. OPTICAL SCHEMATIC OF ERIM EXPERIMENTAL M7 MULTISPECTRAL SCANNER

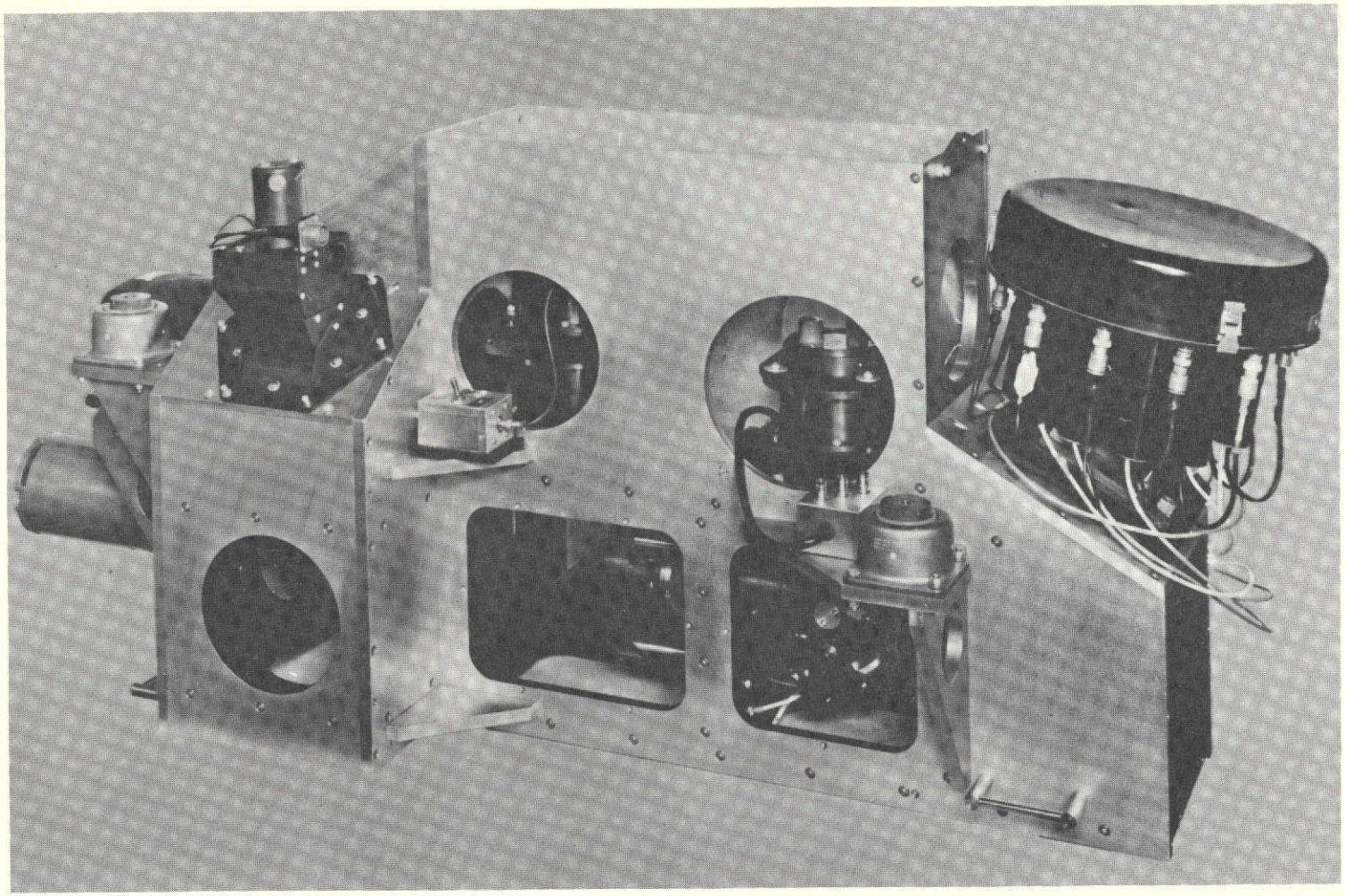

FIGURE 5. ERIM EXPERIMENTAL M7 MULTISPECTRAL SCANNER. View with inspection panels removed.

infrared radiation through fiber-optic bundles (sixteen in all) onto as many as twelve photomultiplier tubes. In the current configuration, the sixteen fibers (some are grouped together) are directed onto nine separate photomultiplier detectors.

Radiation reference sources currently in use with the system are: (1) a quartz-iodine lamp (traceable to NBS standards) packaged to simulate a point source, (2) two temperature-controlled blackbody thermal references that fill the collected aperture, and (3) a sky illumination reference consisting of an opal glass diffusing plate mounted in the top of the aircraft. The operator has control of the radiation from all reference sources through electronic control of the lamp and blackbodies and attenuating optical filters for the sky illumination. The calibrated outputs of these sources are monitored and recorded manually by the operator during data collection. Periodically, these internal references are calibrated against external standards in the laboratory.

Table 2 shows the detector assemblies currently available for use in the M7 Scanner System and those planned for the near future. For all data collected during the last half of 1971 we used the specific detectors listed in the top row of the chart. A 9.3-μm long-wavelength pass filter was used with the HgCdTe detector in Position 1 to provide thermal coverage. Of the new detectors planned for FY73, some became available for use in the spring of 1972; all were operational by the end of 1972.

Figures 6a and 6b show the ERIM C-47 aircraft which normally transports the multispectral mapping system, and an internal view of the instrumentation installed in the aircraft. The internal view looks forward in the aircraft. The M7 scanner assembly with reference sources and radiation detectors installed is in the lower right-hand corner of the figure. The scanner rests in an instrument well built through the floor of the aircraft. Forward of the scanner position are the supporting electronics and operator positions for the system. The modified multispectral system weighs about 1200 pounds, which is about half the instrumentation payload of the C-47 aircraft. Therefore other systems may be installed and operated that complement the multispectral mapping functions.

The M7 multispectral system can also be installed in another ERIM aircraft, a C-46, which normally contains a high-resolution, side-looking airborne radar (SLAR) system likewise used for earth resource applications. However, the two systems cannot be operated simultaneously and, because of reduced aircraft fuel capacity with both systems installed, the flight time available for data collection is reduced. Thus the combined system installation in the C-46 is usually a temporary one to allow both IR and radar mapping with a single aircraft on the same field trip.

In addition to our continued development of new detector assemblies and electronic components to improve scanner performance, we are investigating several other techniques. One

TABLE 2. DETECTOR CONFIGURATIONS FOR M7 SCANNER

	Detector Serial Number	Spectral Band (μm)	Spatial Resolution (mrad)	Detector Serial Number	Spectral Band (μm)	Spatial Resolution (mrad)	Detector Serial Number	Spectral Band (μm)	Spatial Resolution (mrad)
FY72	Position 1 (0.3 to 15.0 μm)			Position 2 (0.9 to 2.6 μm)			Position 3 (0.4 to 0.9 μm)		
	HgCdTe 1-3	2.0†-11.8†	3.2 × 2.9	InAs 3-5	2.0-2.6	2.0 × 4.0	PM 12-1	0.67-0.94	2 × 2
	HgCdTe 1-2	2.0†-15.0†	6.8 × 6.6		1.5-1.8	2.0 × 4.0		0.62-0.70	2 × 2
	HgCdTe 2-2	2.0†-10.9	21 × 28		1.0-1.4	2.0 × 4.0		0.58-0.64	2 × 2
		9.4 -12.1	21 × 21	InSb 3-6	2.0-2.6	2.0 × 4.0		0.55-0.60	2 × 2
					1.0-1.4	2.0 × 4.0		0.52-0.57	2 × 2
								0.50-0.54	2 × 2
								0.48-0.52	2 × 2
								0.46-0.49	2 × 2
								0.41-0.48	2 × 2
							PM 12-2	same as PM 12-1	
New for FY73	Position 1A (1.0 to 15.0 μm)			Position 2 (1.1 to 2.6 μm or 8.0 to 14.0 μm)			Position 3 (0.4 to 0.9 μm)		
	HgCdTe 3-1	2.0†-9.1	20 × 20	InAs 3-6	2.0-2.6	2 × 4	same as FY72		
		8.7 -10.7	20 × 20		1.5-1.8	2 × 4			
		9.9 -14.0	20 × 20		1.0-1.4	2 × 4			
	HgCdTe 1-5	2.0†-12.0†	3.2 × 3.3	HgCdTe 2-3	2.0-2.6	2.0 × 2.0			
					1.0†-1.8	2.0 × 2.0			
	Position 1B (0.3 to 0.7 μm)								
	PM 1-3	0.3†-0.7†	3 × 3	HgCdTe 1-2	2.0†-15.0†	4.0 × 4.1			

*Cutoff established by replaceable dichroic mirror.

†Bandpass established by external optical filter.

(a) Exterior View

FIGURE 6. ERIM C-47 REMOTE SENSING AIRCRAFT

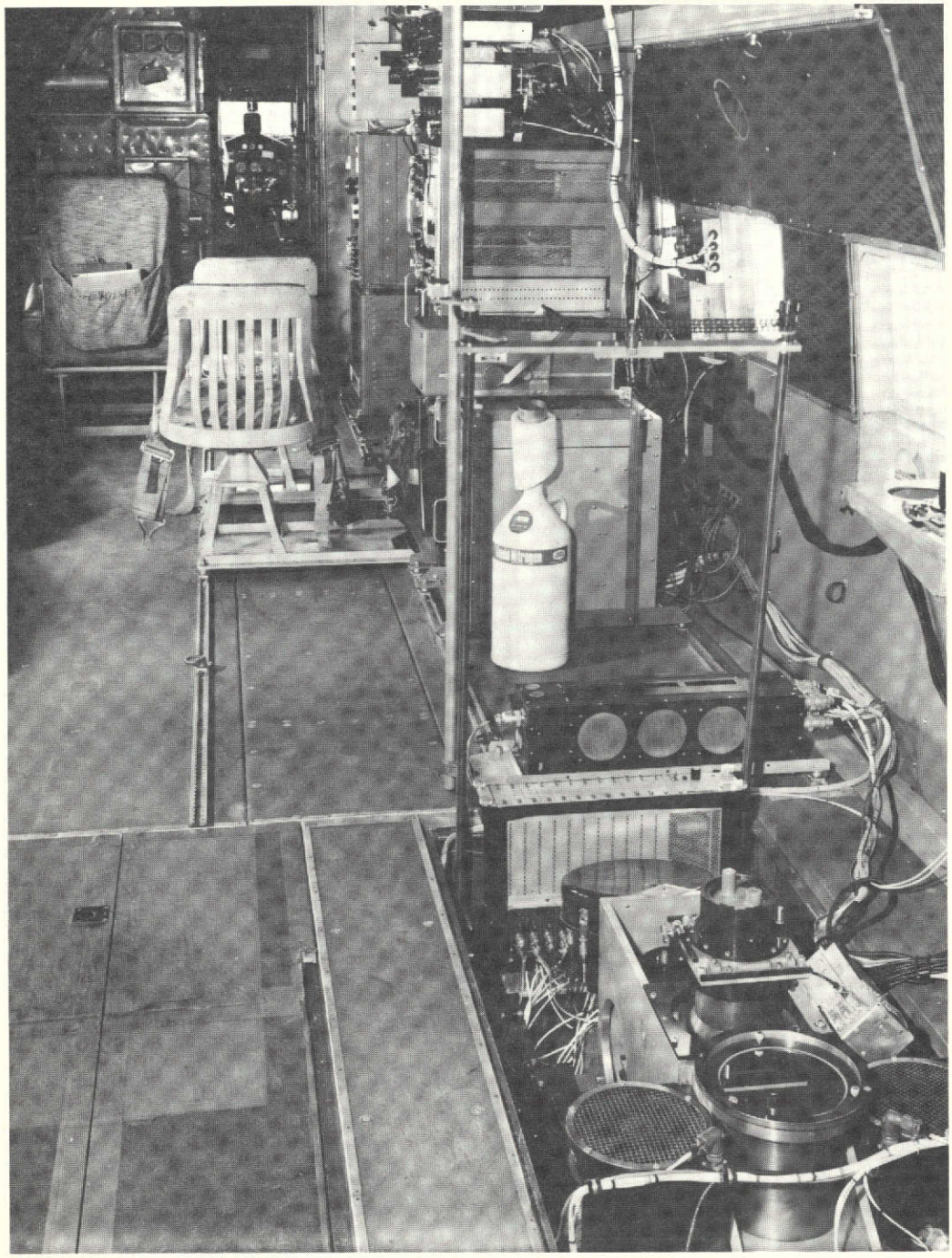

(b) Interior View Showing Multispectral Mapping System

FIGURE 6. ERIM C-47 REMOTE SENSING AIRCRAFT (Concluded)

is a provision for scanning across the aircraft track in an oblique instead of a vertical plane. The oblique view of vegetation should show more vegetation and less ground in a resolution element. The mix of soil and crop in a common resolution element has been a problem in remotely identifying farm crops in the past and the oblique view technique will benefit not only this but other applications as well. Another new technique of potential benefit is one of actively scanning in selected wavelength bands and to record these along with certain passively scanned bands; laser radiation sources can be coupled with line scanners to provide this capability. Still another technique being explored is one of registering selected spectral bands in dual polarized outputs. Because the polarization of reflected radiation is known to cause variations in signal level along a scan line, these variations can possibly be used to advantage as an aid in remotely identifying the reflecting surface.

2.2 AERIAL CAMERAS

The aerial cameras we use with the M7 scanner system provide the high spatial resolution (not provided by the scanner) required for shape identification of some terrain features and conditions. Aerial camera coverage is of course secondary to multispectral scanner coverage; the current cameras (military surplus) provide adequate boresight data for the analysis of scanner imagery.

ERIM's aerial camera inventory consists of two K17 cameras, three KB8 or P220 cameras, and five P2 cameras—all of military type. The characteristics of these cameras are noted in Table 3. Although five cameras is the maximum number possible, we try to limit aerial camera coverage on any given mission to that afforded by three (one of each type) or fewer cameras. All cameras are mounted directly to the airframe with manual in-flight leveling adjustments. The camera operator has in-flight access to the cameras for magazine changes and exposure adjustments. No stabilization, image motion compensation, or automatic exposure control is available for any of the cameras.

ERIM stocks panchromatic (Kodak type 2403) and infrared black-and-white film (Kodak type 2424) for all the above cameras. Color (Kodak type SO397) and color infrared (Kodak type 2443) film is stocked in the 70 mm size only. None of the cameras has color-corrected lenses but all produce apparently acceptable color fidelity. The use of color film in the K17 is not recommended because of the slow lens; however, under bright illumination conditions, acceptable color fidelity has been obtained with this camera.

From a variety of filters available for these cameras, the following film/filter combinations are most often used:

TABLE 3. PERFORMANCE CHARACTERISTICS OF AERIAL CAMERAS

	K17D	KB8A P220	P2
Magazine type	A5A	LA97A	LA97A
Film capacity	9.5 in. × 200 ft	70 mm × 50 ft	70 mm × 50 ft
No. of exposures	250	230	230
Max. cycling rate	3 sec/cycle	5 cycles/sec	5 cycles/sec
Shutter speeds	1/50 to 1/400	1/500 to 1/2000	1/500 to 1/2000
Max. AWAR resolution	25 lines/mm	42 lines/mm	30 lines/mm
Focal length	6 in.	38 mm	3 in.
Max. aperture	f/6.3	f/4.5	f/2.8
Angle of view	$73^{o}44'$	$73^{o}44'$	$41^{o}06'$

Film Type	Filter
2403	W12, W15, 25A
2424	25A, 87C, 89B
S0397	1A, 2B
2443	W12, W15

Most of the filters are glass-mounted. The viewport in the aircraft is covered with plexiglass, the optical transmission of which is uniform for film-sensitive wavelengths.

The ERIM photographic laboratory processes all black-and-white film; we send color film to the Mead Corporation in Dayton, Ohio for processing.

2.3 DELIVERABLE DATA FROM A MULTISPECTRAL MAPPING SYSTEM

The following items comprise the usual data ERIM delivers to the sponsor as part of each multispectral mapping mission:

(1) Mission Plan and estimated costs - These depend on user data requirements as specified in the Flight Request and are based on agreements reached with the Principal Investigator concerning site coverage.

(2) Mission Report - Documents the conduct of the mission and provides associated data the user may need in analyzing the mission data.

(3) Analog magnetic tapes - These tapes contain, in analog form, a maximum of 12 channels of multispectral scanner imagery and reference signals.

(4) Four channels of scanner imagery on 70 mm filmstrips. These are reproduced from the original magnetic tapes.

(5) All aerial camera imagery obtained.

The magnetic tapes, if required, are delivered as analog duplicates; the original tapes are retained on file at ERIM. Film imagery is delivered in the form of original film transparencies. Further reproductions of mission data, such as additional scanner channels on film or digitized tapes, are considered a part of data processing and hence not normally included with the data collection effort.

In all, a data collection mission takes about three calendar months. During the first six weeks, the ERIM test conductor works with the contract sponsor and the specific data user to evolve a plan for accomplishing the mission within the frame of available funds and data needs. The outcome of these negotiations is an acceptable Mission Plan with an associated estimate of costs. This plan is usually finalized a week or two before the mission. The mission itself usually takes a week, including transit time, weather standby time, and actual flight time.

Following a mission, approximately two weeks are required to process the aerial camera film and to duplicate the analog tapes (if this is a requirement). Approximately one month is required to reproduce four channels of scanner imagery on film and complete the film processing. By the time all film data are reviewed and labeled and a Mission Report prepared for transmittal to the sponsor, a total of three months will have elapsed since the initial request. Non-routine missions can be completed in one-third this time—if they are infrequent and adequately justified.

Because much of the work following data collection can be accomplished in parallel, ERIM can fly an average of a mission a week between periods of required aircraft maintenance—which must follow every 100 hours of flight time. (Periodic maintenance and calibration of the airborne instrumentation is scheduled to coincide with aircraft maintenance periods.) One week of downtime usually suffices for all such maintenance, although this period may be extended by unforeseen failures in aircraft or instrumentation equipment.

2.4 SCANNER DATA PROCESSING AND ANALYSIS SERVICES

After terrain has been mapped in twelve different spectral channels and the data stored on magnetic tape, machine processing of the multispectral data should help the investigator reach his objective with minimal effort. With the imagery in electrical form from tape playback, the separate channels can be amplified, sliced, ratioed, and combined in different ways to implement almost any function that can be described mathematically. The processing results can be displayed in statistical tabulations, computer paper printouts, in coded grayscale or color film printouts, or in any other display that accepts electrical inputs. Processing and analysis personnel at ERIM are experienced in working with investigators to extract the most information from the data and to help explain why the results appear as they do.

Specific processing and analysis services available at ERIM are detailed in Appendix B.

The next section describes the application of multispectral processing techniques to a particular earth resources investigation.

3
APPLICATION OF MULTISPECTRAL MAPPING TO EARTH RESOURCE PROBLEMS

In the course of developing, testing, and applying multispectral techniques to many surveys of earth resources, ERIM has acquired much knowledge of processing techniques and procedures useful to the investigator. Thus, ERIM personnel can offer invaluable assistance in helping a scientist determine which processing techniques are best for his particular purposes.

An example of the use of earth resource data is presented here, along with a comprehensive bibliography relating to various fields in which feasibility experiments have been performed. The case selected for discussion concerned the 1967 United States Geological Survey water resource investigations in Florida.

In September of 1967, WRL made several data collection flights in southern Florida in collaboration with the Miami and Tampa offices of the U.S.G.S. These data were processed using multispectral techniques to determine the capability of these techniques for identifying or locating features peculiar to areas of sinkhole collapse, and to determine the possibility of mapping different types of vegetation cover and water depth in the Everglades. Preliminary analysis of results indicated a good probability that active sinkholes could be located and mapped. In the Everglades we found that the natural vegetation, water and limestone outcrops could be identified and mapped, and the areas of these features computed automatically as well.

3.1 PROBLEMS AND OBJECTIVES

Tampa-Bartow, Florida. The Tampa area has experienced a continuing development of subterranean cavities in karst topography where sinks may now be more active than previously. Before their actual collapse, the presence of these sinkholes is often not evident from the surface; this fact creates serious problems in urban planning and road site location. Since these sinks are most apt to collapse when the water level is reduced and the sink becomes dry, A. E. Coker of the U.S. Geological Survey (Tampa) hypothesized that local water loss in areas known to contain active sinks could be detected by its effect on vegetation and by certain thermal relationships on the surface. To test this hypothesis it was necessary to map the areas of interest, process the data to detect water-stressed vegetation, enhance the surface thermal effects, and then correlate these processed results. An experiment was begun to gather and process data for this purpose.

The Everglades. The Everglades traditionally has been an inaccessible area known for its unique flora and fauna and thus deserving preservation as a national park. Difficult to evaluate, however, are the effects on the park of changes in the adjacent environment. To detect changes in the park area, it was decided that the area should be mapped periodically to identify most

types of vegetative cover, water levels and areal extent, and features such as limestone outcrops. As a demonstration of the feasibility of remote sensing for recognizing these features, WRL agreed to try to map them and determine their distribution in a limited but representative area. In collaboration with A. Higer and M. Kolipinski of the U.S. Geological Survey (Miami), a series of flights was then made to gather this data.

3.2 PROCESSING APPROACH

As our experience has grown in the use of multispectral data, a variety of analysis and recognition techniques applicable to such problems has been developed at WRL/ERIM. These techniques have included the use of digital, analog, and special-purpose computers suited to the particular requirements of the analysis or recognition problem at hand. In general, digital computing has been employed in the analysis of targets and backgrounds as objects or distributions in multispectral space and for the development and testing of recognition techniques. Conventional analog computing equipment, sometimes used for these same purposes, is more often useful in the development, evaluation, and simulation of concepts for practical high-speed recognition and mapping. Analog techniques have also proven valuable in achieving realistic visualizations essential to more immediate understanding of the effects of various steps and techniques used in processing.

These investigations have resulted in development of special-purpose equipment capable of analyzing data and recognizing objects of interest at the same rate as that at which the data were originally gathered by the airborne scanner. Particular emphasis has been given to the development and use of this "fast" equipment because of the need to process large amounts of data with minimal delay to obtain maps showing the locations of targets of military interest, and to provide maps of objects of ecological and agricultural interest. The time element can be of critical importance, for example, in agriculture, where crop disease or insect infestation may require a remedial response within a few days. Thus the usefulness of a multispectral system is often proportional to its speed. And the faster such a system can supply processed data, the more applications become possible.

3.2.1 PROCESSOR SYSTEM

The processor system, Fig. 7, consists of a playback tape recorder, signal handling equipment, the SPARC processor (SPectral Analyzer and Recognition Computer), and various items of display and recording equipment.

The system operates in two basic modes. In one, the signatures of the target to be recognized and its associated backgrounds may be obtained from a training area or areas; in the other, a complete area is examined by the processor, and the targets are mapped from signatures provided in the first mode.

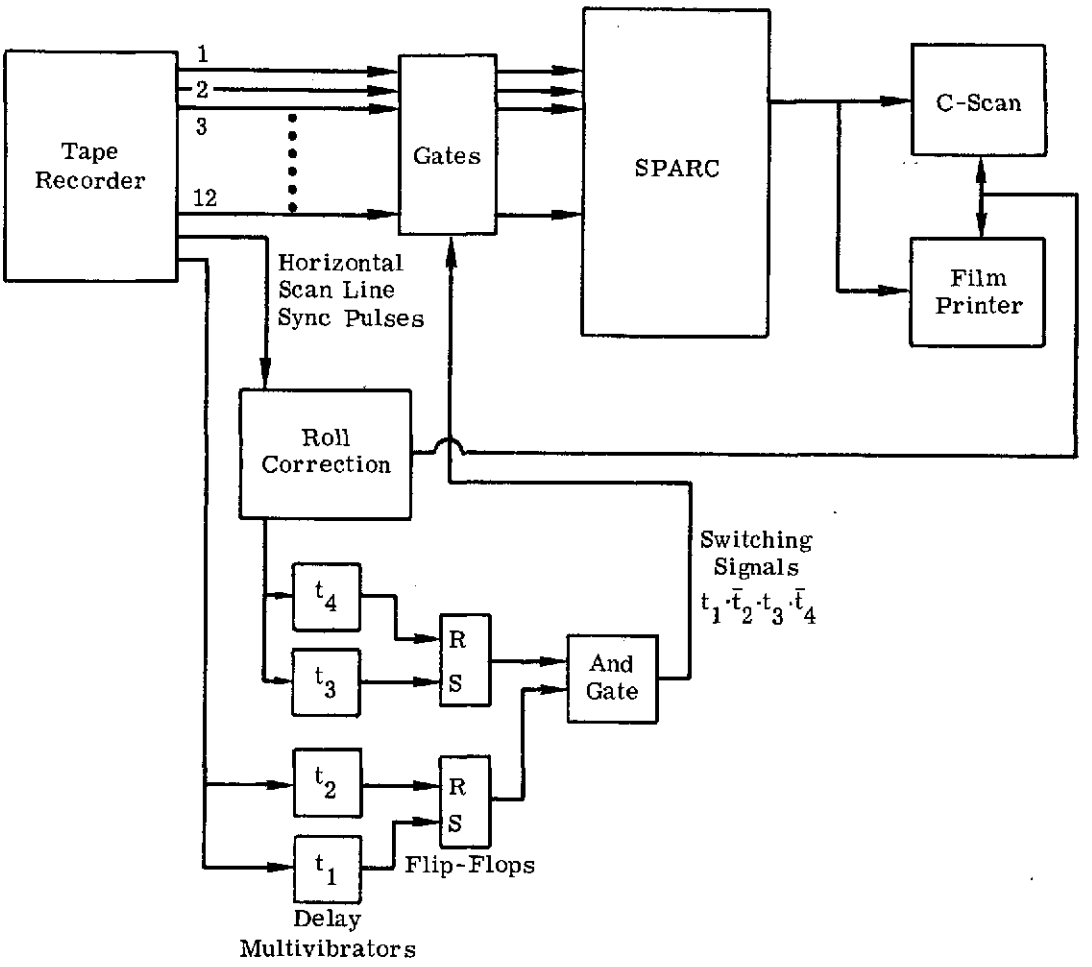

FIGURE 7. LABORATORY EXPERIMENTAL APPARATUS FOR MULTISPECTRAL PROCESSING

The second mode of recognition is accomplished by placing the original tape on the tape recorder and making a map on film of the recognition video signals at the same rate as that at which the aircraft data was originally obtained. At the same time, the areas of the various objects mapped may be cumulatively totalled.

The series of maps obtained for a given area by this means may then be copied, each in a desired ozalid foil color, and overlaid to form a color composite which may be copied on a color positive or negative and used as desired. This color presentation is a useful means of displaying such data. It allows a considerable amount of mapped data to be seen at one time, while preserving good resolution and the actual spatial interrelationships of the objects mapped.

3.2.2 RESULTS OF PROCESSING

The Everglades. A map obtained by processing the area in the Everglades is shown in Fig. 8. As indicated in the figure, nine classes of hydrobiological features have been identified and color coded in this scene, and approximately 80% of the total area classified. Spot checks of the area were made to determine the validity of the classifications, using low-altitude helicopter photography and observation, and photography and observations on the ground. Evaluation of the accuracy of the recognition maps based upon aerial photography obtained during data collection and limited ground truth indicates that the processing technique is more accurate than other techniques used previously. These results were obtained using 12 channels of spectrometer data in the spectral range from 0.4 μm to 1.0 μm.

Tampa-Bartow Sinks. In the area near Bartow, several indications of possible sink patterns appear (see Fig. 9) in addition to those known and used for training areas. These occur in the low herbaceous vegetation (consisting principally of grasses) near the sinks, and were found by processing near-infrared data in three bands: 1.0-1.4 μm, 1.5-1.8 μm, and 2.0-2.6 μm.

Enhanced thermal data (8.0-14 μm) were also obtained by false-color contouring, i.e., quantizing and assigning contrasting colors to adjacent thermal intervals. These data (Fig. 10) indicate patterns similar to those obtained for vegetation recognition, but appear to have better relevance to the hydrological features of interest.

Of particular interest is an area north of the known sinkhole. The area was overflown in September of 1967, processed and examined in February of 1969. Up to that time, no surface signs of collapse had been noted. But further observation produced evidence that the road is subsiding.

In several areas where processing suggested closer inspection, drilling tests have been made and cavities located. It appears that sink activity as much as 60 ft underground can produce surface indications. This was rather surprising and tends to confirm the original hypothesis.

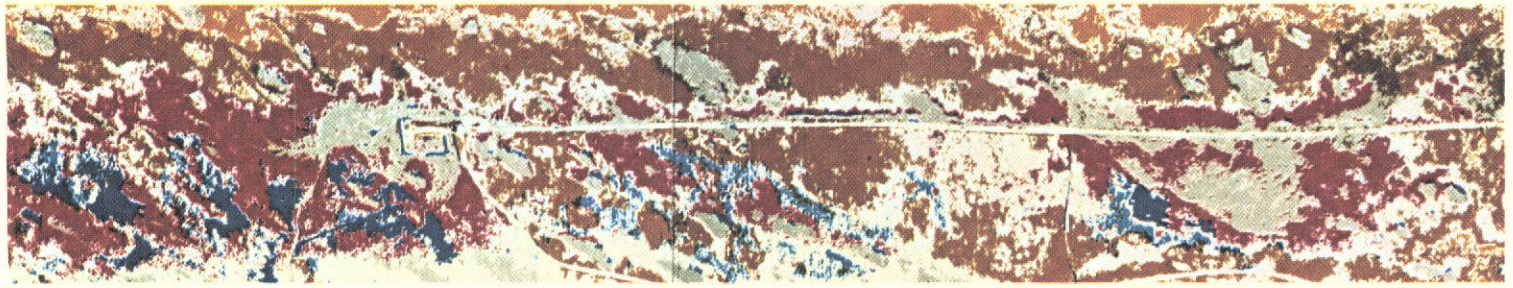

Color	Feature
Dark Blue	Water depth greater than 1 ft
Light Blue	Water depth less than 1 ft
Light Green	Trees and woody vegetation
Red	Dense sawgrass marshes and associated communities

Color	Feature
Brown	Sparse sawgrass marsh
Purple	Wet prairie communities
Dark Yellow	Prairie communities, dry or damp
White (lines)	Roads
Black	Limestone outcrops
White	Unresolved features

FIGURE 8. PORTION OF A RECOGNITION MAP OF THE EVERGLADES

Color	Feature
Blue	Dry marsh vegetation
Green	Dry grass, mowed field
Red	Dry grass, mowed, near center of sink area
Brown	Dry grass, unmowed

FIGURE 9. PORTION OF A RECOGNITION MAP OF VEGETATION IN A SINK AREA

Color	Average Apparent Temperature (°F)
Cyan	77
Violet	79
Orange	80.5
Black	82
Yellow	83.5
Red	85
Blue Green	86.5
Dark Brown	88
Yellow Green	90
Magenta	93
Olive	96
Dark Blue	98.5

FIGURE 10. FALSE COLOR THERMAL CONTOUR MAP OF SINK AREA

4
DESIGN DESCRIPTION OF M7 SCANNER

One might wonder at first why the optical-mechanical scanner of Fig. 1 in Section 2 could not simply be converted to a multispectral scanner by replacing its detector with a dispersing monochromator or spectroscope. However, we should remember that the single detector at the output end of a conventional laboratory-type spectroscope observes just one spectral resolution element at any one time, and that the system scans in time through the spectral range of interest. Frequently, too, if this spectral range is broad, it is necessary to change the dispersing grating or prism at mid-scan and to utilize different detector types for different parts of the spectrum.

But airborne scanners of the kind in which we are interested scan across one ground-resolution element in times which are short compared to the fastest spectrally scanning spectrometers. Thus the airborne multispectral scanner must be able to detect all spectral resolution bands simultaneously. This stipulation poses rather severe requirements and can result in a system employing a variety of optical beamsplitters and spectral dispersing elements as well as a multiplicity of detectors—in other words, a system of complex design.

The specific purpose of this section is to consider the basic design of the M7 Scanner and to present the rationale followed in arriving at this design.

4.1 OPTICAL SYSTEM

The optics of a multispectral scanner system can be configured in at least two different fundamental forms. Examples of these two forms, both with identical rotating mirror systems to accomplish the spatial scanning, are shown in Fig. 11, parts (a) and (b). They differ basically, however, in that (a) has a single field stop common to all spectral bands while (b) has multiple field stops, some of which may include the physical outlines of individual detector flakes. Example (a) has the distinct advantage of forcing all spectral bands to view precisely the same spatial resolution patch at all times. Within the spectrometer, each detector element must be focused upon the common field stop or it sees nothing at all. The optics of such a system tend to be cascaded and hence somewhat interdependent. In general, the optics also tend to be more complex and more compactly or tightly packaged. Also, because of the cascading effect, optical efficiencies are often lowered. Example (b), on the other hand, lacks the positivism of coincident fields of view for all detector channels. As explained later, certain precautions must be taken in the alignment of the system to assure superposition of the fields of view for the various detectors.

We chose the latter approach primarily for its simplicity and flexibility. We felt too that since the optics for such a system were within the current realm of practice, much development

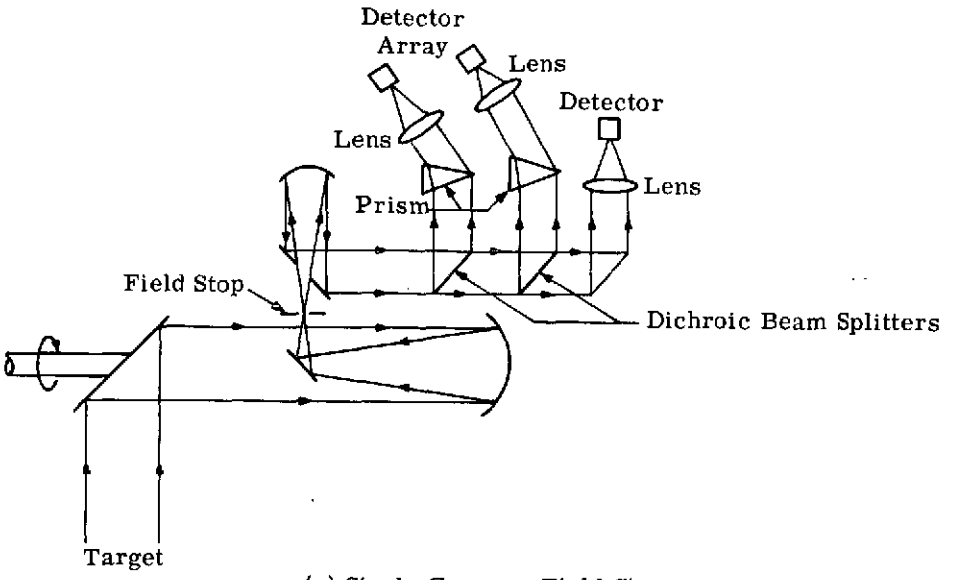

(a) Single Common Field Stop

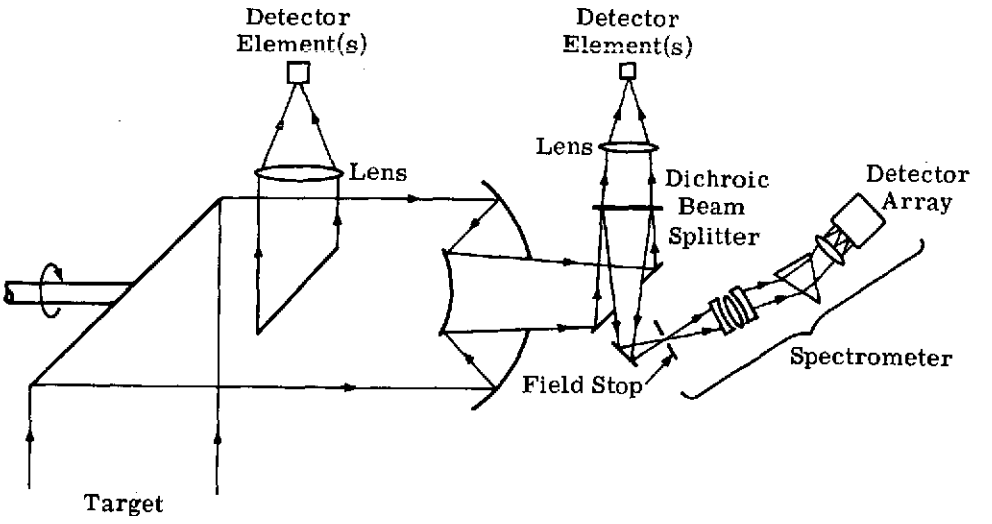

(b) Multiple Field Stops

FIGURE 11. EXAMPLES OF TWO FUNDAMENTALLY DIFFERENT MULTISPECTRAL SCANNERS

time and cost could be avoided. Moreover, such a design facilitates access to the optical components and detectors, and provides more opportunities for keeping the system flexible. Such attributes as accessibility and flexibility were deemed extremely important for a general-purpose experimental system.

The system which has ensued as a result of adopting the concept illustrated in Fig. 11(b) is often called a common line-of-sight scanner. This is in fact the case, since the optical lines of sight of the various detectors are caused to be superimposed through certain alignment procedures. Refer to Fig. 4 for a descriptive view of the M7 system. A summary of system specifications appears in Table 4.

The scanner baseline (item 1 in Table 4) is the backbone of the system and remains relatively inflexible to change; it consists of the scan mirror and drive, the Dall-Kirkham telescope, and several folding flats located fore and aft of the telescope. These components are arranged in-line (sharing a common optical axis). The other subsystems are then folded off generally at right angles to this axis. Those components located off the axis are mounted in a manner amenable to change or replacement as experimental parameters change.

The heart of the baseline is the scan mirror and drive. The mirror is a monolithic structure fabricated from aluminum; it is affixed to a shaft with a bolt that passes through a small relieved hole in the center of the mirror. The shaft, supported by two pairs of preloaded ball bearings, is directly coupled to an a-c synchronous motor. Either one of two motors is used—a 60-Hz, 3600-rpm motor, or a 400-Hz, 6000-rpm motor. The system has been designed for balanced operation and retention of the mirror's optical figure to within a flatness of 0.1 mrad at either drive speed. Enclosing the mirror is a cylindrical, eccentrically mounted balance tube whose axis is parallel to the spin axis of the mirror. The tube is designed to counteract the dynamic forces of the truncated scan mirror which has an inherent imbalance. A port in the side of the balance tube permits passage of the folded optical scan beam.

The telescope is a traditional Dall-Kirkham system having a slightly aspheric primary and a spherical secondary mirror. Both elements are fabricated from pyrex. Overall, the system has a collecting aperture of 5 in. with a 3 in. diameter center obscuration because of the secondary mirror. The focused cone emanating from the telescope converges at a speed of f/4, and the effective focal length is 20 in. Immediately ahead of the telescope in that portion of the beam obscured by the secondary mirror is a 45° diagonal mirror fabricated from aluminum. Immediately behind the telescope are several pyrex folding mirrors that fold the converging f/4 beam to the respective detectors. All reflective optics are coated with an aluminum alloy optimized for reflectivity in the 0.3- to 15-μm band and having a minimum reflectivity of 88% for one reflection. The coating was selected for uniform spectral reflectivity as well as high durability and good cleanability; high reflection enhancement was of secondary importance.

TABLE 4. SPECIFICATIONS OF MICHIGAN EXPERIMENTAL MULTISPECTRAL SCANNER, M7

1. The Scanner Baseline*	
Scan mirror	single-face, elliptical mirror at 45° to spin axis
Scan mirror collecting aperture	5 in. diameter
Effective collecting area	19.33 in.^{2}
Rotational Speed	constant speed of 3600 rpm or 6000 rpm
Drive	in-line, direct-coupled synchronous motor (choice of 3600 rpm/60 Hz or 6000 rpm/400 Hz)
Angular width of scanned field	±45° (from nominal scanner nadir)
Calibration ports	5
Calibration port locations	±90°, ±35°, 0° (from nominal scanner zenith)
Collecting aperture	3 in. dia. central folding mirror
Collecting aperture	5 in. dia. Dall-Kirkham telescope
Effective collecting area	12.57 in.^{2}
Primary mirror f/no.	1.5
Telescope f/no.	4
Telescope blur circle	0.2 mrad (90% of energy)
2. Detector Position 1A†	
Effective collecting aperture	6.18 in.^{2}
Lens	f/1, two-element, germanium, anti-reflection coated
Spectral bandpass	defined by bandpass filter, nominally 9.3-11.7 μm for single-element detector; separately filtered, multi-element detectors also used
Instantaneous field of view	defined by detector element size; nominally 3.3 × 3.3 mrad for single-element detector
3. Detector Position 1B†	
Dichroic beamsplitter	germanium substrate, convex-concave, with concentric radii of curvature; dichroic coating on concave surface, convex surface is anti-reflection coated. (See text for coating specs.)
f/no.	2.8
Effective collecting area	6.18 in.^{2}
Effective f/no.	3.03
Spectral bandpass	defined by bandpass filter placed after field stop; 0.33-0.38 μm and 0.71-0.73 μm bands have been used
Instantaneous field of view	3 mrad × 3 mrad

*See Fig. 11b for scanner geometry and locations of optical elements.

†Because the M7 system may be reconfigured from time-to-time, the specifications given here—while current at the time of writing—must be considered nominal.

TABLE 4. SPECIFICATIONS OF MICHIGAN EXPERIMENTAL MULTISPECTRAL SCANNER, M7 (Cont.)

4. Detector Position 2**	
Effective collecting area	12.57 in.^{2}
Condensing lens spectral band-pass	condenses beam from f/4 to f/1; 4-element, glass and barium fluoride, achromatic between 1.0 and 2.5 μm; elements anti-reflection coated. (A single-element germanium lens coated and achromatized for the 8-13 μm region is available for substitution.)
Effective f/no.	1.25
Spectral bandpass	defined by bandpass filter(s); nominally a multi-element detector filtered for simultaneous operation in 1.0-1.4 μm, 1.5-1.8 μm, and 2.0-2.6 μm regions is used
Instantaneous field of view	defined by detector element size (2 mrad × 4 mrad for 3-element detector described above)
5. Detector Position 3†	
Dichroic beam splitter	currently of a quartz substrate, plane-parallel. See text for coating specs. (A nearly similar barium fluoride substrate dichroic is also available.)
Effective collecting area	12.57 in.^{2}
Effective f/no.	5
Detector type	multi-channel spectrometer. See text for further description, including spectral bands.
Instantaneous field of view	defined by spectrometer entrance slit dimensions of 2 mr × 2 mr

†Because the M7 system may be reconfigured from time-to-time, the specifications given here—while current at the time of writing—must be considered nominal.

The optics associated with Detector Position 1A in Fig. 4 consist of a dichroic beamsplitter and a two-element germanium lens. The beamsplitter has a germanium substrate while its two optical surfaces have slightly spherical figures with concentric radii of curvature. As a first approximation, the net effect of the dichroic insofar as Position 1A optics are concerned is to transmit a certain chromatically chosen beam of parallel rays without refracting them. The lens subsequently focuses this beam. The speed and effective focal length of the lens are f/1 and 3 in., respectively. The lens in current use has been anti-reflection coated and achromatized for optimum performance over the 8- to 14-μm range. The imaging quality of the lens over this range has been analytically shown to be near the diffraction limit whether or not the dichroic beamsplitter is inserted in the incident beam. In addition, the option exists for duplicating this lens and applying to the duplicate an antireflection coating appropriate to other spectral regions—4.5 to 5.5 μm for example—where lens analysis indicates that imaging qualities would be equally good.

The detector normally used in Position 1A is a single-element, cooled, mercury-cadmium-telluride photoconductor with a separate optical interference filter to limit the spectral response of the detector to a bandpass of 9.3 to 11.7 μm. The bandpass has been chosen to minimize the effects of variations in atmospheric attenuation on the incoming radiation stream. This detector's sensitive flake size (i.e., the virtual field stop) is such that a 3.3 by 3.3 mrad instantaneous field of view is defined. Other more specialized detectors have been utilized; duscussion of them will be found in Section 4.3.

Detector Position 1B effectively utilizes a Newtonian-type telescope, with the first surface of the dichroic beamsplitter serving now as the primary mirror or focusing element of the telescope. A convergent f/2.8, 8.5-in. focal length beam results. The dichroic coating in current use has been designed primarily to optimally reflect ultraviolet radiation and transmit thermal infrared radiation. Its reflecting and transmitting characteristics are shown in Fig. 12. The detector in this position is a photomultiplier preceded by a field stop. In practice a bandpass filter positioned immediately behind the field stop defines a specific spectral band. To date, filters providing passbands of 0.33 to 0.38 μm and 0.71 to 0.73 μm have been used. Other passbands are feasible, and a modification of the dichroic's reflecting characteristics would permit selection of still others.

Detector Position 2 employs a condensing lens to convert the f/4 beam emanating from the Dall-Kirkham telescope into a convergent f/1 beam. For solid-state-type detectors, reduction in the f-number of the incident cone of radiation improves the noise equivalent power or sensitivity of the detector. In practice, the lens consists of three glass elements and one barium fluoride element. This refractive system is coated and achromatized for optimal operation in the 1.0- to 2.5-μm region. Over this spectral range the design goal has been to achieve

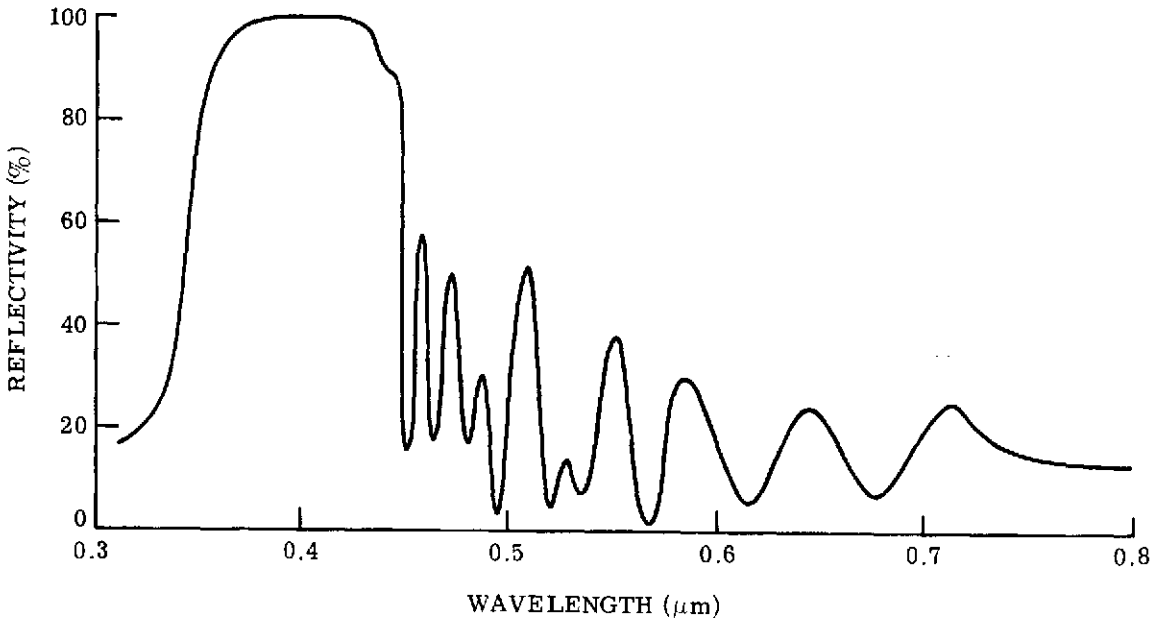

(a) Reflectivity to Detector Position 1B

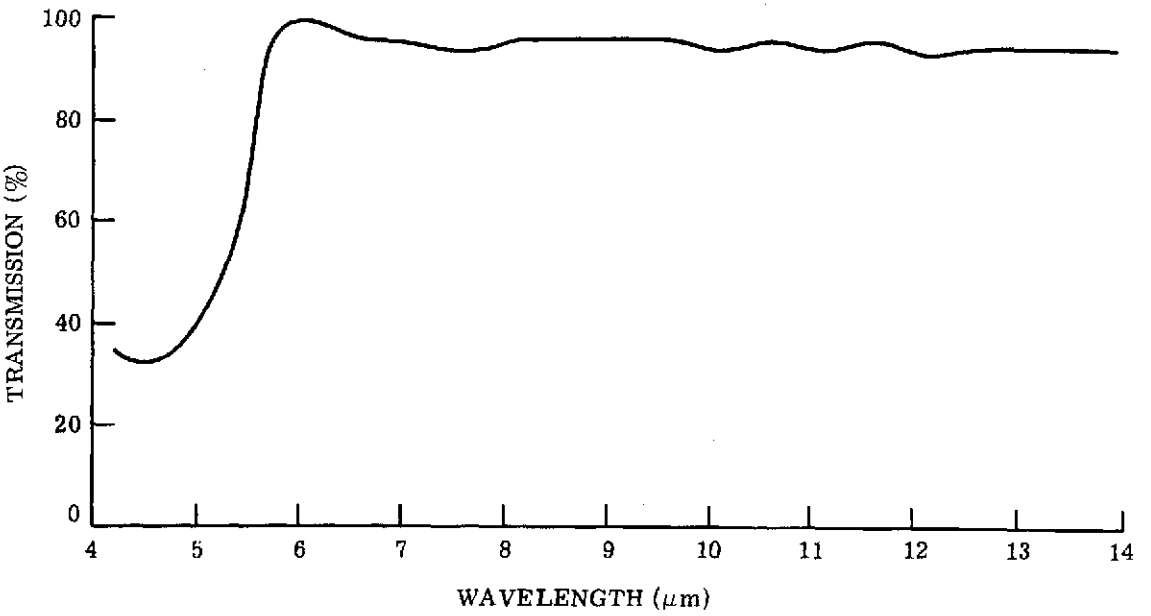

(b) Transmission to Detector Position 1A

FIGURE 12. DICHROIC BEAMSPLITTER

a blur circle of less than 0.2 mrad dimension. Similarly, another lens—this one a single-element germanium refractor—has been designed and fabricated, except that it is coated and achromatized for the 8- to 14-μm range. To date it has not been employed in the system. Typically the detector utilized in Position 2 is a three-element linear array of indium-arsenide flakes with each flake individually filtered by a different multilayer interference filter placed immediately in front of it. The detector-filter combinations have been chosen to give a response in the 1.0-1.4, 1.5-1.8, and 2.0-2.6 μm bands, respectively. At nominal aircraft nadir the optical projection of this array onto the ground is oriented in the direction of scan (i.e., orthogonal to the ground track) so that objects directly beneath the aircraft are scanned in succession by the three elements. Since the spacing between detector elements and the scan rate is a known, fixed parameter, the use of time-delay circuitry at the time of data playback allows all elements to be brought into spatial registration. These elements are sized such that an instantaneous field of view of 2×4 mrad is defined for each element while a 3-mrad spacing exists between elements. Additional details on this detector will be found in Section 4.3.

The linear array described above suffers one serious drawback. The geometry of scanning rotates or twists the projection of the linear array on the ground with respect to the scan line as the scan angle increases away from nadir. For example, at 45° from nadir (the M7 scanner's maximum departure from nadir for external scanning) the array is twisted 45° with respect to the scan line. The result is that at scan angles significantly away from nadir, strict point-by-point spatial registration cannot be achieved. It is intended that this situation will be corrected, probably through the use of a layered or superimposed detector array—a concept which is discussed further in Section 4.3.

A multichannel spectrometer is located at Detector Position No. 3. This spectrometer is capable of sensing as many as 12 spectral channels. Since its incorporation in the M7 Scanner, it has been configured in a 9-channel mode. The instrument is a prism-type spectrograph with its entrance slit located at one of the focal points of the scanner collecting optics (where the detector flake of a single-element detector might normally be located). The lenses are conventional off-the-shelf components. The collimator uses a 200-mm, f/4 lens matched to receive the f/4 cone emanating from the Dall-Kirkham telescope. A 100-mm, f/2 lens is employed at the telescope or imaging end of the spectrograph. The dispersing element is a dense flint prism having an apex angle of 60°. The spectrum formed at the telescope focal plane is picked up by an image slicer consisting of an array of fiber-optic bundles. These bundles distribute the energy to as many as 12 separate photomultiplier detectors arranged in a ring around the top of the assembly.

Figure 13 shows the spectrometer detector with the cover removed. Clearly visible are the fiber-optic bundles as they radiate from the focal plane to the photocathode surface of the

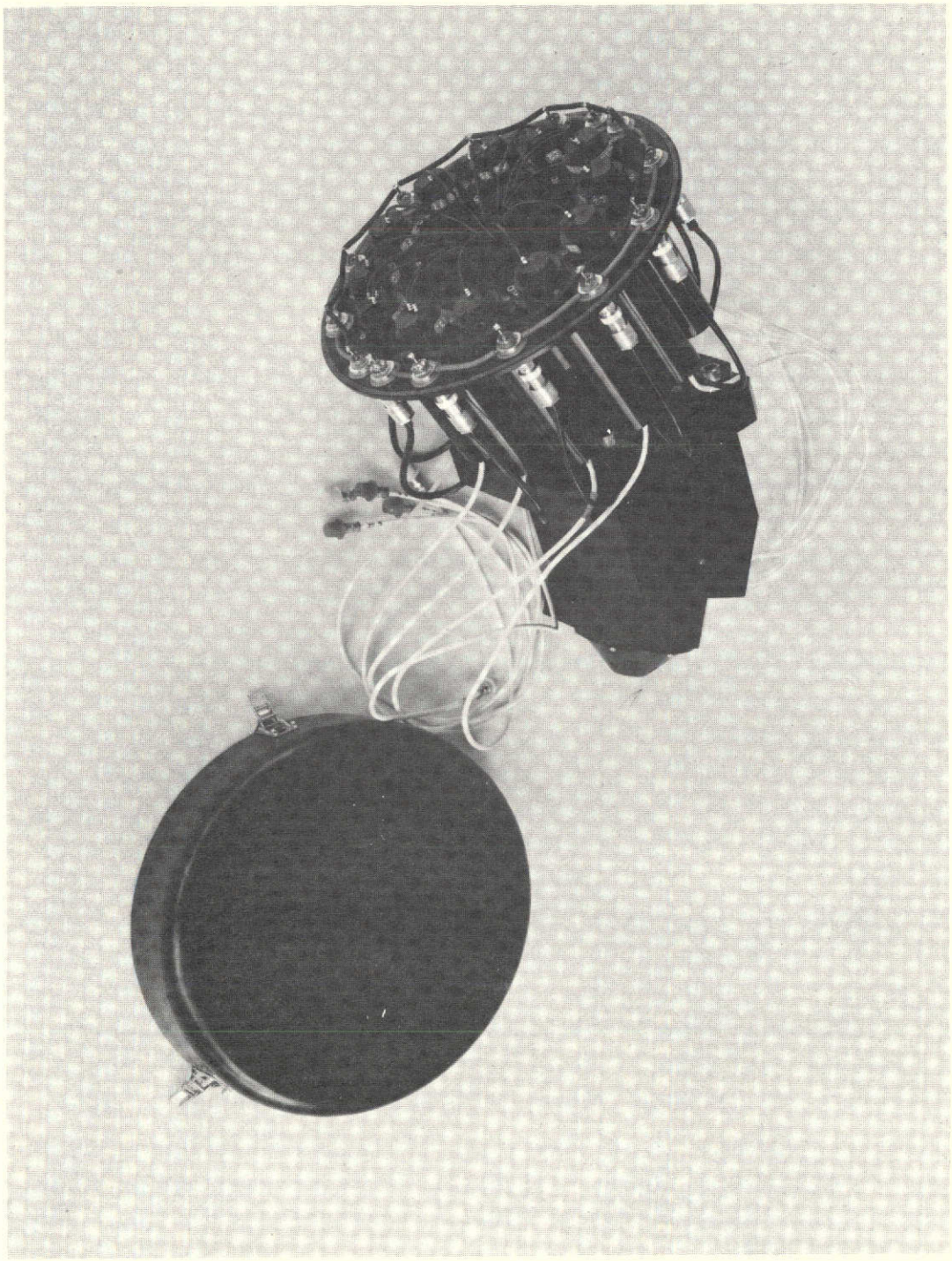

FIGURE 13. SPECTROMETER WITH COVER REMOVED TO SHOW FIBER OPTICS

several photomultipliers. One to six fiber bundles may be grouped at each photomultiplier to establish the wavelength resolution of each channel. Figure 14 plots the normalized response of the respective spectral channels for the current operating mode of the instrument.

Intimately associated with optics of Detector Positions 2 and 3 is a dichroic beamsplitter located immediately behind the telescope's primary mirror. This beamsplitter has a standard Kodak cold mirror coating deposited on one surface of a plane-parallel fused quartz disk. Initially, an IRTRAN 2 substrate had been tried but adherence of the coating to that material was found not sufficiently durable. Transmittance and reflectance properties of this cold mirror (i.e., the dichroic beamsplitter) are shown in Fig. 15.

Several imminent changes are planned with regard to the detectors at Positions 2 and 3: first, reduction of the 3-element detector of Position 2 to a 2-element array, probably through elimination of all or part of the 1.0- to 1.4-μm spectral band; and secondly, extension of the spectral range of the spectrometer at Position 3 to 1.1 μm. These two changes require a basic modification in the dichroic beamsplitter—and in fact a new dichroic which will eventually replace the cold mirror has been procured. The characteristics of this replacement dichroic are shown in Fig. 16. Besides a new reflectance-transmittance cross-over point, this beamsplitter differs in that the substrate is barium fluoride. The newer dichroic appears to offer improved reflectivity near 0.4 μm, and because of the substrate change, its long-wavelength transmission is extended to beyond 11 μm at 90% transmission, with a rolloff to 40% at 14 μm.

4.2 OPTICAL ALIGNMENT

As emphasized in Section 4.1, the optical alignment of a scanner—and particularly the alignment of detectors for this type of scanner—is a critical function. The bulk of the alignment tasks have been dependent upon use of the large collimator shown in Fig. 17. This instrument employs a large paraboloid having a focal length of 100 in. and several folding flats. A variety of illumination sources may be used for inserting radiative signals into the system. The source is inserted through a field-defining aperture located near floor level in the foreground of the figure. It is collimated, projected horizontally, and subsequently folded upward into the collecting aperture of the scanner which rests atop the apparatus. This equipment, along with optical flats, a traveling microscope, and an autocollimating theodolite, were extensively used for in-process assembly and alignment of the M7 scanner optics.

Subsequent to the assembly of the scanner itself, the collimator was used (and continues to be used) for detector alignment. All detectors are provided with integral mounts permitting three-axis orthogonal adjustments. Figure 18 illustrates a typical cooled-detector assembly and its integral mounting fixture. The fixture in turn is positioned on the scanner with two close-tolerance dowel pins. Alignment is accomplished by projecting through the collimator

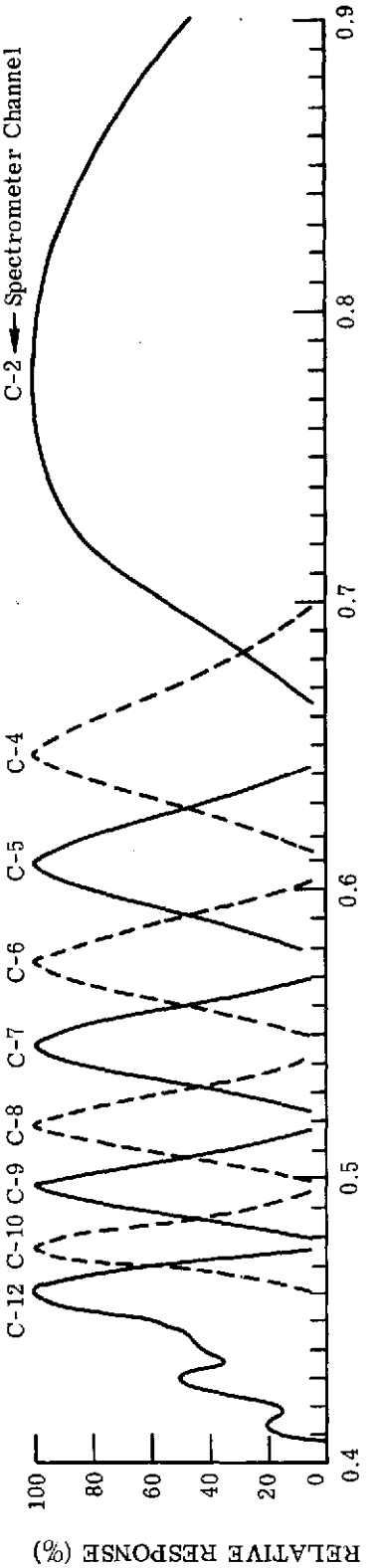

FIGURE 14. SPECTROMETER SPECTRAL SENSITIVITY

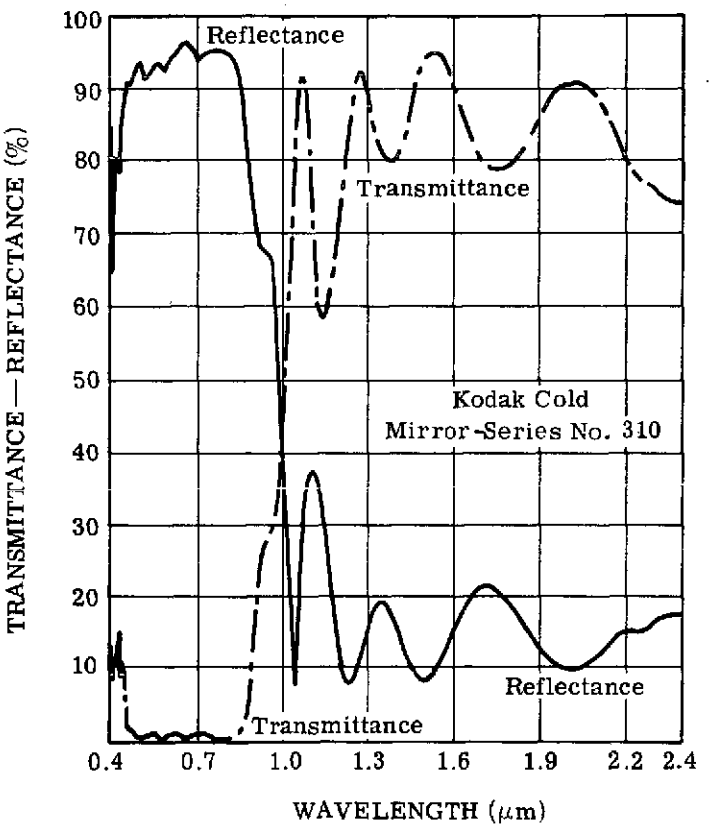

FIGURE 15. DICHROIC COLD MIRROR BEAMSPLITTER RESPONSE

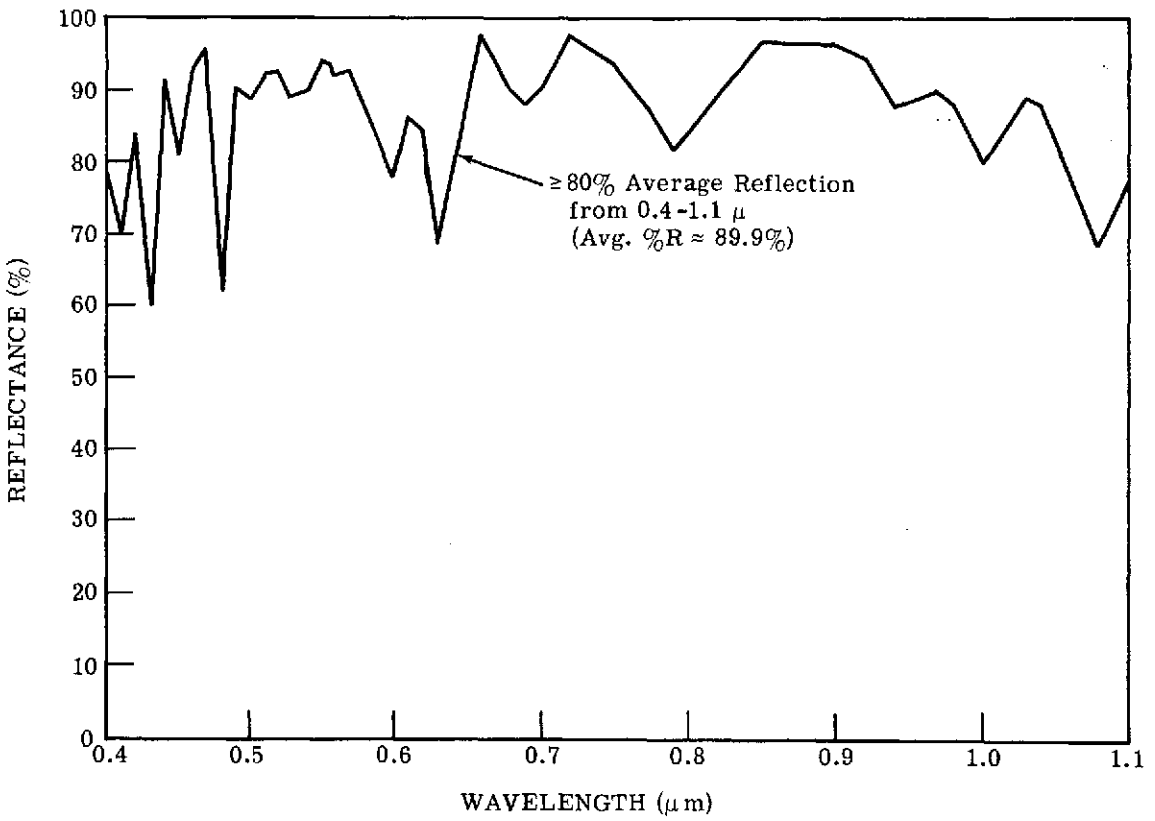

(a) Reflectivity to Detector Position 3

FIGURE 16. REPLACEMENT DICHROIC BEAMSPLITTER

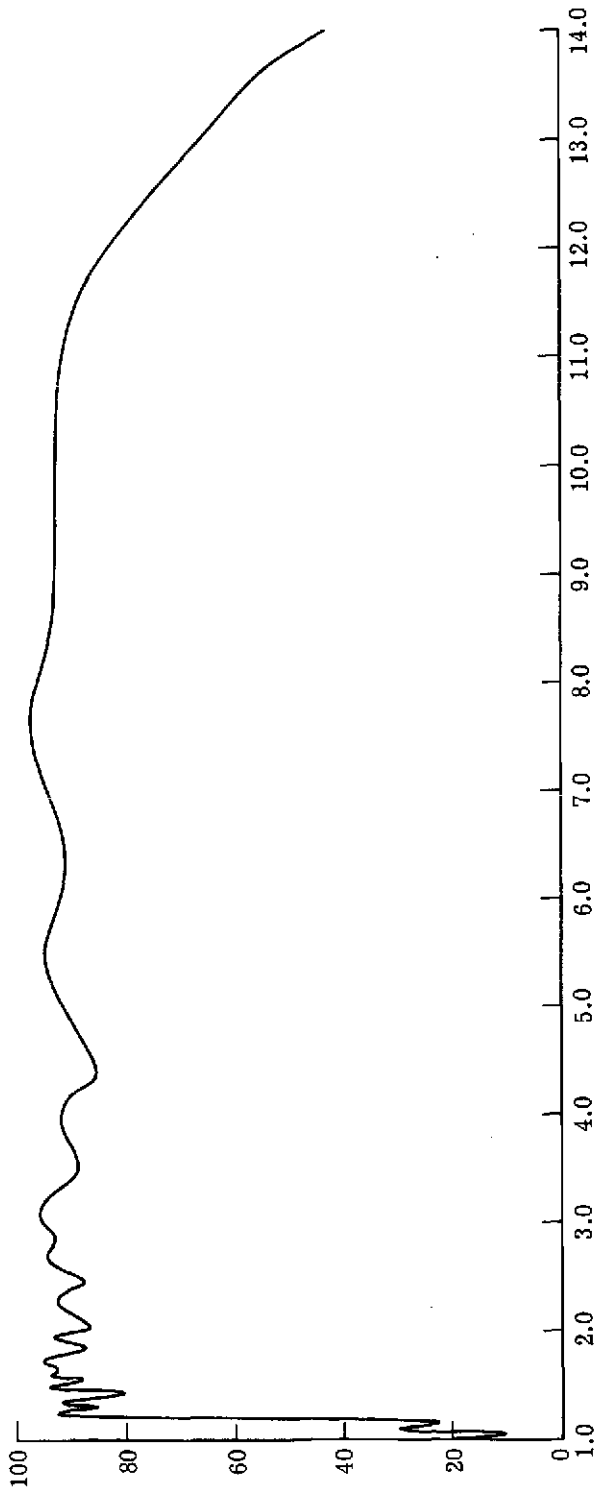

(b) Transmission to Detector Position 2

FIGURE 16. REPLACEMENT DICHROIC BEAMSPLITTER (Concluded)

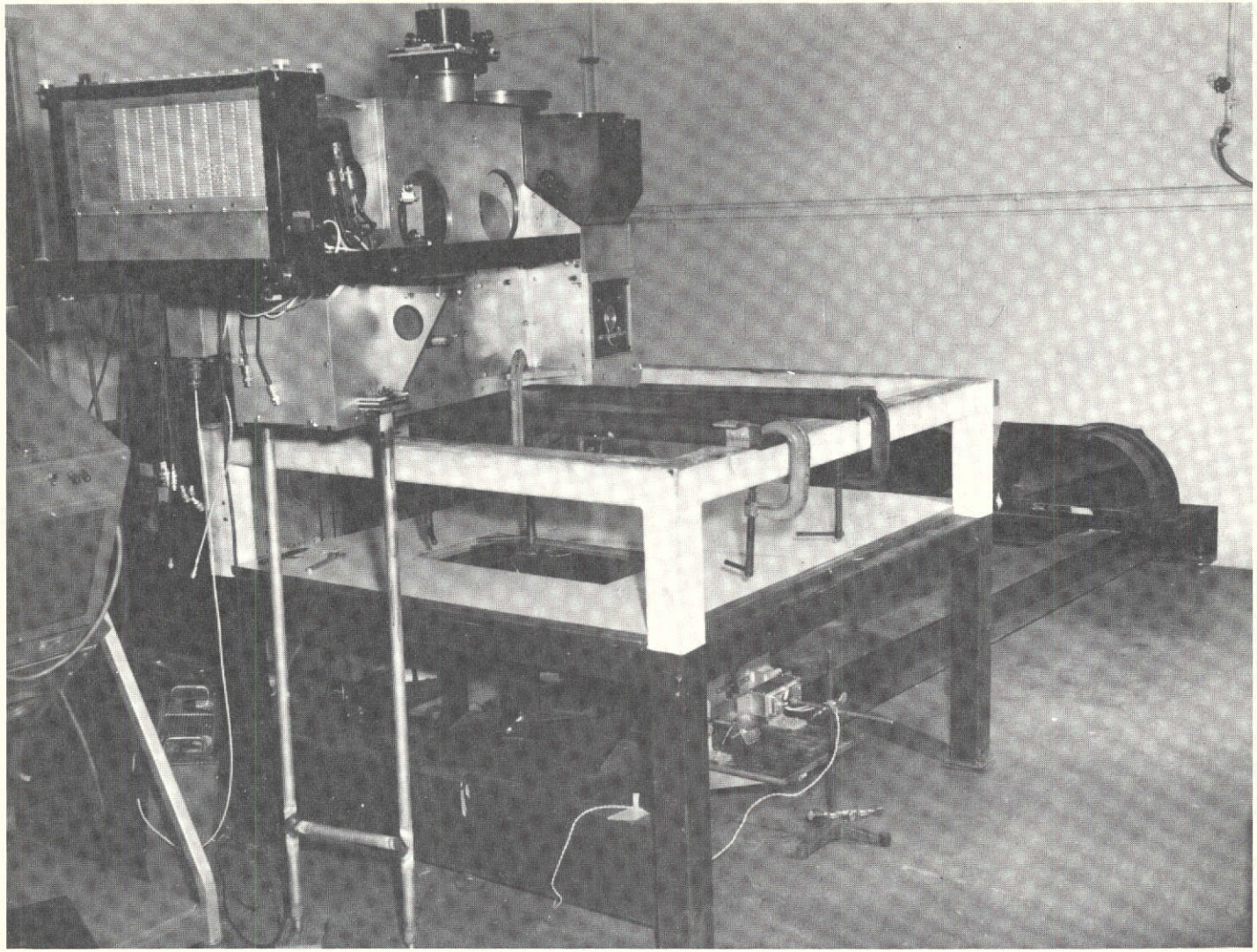

FIGURE 17. ALIGNMENT OF M7 SCANNER OPTICS AND DETECTORS ON LARGE LABORATORY COLLIMATOR

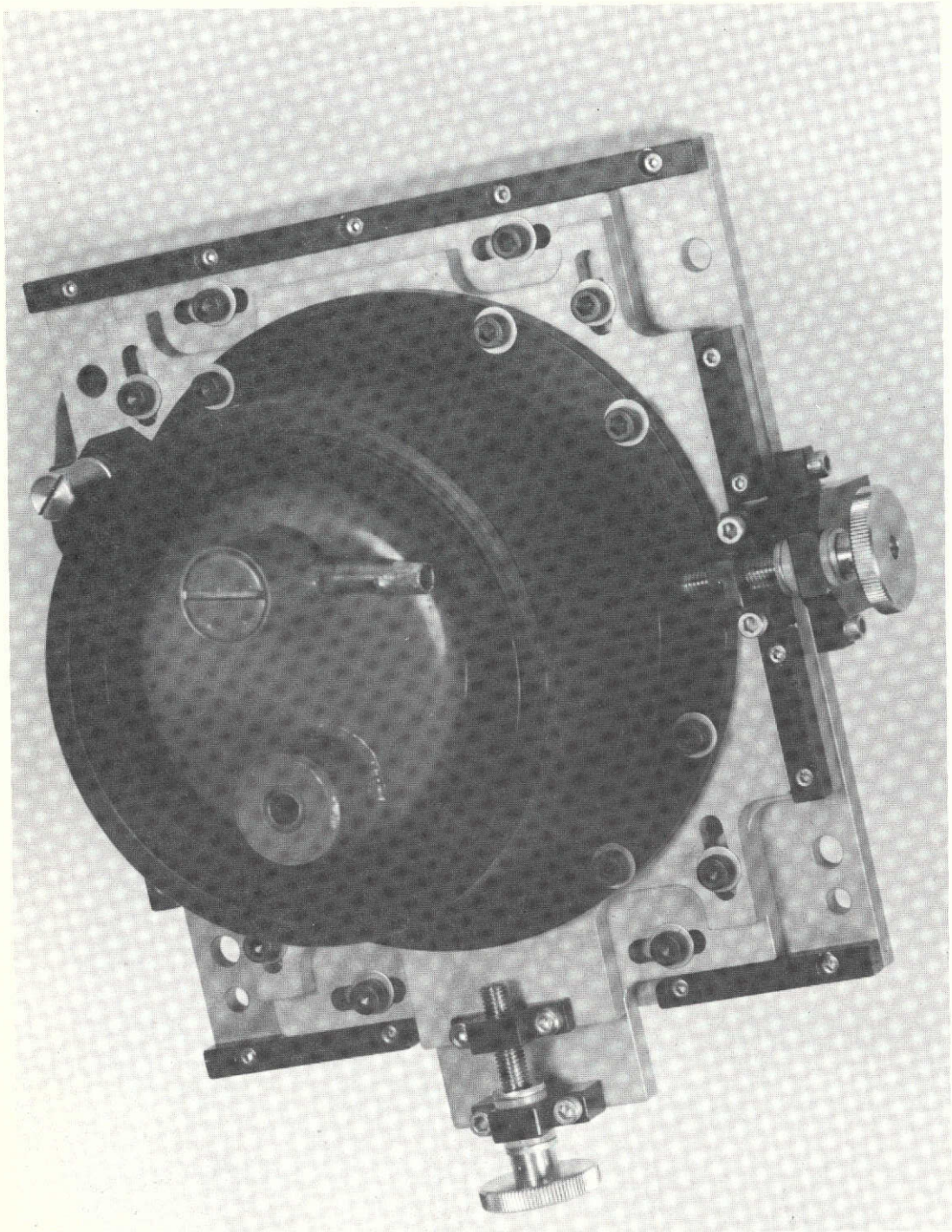

FIGURE 18. COOLED DETECTOR ASSEMBLY AND INTEGRAL POSITIONING FIXTURE

energy from a source apertured to simulate the instantaneous field of view of the detector. By using the orthogonal adjustments, the detector element is brought into coincidence with the target image as optically formed within the scanner. Upon completion of its alignment, the detector is secured with all adjustments locked out. Similarly, the other detectors are then adjusted so that all share a common optical line of sight. Operating procedures are such that the entire inventory of available detectors may thus be pre-aligned. As a result, a variety of detectors are available for configuring the scanner to specific mission requirements prior to flight, and spare detectors are available for rapid substitution should an in-flight failure occur.

The large collimator is also extensively used for both spatial and spectral resolution testing and evaluation of scanner performance. Measurement methods and results are discussed and depicted in Sections 6.2 and 6.3. In the course of this work, a variety of sources have been available for projection through the collimator; these include tungsten-halogen lamps, ultraviolet lamps, tungsten ribbon filament lamps, gaseous discharge lamps, thermal radiation sources, and a Leiss double-pass monochromator.

4.3 RADIATION DETECTORS

Although the M7 Scanner is able to accept a great variety of detectors, the following discussion is largely limited to a description of the general type of detectors currently in use or envisioned for use in the near future. Several highly specialized detectors unique to the ERIM system are, however, described in some detail. The reader is again referred to Table 2, wherein current and near-future detectors are listed.

In recent years mercury-cadmium-telluride (HgCdTe) detectors have improved substantially in spectral coverage and D^* (a measure of signal to noise normalized with respect to bandwidth and detector size). D^* values for HgCdTe now approach those for mercury-doped germanium (Ge:Hg) detectors. As a result, the latter type of detector is not used with the M7 scanner. Reduced cooling requirements ($77^{\circ}K$ for HgCdTe vs. $28^{\circ}K$ for Ge:Hg) are thus realized. Ordinarily a 1/4-mm-square HgCdTe detector is used in the scanner in Detector Position 1A. This detector is filtered to receive energy in the 9.3- to 11.7-μm band. A D^* above 2.0×10^{10} cm $Hz^{1/2}$/watt has resulted in the realization of an NEΔT of $0.1^{\circ}C$.

Indium arsenide (InAs) and indium antimonide (InSb) detectors are used in the reflective infrared spectral region (1.0 to 2.6 μm). Photovoltaic InSb and InAs detectors have been developed to the point where sensitivities approaching the theoretical limit of detection are being realized. The recently realized improvements can be attributed largely to the reduction of background current, which is a fundamental noise source in this type of detector. The background noise has been reduced as a result of spatial filtering (i.e., cooled field-of-view limiting stops) and spec-

tral filtering (i.e., cooled bandpass optical filters). Both spatial and spectral filtering are effective since they reduce the number of incident photons from background radiation.

The InAs and InSb detectors used in the M7 Scanner are, in fact, a specialized breed of this detector manufactured by Barnes Engineering Co. The detector assemblies consist of an integrated linear array of three detector elements. Each element has a restricted field-of-view of 60^{o} (adequate for receiving an incident f/1 cone of radiation) and is covered with a different bandpass filter. In essence then, this type of detector is a real-time, three-color detector system utilized in Detector Position 2. A schematic cross-section of the detector in Fig. 19 shows the spectral filters and the spatial field-of-view stops. In addition, baffles have been placed between detector elements to minimize optical cross-talk from multiple interval reflections. Perpendicular to the plane of the figure, the detector elements are typically 0.020 in. long. The spectral bands purposely chosen to lie within atmospheric transmission windows and which are defined by the bandpass filters are: (1) for the InAs assembly - 1.0 to 1.4 μm, 1.5 to 1.8 μm, and 2.0 to 2.6 μm; and (2) for the InSb assembly - 1.0 to 1.4 μm, 2.0 to 2.6 μm, and 4.5 to 5.5 μm. Unfortunately, the use of glass elements in the lens associated with these detectors precludes use of the 4.5- to 5.5-μm channel in the M7 Scanner. Typically, sensitivities or D^*s better than 2.0×10^{11} cm $Hz^{1/2}$/watt at 1000 Hz are achieved for all three spectral bands of the InAs and InSb detector arrays.

Previously (in Section 4.1) it was mentioned that true spatial registration cannot be achieved at scan angles significantly different from nadir for detector arrays which have side-by-side elements. Recently Honeywell, Inc. has begun manufacturing stacked layers of HgCdTe elements. In such a detector, the first or top element responds to photons up to a cut-off wavelength inherent to that element as manufactured. Beyond this wavelength, the top element transmits photons to the second element. The second element responds to photons it receives, and similarly may transmit longer wavelength energy to still a third detector if the stack should include three layers. The technique is illustrated in Fig. 20. To date, ERIM has used this type of detector solely in the thermal infrared. Both a two-element detector (bandpasses of 8.0 to 10.9 μm and 9.4 to 12.1 μm) and a three-element detector (bandpasses of 8.0 to 9.1 μm, 8.7 to 10.7 μm, and 9.9 to 14.0 μm) have been utilized. Unfortunately, in order to achieve acceptable sensitivity, the sizes of the individual elements of these layered detectors have had to be inordinately large. As a result, spatial resolution for those wavebands is degraded (i.e., the instantaneous field-of-view becomes large).

Recent developments by the manufacturer have shown that the constituent mixing ratios of a HgCdTe detector can be varied so that a D^* is achieved which is similar to that of indium arsenide or indium antimonide. Accordingly, ERIM is now procuring a two-element layered detector which will replace the three-element InAs and InSb linear arrays and avoid the aforementioned spatial registration problems. We anticipate that the elemental size of this new

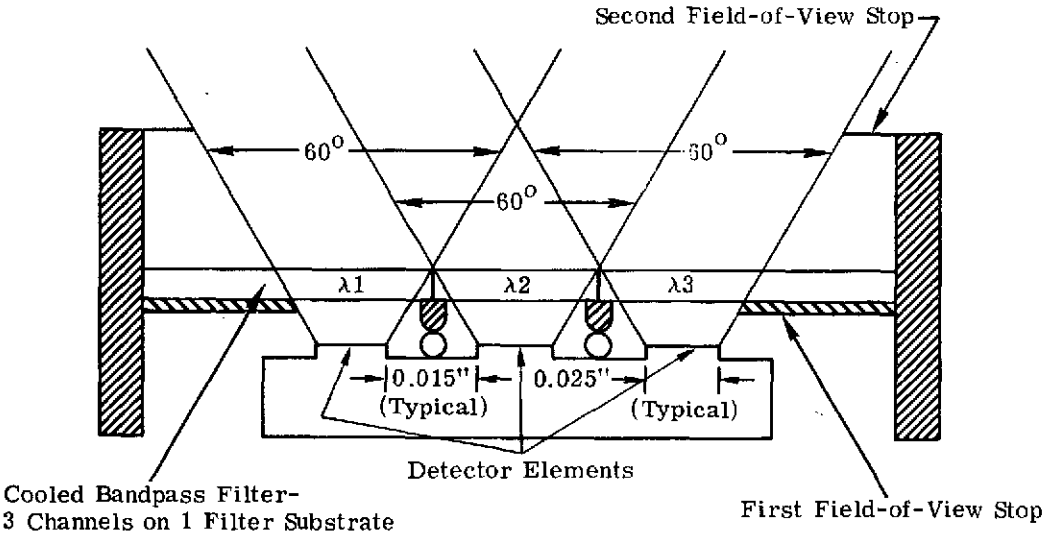

FIGURE 19. REAL-TIME, THREE-COLOR DETECTOR WITH COLD FILTERING

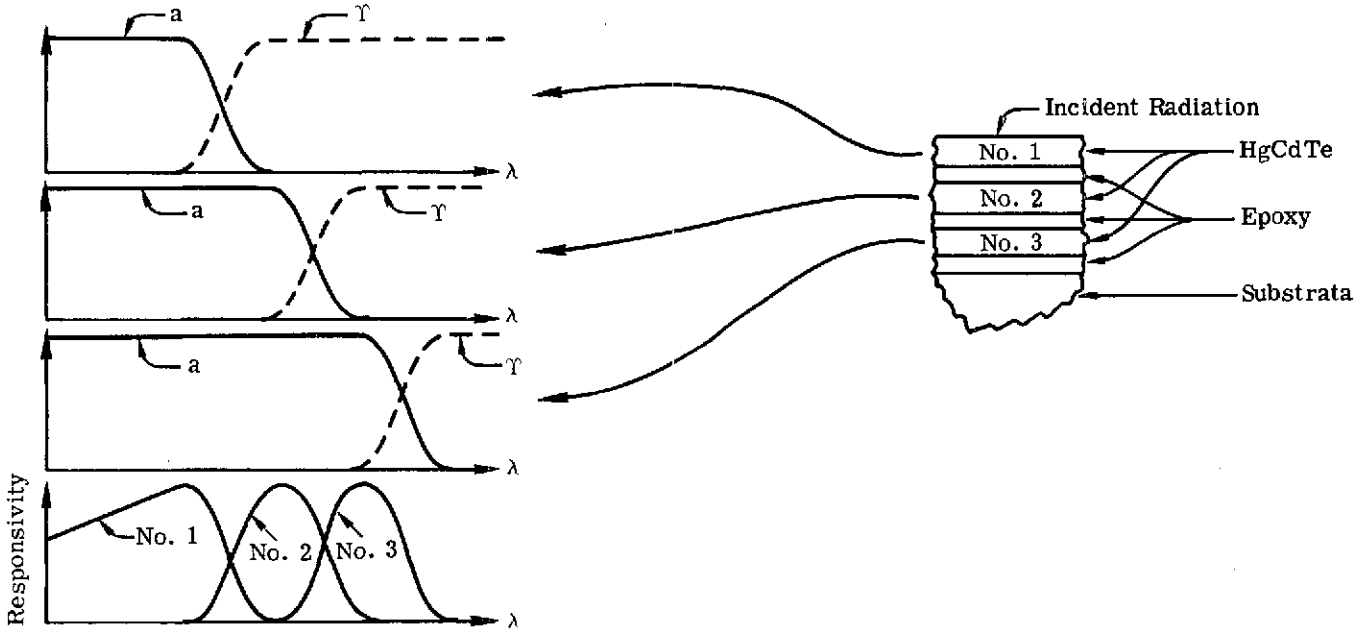

FIGURE 20. HgCdTe SANDWICH DETECTOR

stacked array will not be inordinately large. In fact, a slight improvement in spatial resolution is expected. The responsivities of the two elements are to be peaked in the 1.0- to 1.8-μm and the 2.0- to 2.6-μm bands, respectively. It is expected that the former band will normally be limited to operation in the 1.5- to 1.8-μm region by use of a cut-on filter and that the spectral range of the spectrometer (Detector Position 3) will be extended to 1.1 μm to partly offset the absence of a 1.0- to 1.4-μm band.

Detectors of the HgCdTe, InAs, and InSb varieties all require cooling to liquid nitrogen temperatures. Automated open or closed-cycle transfer systems and mechanical refrigerators can be deplorably unreliable, inefficient, and in some cases microphonic. Therefore, ERIM—with ready access to its equipment—prefers to use liquid nitrogen in a simple bulk, direct-pour fashion. This method is quite reliable, expeditious, and economical. Dewars manufactured by Cryogenic Associates are used in conjunction with all cooled detectors. The dewars have a liquid capacity of 0.22 liter and a hold time of 5 to 8 hours. In addition, the dewars are internally accessible so that detector elements may be repaired or replaced when necessary.

To date, all uncooled detectors utilized with the M7 system have been photomultiplier tubes having either an S-20 or S-1 response, depending upon the sensed spectral waveband. For the sake of interchangeability, two tube types—each manufactured by RCA—have been standardized upon. Both types have integral voltage dividers and magnetic shields, and both are identical in physical dimensions. These tubes are used with the spectrometer at Detector Position 3 as well as with the one in Position 1B. Studies currently underway may lead to the eventual use at the near-IR wavelengths of silicon photodiodes in lieu of photomultipliers.

4.4 REFERENCE SOURCES

The M7 Scanner incorporates five ports through which a variety of calibration references may be introduced. All five ports are in line with the scan mirror, so that each source is seen and registered sequentially once for each and every scan line. Calibration sources have thus far consisted of three blackbody plates, a lamp reference, and a sky illumination reference. Generally the references can be thought of as reflected (solar) radiation sources or as self-emitted (thermal) radiation sources. Figure 21 shows schematically the arrangement of the calibration sources, while Fig. 22 is a functional block diagram of the controls for the sources.

The reflected radiation range of the optical spectrum may be defined as that spectral range in which the dominant radiant energy from a scene is reflected sunlight. During daylight hours, radiation is predominantly reflected in the spectral range from 0.3 to 3.0 μm. Within this range, the lamp reference and the sky illumination reference are principally utilized. In the case of the lamp reference, a conscious effort has been made to match the spectral characteristics of this source with the spectral characteristics of the sun. The sun's spectral energy as

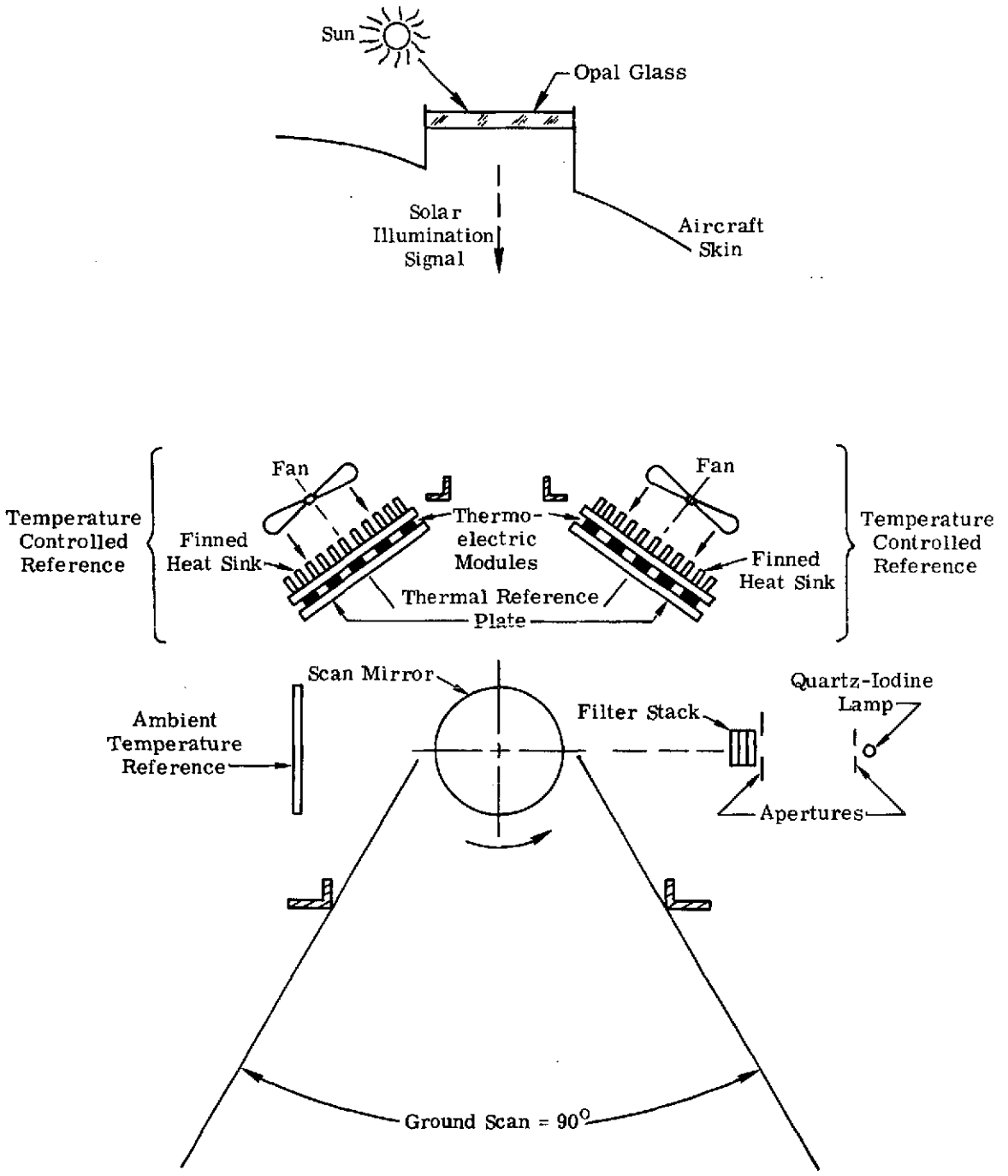

FIGURE 21. CONFIGURATION OF REFERENCE SOURCES

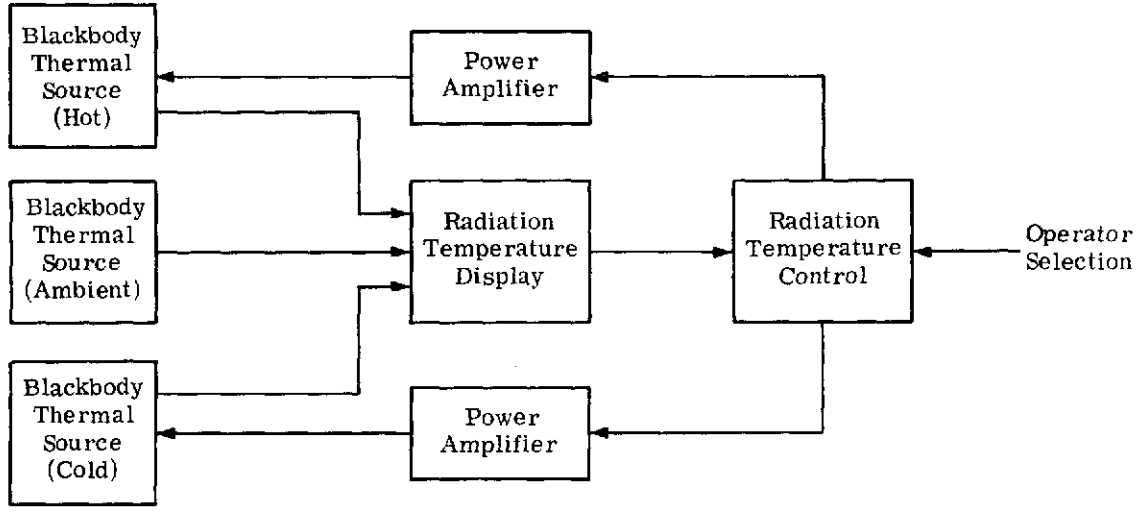

(a) Radiation Reference for 8.0 to 14.0 μm Wavelengths

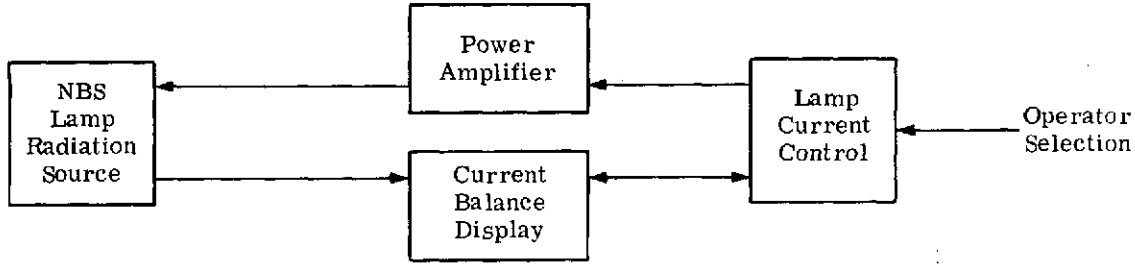

(b) Radiation Reference for 0.4 to 2.6 μm Wavelengths

FIGURE 22. RADIATION SOURCE REFERENCE CONTROLS

viewed through the atmosphere is approximately that of a 5800°K graybody with some attenuation in the 0.4- to 0.5-μm region and more in the 0.3- to 0.4-μm region. The lamp reference source consists of a 100-watt, tungsten-filament, quartz-iodine lamp shining through a series of optical filters and two apertures or stops, thence onto the rotating scan mirror. The lamp itself has a color temperature of 2950°K at a maximum current of 6.6 amps. The optical filters shape the lamp's spectral output toward an approximation of incident solar radiation. Figure 23 shows the approximate spectral geometry of the sun and of the quartz-iodine lamp at its maximum rated current. Figure 24 shows the transmission characteristics of the composite of three filters used to modify the lamp's spectral output (i.e., to reduce its near-infrared output relative to its visible output). In practice, lamp current is varied over a 4- to 6-amp range in order to obtain, in the scanner's reflective spectral channels, a lamp signal level approximating the average signal levels received from the ground in this spectral range. Thus, depending upon the operating current supplied, the spectral curve may be shifted somewhat from that shown in Fig. 24.

The apertures or stops used with the lamp ensure (1) that light from the lamp filament rather than from its quartz envelope is fed into the scanner, and (2) that the lamp signal is sharpened so that only a narrow pulse is seen by the scanner. Shaping is such that the scanner sees the lamp for a peak pulse width lasting for 3.6° of scanner rotation. Once set, lamp current is maintained to a constancy within ±0.02 amp by a servo feedback loop. As an additional means of obtaining a reflected region calibration reference, the blackened surfaces of the thermal calibration plates serve as dark-level (zero-radiation) references.

The sky reference port, located opposite to or 180° from nominal scanner nadir, extends through the roof of the aircraft to a flashed-opal glass diffusing plate. Direct solar and diffuse sky radiation illuminate this plate, which in turn is viewed by the scanner once each revolution for approximately 1° of scan. This arrangement affords an approximate means of comparing the illuminating radiation with reflected radiation seen by the scanner when it is viewing the ground. This comparison is a measure of ground target reflectance, which in the solar-reflected spectral range is considered the target signature. The term "approximate" applies because the diffusing plate is not at ground level (i.e., an atmospheric path at lease twice the altitude of the aircraft affects the comparison), and the opal glass plate is neither a perfect Lambertian receiver nor transmitter. In addition, the glass plate is not transparent below 0.4 μm, and studies have shown that the flashed opal is poor diffusion material beyond about 1.0 μm. A design is currently being developed to replace the opal glass plate with a refractive-type diffusing material permitting separation of direct solar radiation and diffuse sky radiation. The change is expected to be implemented during 1973.

In the solar reflective regions, the spectral signature of a target results wholly from surface reflectance characteristics. Hence, lamp and sky illumination sources must be considered

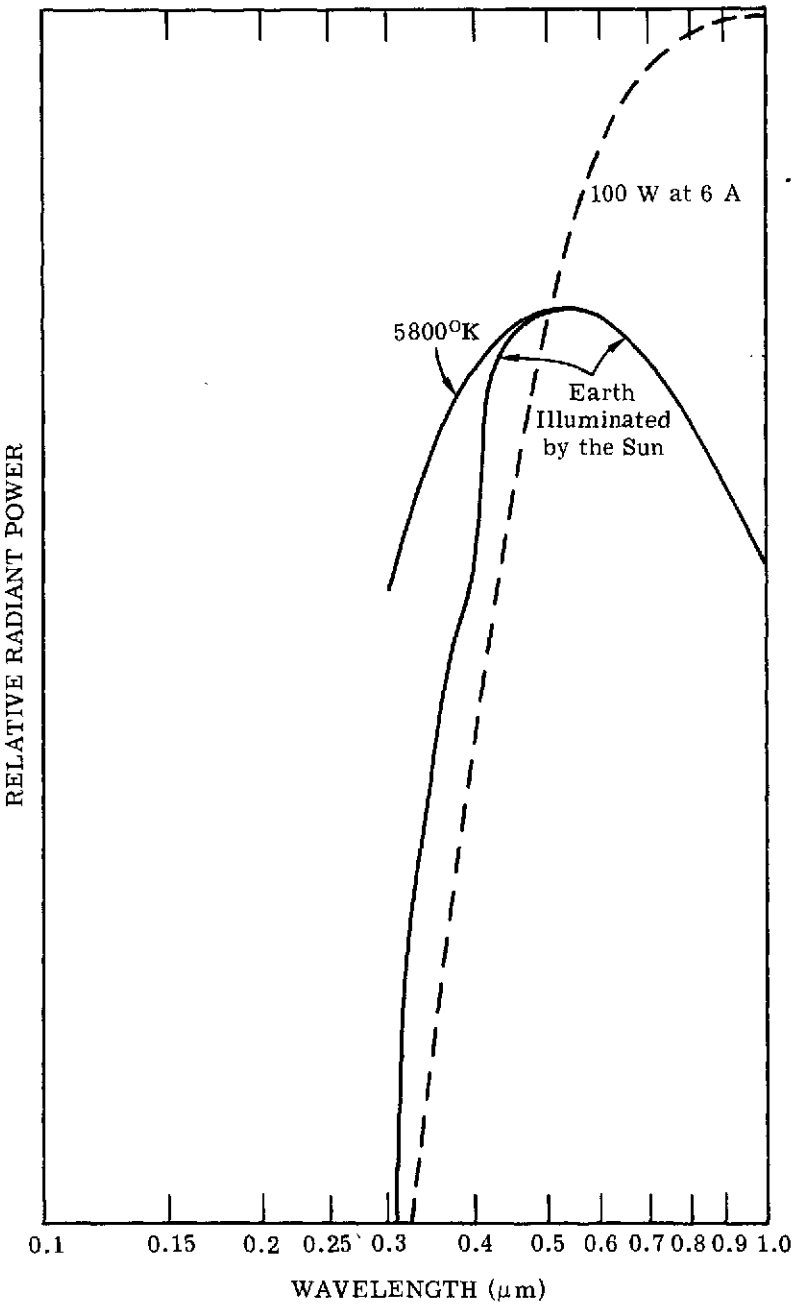

FIGURE 23. APPROXIMATE RELATIVE SPECTRAL CHARACTERISTICS OF SUN AND 100-WATT QUARTZ-IODINE LAMP

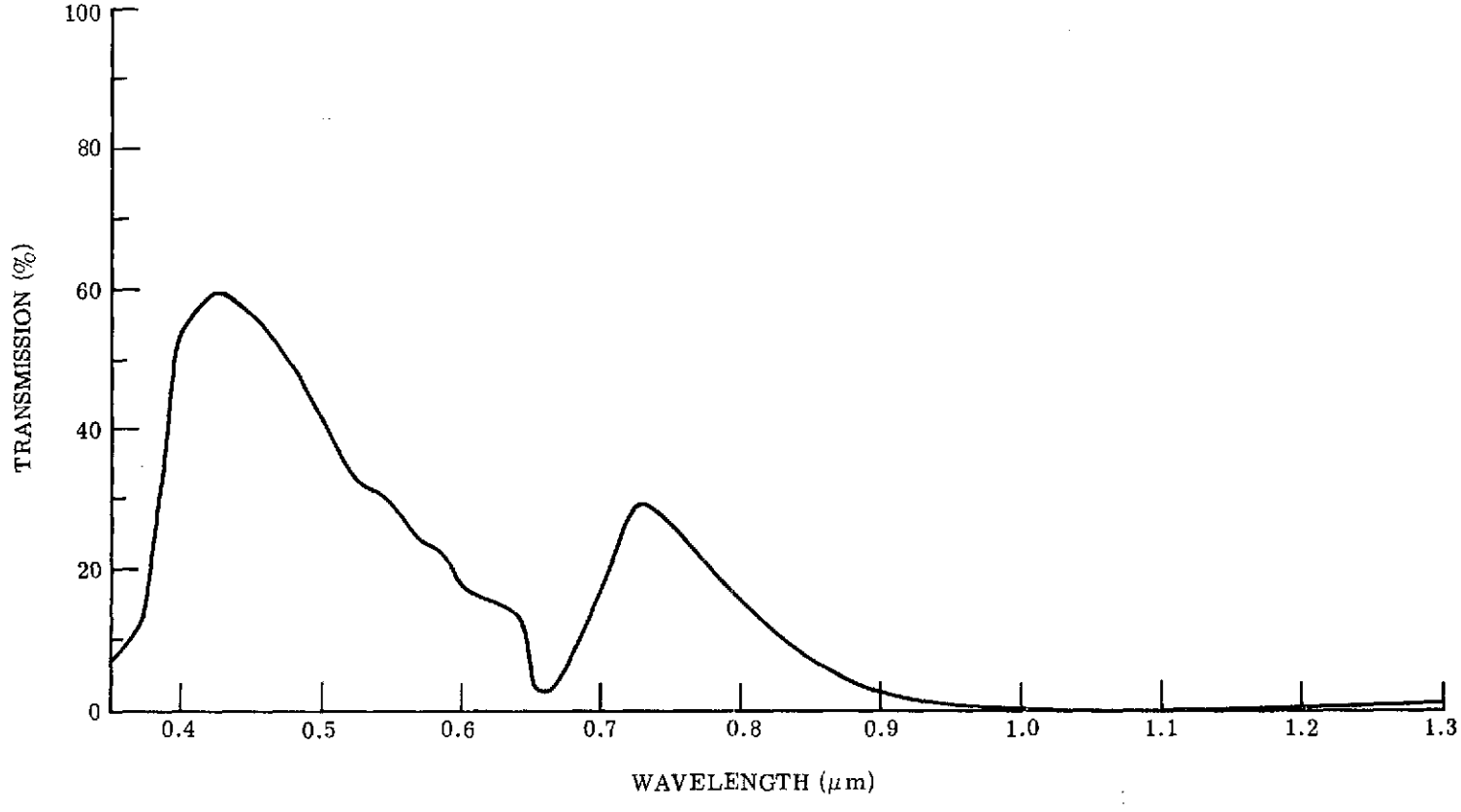

FIGURE 24. COMPOSITE LAMP REFERENCE FILTER CURVE

as secondary calibration references. However, a ground reflectance panel of known characteristics placed in the target scene could be (and has been) used as a primary calibration source. So because the reference lamp and opal glass sources serve to relate this primary calibration to actual targets, they are considered transfer or secondary calibration sources. Since the lamp does not fill the scanner's aperture, it does not fully exercise the transfer function of the scanner's total optical system. For this reason, lamps employed as references require careful evaluation.

One way to assess the transfer characteristic of the lamp reference is to use ground-based reflectance panels in the manner suggested above. As an alternative, a laboratory method is also periodically employed; illustrated in Fig. 25, it entails the use of two 200-watt, traceable to NBS, quartz-iodine lamps and a sheet of flame-sprayed aluminum for which the diffusion characteristics have been verified. This calibration technique and some test results are further described in Section 6.

In the infrared beyond 4.5 μm, target radiation is primarily thermal emission. Since the radiation from the three blackbody plates is determined directly by applying Planck's radiation law to the measured temperatures of the plates, these plates may be considered primary calibration sources. Two of the plates are temperature-controlled and the third is allowed to remain at ambient. The two controllable plates are usually set to temperatures that bracket temperatures in the ground scene.

Maintenance of the plates at these predetermined temperatures is accomplished through the use of thermoelectric modules or heat pumps tightly sandwiched between dual plates. The front plate of the sandwich is copper with a blackened surface which is, in fact, the reference surface. It is either heated or cooled, depending upon the direction of current flow through the thermoelectric modules. The rear plate is a finned assembly; it is coupled to ambient air by a fan that directs air upon the fins. The temperature of each plate is held constant by a closed-loop servo with a thermistor embedded in the plate as a sensor. The maximum heating or cooling rate of a plate is $0.2^{\circ}C$/sec. Once stabilized, it is controlled to within $\pm 0.1^{\circ}C$. Both plates are calibrated to operate over a 0° to $52^{\circ}C$ range.

In designing the thermal reference plates, the possibility of using deeply grooved plates to achieve a higher surface emissivity was considered. Prudence ruled against doing so for two practical reasons: the difficulty of machining sharp accurate grooves in the soft copper, and the difficulty of making the still-necessary emissivity correction for this more complex surface. Instead, it was decided to leave the plates flat while coating them with a thin layer of flat black paint of known spectral emissivity. Hence, retrieval of data from these so-called "blackbody" plates is a straightforward procedure.

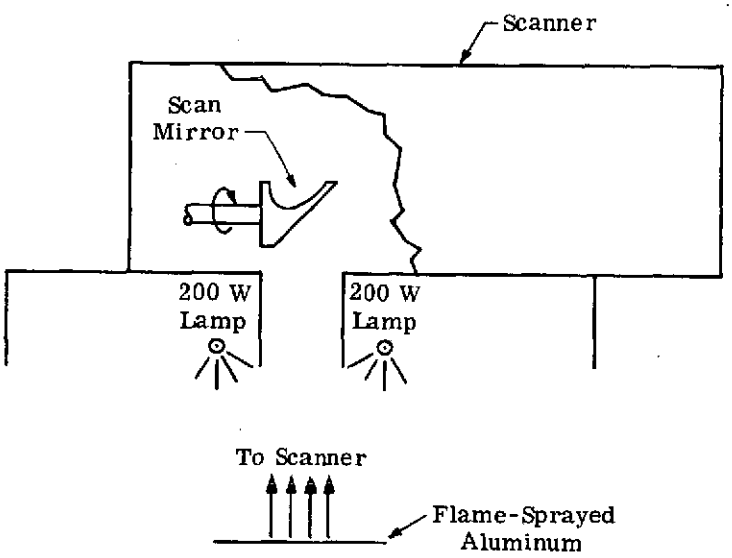

FIGURE 25. TECHNIQUE FOR DETERMINING LAMP REFERENCE TRANSFER FUNCTION

4.5 VIDEO AMPLIFICATION

The approach used in video amplification was to amplify linearly the low-level output of the radiation detector as close to the detector as possible, and to optimize the impedance match of the detector and associated amplifier string to realize optimal detector response.

For the cooled infrared detectors this was accomplished by building custom preamplifiers, each containing a current amplifier impedance-matching stage mounted on the dewar within an inch of the detector flake. The output of this stage couples to a specially compensated preamplifier which also provides detector bias. The impedance-matching current amplifier is an integral part of each infrared detector assembly.

The preamplifier package, mounted within 1 ft of the detector assembly, contains a plug-in preamplifier card compensated for a particular detector. The output of each preamplifier goes to an array of twelve operational amplifiers also located in the scanner assembly. Since the preamplifier function is accomplished within the photomultiplier tube, outputs of the photomultiplier detectors are connected directly into the operational amplifier array.

As shown in Fig. 26, as many as nineteen different spectral bands of video information can be generated in the M7 scanner, but only twelve can be transmitted beyond the scanner because of the limited number of video amplifiers and magnetic tape channels. The selected twelve channels are sent through coaxial cables to the operator console located about 10 ft from the scanner assembly. At the console assembly, each video channel passes through two more operational amplifier stages before being displayed and recorded. Referring to the video display at the console, the operator selects the appropriate gain in the operational amplifier chain to present a 0- to 3-volt signal for display and recording.

The nominal bandwidth of the video amplifier chain is dc to 300 kHz. The actual bandwidth is a function of the amount of gain selected and the compensation required in the detector output. Often the low-frequency drift from a cooled detector is so great that ac coupling must be employed to reduce the noise. The signal is dc-restored in processing by reference to a constant radiation source which appears in the video signal. Because the coupling is made to a fraction of a Hertz, the droop between periods of restoration is less than 1%.

The fundamental signal bandwidth required to transmit the scanner signals varies from 9.4 kHz to 157 kHz, depending on the size of the radiation detector used and the scan rate. The radiation detectors currently in use have an instantaneous field of view ranging from 30 mrad to 2 mrad. The scan rate can be either 60 scans/sec or 100 scans/sec. The most common configuration is a scan rate of 60 scans/sec with nominal instantaneous field of view of 3.3 mrad. This requires a signal bandwidth in the system of dc to 57 kHz.

In addition to amplification, the video amplifiers also perform clipping to prevent signals exceeding +3.5 volts from entering the tape recording system; such clipping is necessary

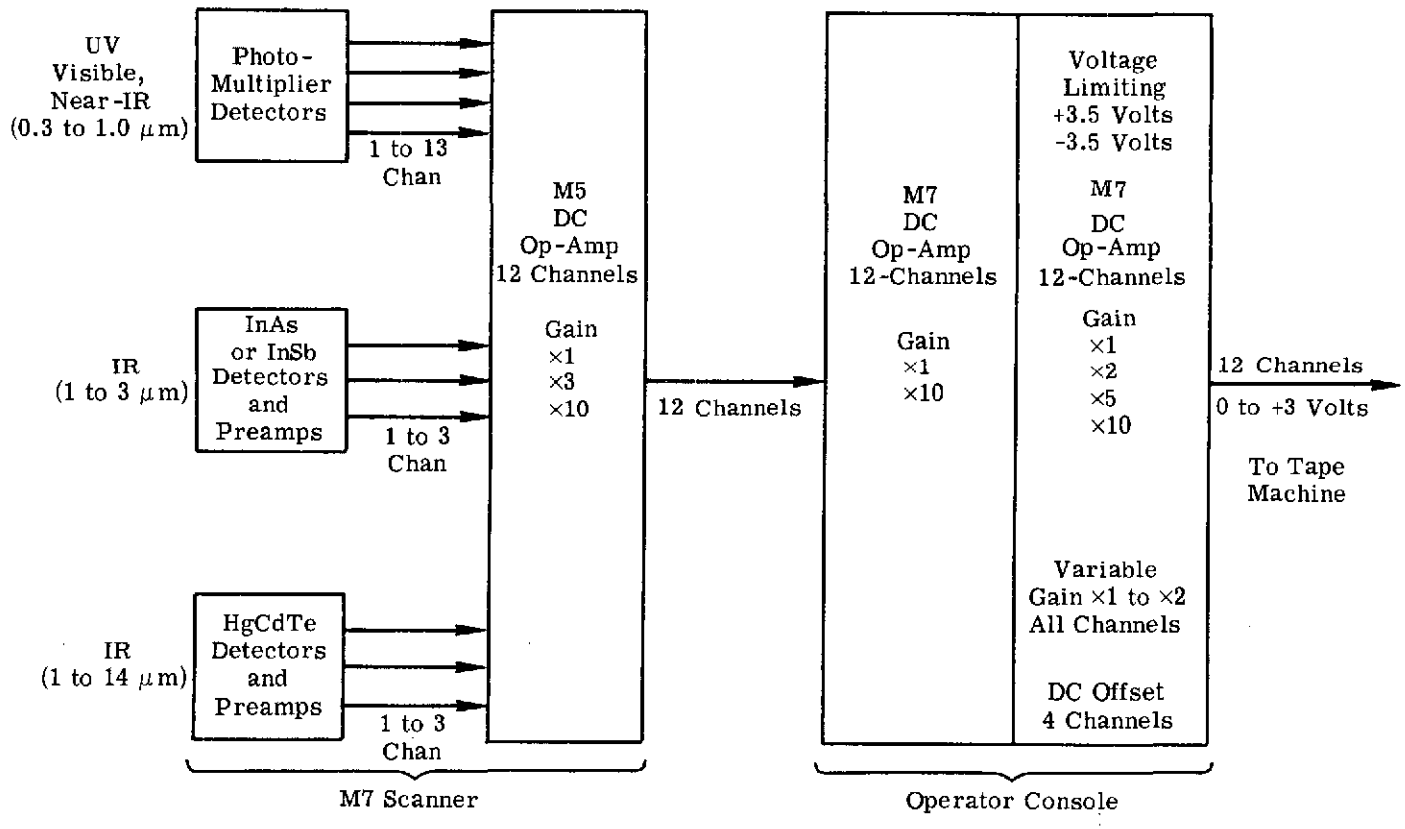

FIGURE 26. VIDEO AMPLIFIERS — BLOCK DIAGRAM

because the FM modulators in the recording system become nonlinear when overdriven. Four of the twelve video amplifier chains also have provision for dc offset of the detector signal so that the recorded 0 to 3 volts can be shifted to represent the signal variation of interest rather than the total signal variation. This offset provision is particularly necessary for the thermal infrared signals.

In summary, the video amplifier chain is customized at the input end to match individual detector characteristics. Then, beyond these linear preamps, all channels include three stages of linear amplification by standard operational amplifiers. The first such stage provides a gain selection of 1, 3, or 10; the second stage, 1 or 10; and the third stage, 1, 2, 5, 10, and variable 1 to 2. The third stage also provides clipping and offset. This video amplifier configuration was established after the first year of M7 system operation. Two interim video amplifier configurations are described in Appendix A.

4.6 VIDEO DISPLAY AND RECORDING

The video display and recording functions are illustrated in block diagram form in Fig. 27. The operator display and its associated controls consist of a 4-channel Tektronix oscilloscope and a video selector panel. The operator selects video signals for viewing in groups of three along with the scanner sync signal; these video signals can be either inputs to the magnetic tape machine or signals reproduced from the tape. The video signals are displayed with signal amplitude as the vertical CRT deflection, and time or scan angle as the horizontal deflection. The display is calibrated vertically in volts and horizontally in time.

The analog magnetic tape system is a Mincom PC-500 tape machine with fourteen Data Control Systems frequency modulation units and four FM demodulation units. This 14-track machine can direct-record signals over a bandwidth of 400 Hz to 1.5 MHz. The machine has staggered heads and uses 1-in. tape at tape speeds up to 120 ips. At a tape speed of 60 ips, 12 minutes of recording time is available on 3600-ft, 10-in. diameter reels. The machine can accept 14-in. reels. Scotch type 871 magnetic tape is used.

The FM units are adjusted to accept 0 to +3 volts with a center frequency of 216 kHz. The deviation is set for a nonstandard ±30% to provide a nominal dc to 100 kHz bandwidth with some sacrifice in signal-to-noise performance. The polarity is such that 0 volts is represented at 281 kHz and +3 volts at 151 kHz. Zero volts represents cold or dark radiation signals, and +3 volts represents hot or bright signals.

Although the tape machine and associated FM units are capable of recording dc to 500 kHz signals upon proper selection of FM center frequency and maximum tape speed, they are operated as described for compatibility with laboratory data reproduction and processing equipments. Until this system was fielded, previous multispectral data were recorded on an Ampex FR-1300

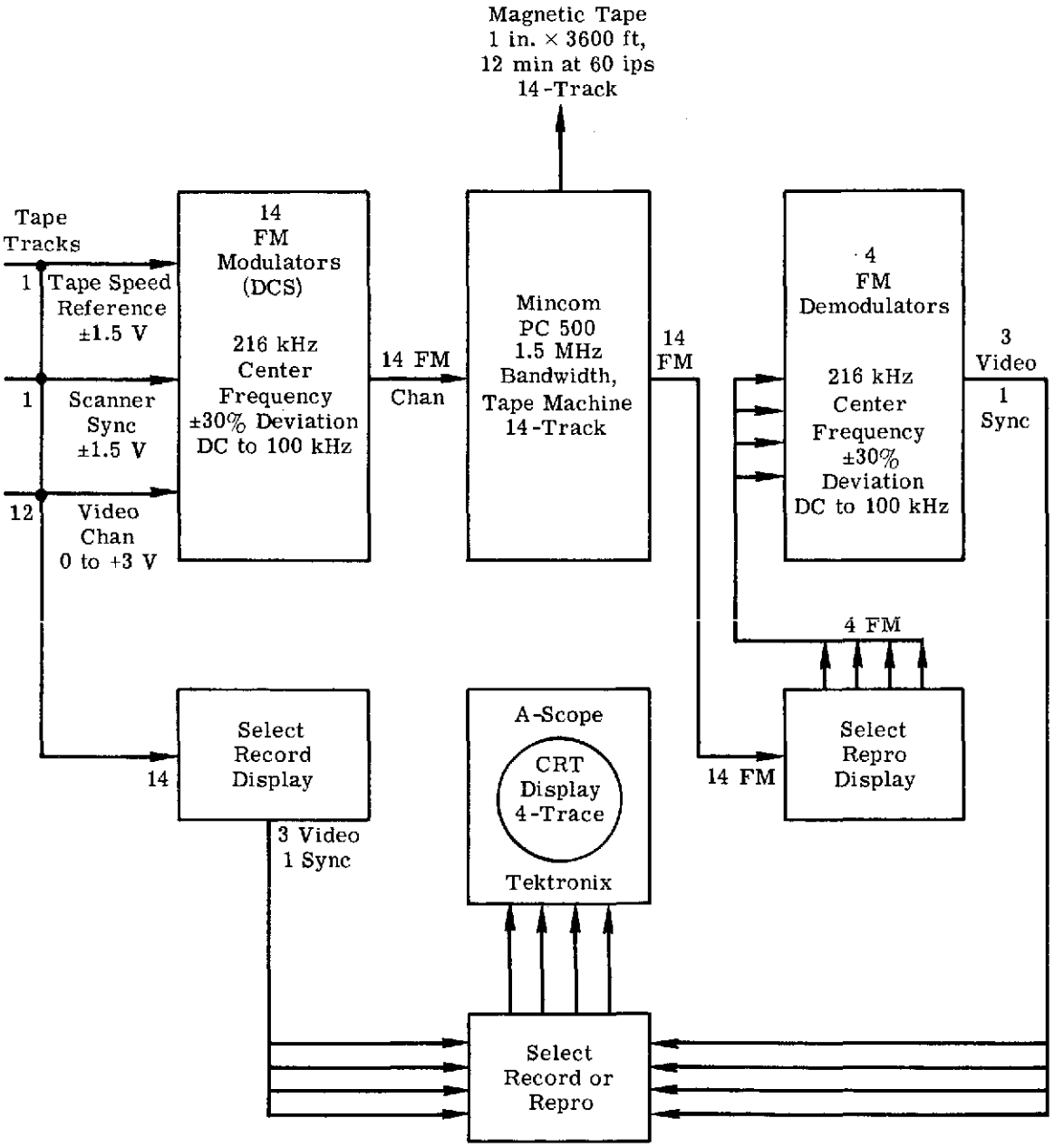

FIGURE 27. VIDEO RECORDING AND DISPLAY — BLOCK DIAGRAM

machine rated as having a maximum capability of recording at 108 kHz FM center frequency at a maximum tape speed of 60 ips. Further, most of our analog processing equipment was designed with a dc- to 100-kHz bandwidth. Tapes recorded on the PC-500 at 60 ips can be reproduced on Ampex FR-1300 machines at 30 ips, so—in real-time processing—the maximum recorded bandwidth of scanner data does not exceed the bandwidth of the analog processing equipment. Nevertheless, if the full information rate of the scanner is to be realized, wider bandwidth recording and processing of the data will be eventually required. Given current recording and processing practices, there is obviously no need for scanner spatial resolution smaller than 3 mrad even at the slowest rate of 60 scans/sec. But when the ground station becomes capable of accepting the data, the M7 airborne system does have the capability of being upgraded to its full performance of 2 mrad spatial resolution at 100 scans/sec.

4.7 ELECTRONIC REFERENCE SIGNALS

The electronic reference signals consist of the following:

(1) A marker pulse which registers the position of the instantaneous scan FOV relative to the scanner housing at one instant in time during each scan.

(2) A marker pulse which registers, once each scan, the nadir or center of the ground scan stabilized for scanner housing angular motion in the scan plane. Because for vertical scanning, aircraft roll motion would be in the scan plane, this pulse is roll-stabilized.

(3) A binary code count of line scans from a selected reference point such as the beginning of a run.

(4) A mix of reference frequencies from a precision oscillator for use in tape speed control during data reproduction.

The first three reference signals listed above are mixed in a common data channel for recording on tape; in reproduction they are discriminated by either polarity or amplitude. The two marker pulses are both of 1.5 volts amplitude but have opposite polarities; spacing is close, with the unstabilized pulse appearing first. The line count binary code is a series of square-wave pulses of 0.75 volt amplitude synchronized to follow the pair of marker pulses for each line scan. The line count code is completed before the beginning of the next scan.

The fourth reference signal cited above may change from time to time as data reproduction requirements vary. It is usually a mix of selected precision sinewave oscillator signals for use in tape speed control. At times, however, it has been a recording of 60 Hz and 120 Hz square wave signals. Essentially, its reference track is reserved to record whatever reference signal is required for data reproduction. The 3-volt p-p signal can be recorded either direct for high-frequency signals, or frequency modulated for dc and low frequencies.

4.8 AERIAL CAMERA CONTROLS

The aerial camera control panel consists of a power switch for activating the camera controls, intervalometers for selecting the firing interval for each camera, and a frame counter for each camera. The camera control panel is mounted adjacent to the scanner operator's console within easy reach of either the scanner operator or a camera operator.

Three types of intervalometers are used to trigger the cameras. The CP3 type produces intervals of less than 6 sec and is used primarily with the 70mm cameras equipped with lenses of 3-in. focal length. The modified B3B type produces intervals in excess of 2 sec and is used with 70mm cameras equipped with 38mm lens. The standard B3B type also produces intervals in excess of 2 sec and is used with the 9.5-inch camera equipped with a 6-in. lens. The 70mm cameras require a trigger pulse of 110 msec duration, whereas the 9.5-in. camera takes a 250-msec duration pulse.

The cable junction box and the aerial camera assemblies are located in the left instrument well of the aircraft.

5
DATA RETRIEVAL

Previous sections have described the data produced by the M7 multispectral scanner system and some of the things that can be done with such data. This section describes the retrieval of scanner data from the analog tapes and shows examples of what scanner imagery looks like when reproduced on film.

5.1 TAPE-RECORDED DATA FORMAT

The scanner data is recorded in analog form on a 14-track magnetic tape machine. The machine uses 1-in. Scotch type 871 tape (or its equivalent) on 10-in. reels. The tape machine also accepts 14-in. reels. The twelve scanner video and two reference signals are recorded at 60 ips via FM electronics which, through special filtering in reproduction, provide an electronic bandwidth of dc to 100 kHz. This full bandwidth is reproduced on film but in multispectral processing is degraded to either 80 kHz or 40 kHz. The FM electronics are set for ±30% deviation about a center frequency of 216 kHz to record an input signal of 0 to 3 volts. In record mode, however, the tape machine electronics have been set up to operate in an abnormal manner to obtain maximum performance. For zero signal input, the carrier frequency rests at 280.8 kHz instead of at the normal center frequency of 216 kHz. For positive signal input (no negative signals present), then, the carrier frequency shifts downward to 151.2 kHz. Zero volts for this tape machine represents dark or cold targets.

There is no permanent assignment of a particular scanner spectral band to a particular tape channel. Our usual practice, however, is to record the scan-synchronizing reference and line count on tape track 7 and the processing reference on track 14. And since the tape machine has staggered heads, we prefer assigning the six spectral bands most likely to be machine-processed to odd tracks along with the sync in order to minimize misregistration of the multispectral data because of tape transport characteristics (skew, stretch, etc.). When optimized registration of the imagery in all tape channels is desired, analog delay lines are used in tape duplication on the processing tape machine to bring common objects in the imagery into exact registration.

Duplicate analog tapes are just what this name implies—duplicates of the signals on the original tape with the same track assignments and voltage gains. A special analog tape duplicating setup transcribes the FM signals to the second tape, normally without going through the demodulation and remodulation process. Where faults exist in the original tapes, these can often be corrected or relieved in the duplicated tapes. Examples are polarity reversals in a particular track, or minor misregistration of the imagery between tracks. Because the correction of such faults usually requires demodulation and remodulation of the FM signals, some signal-to-noise is then sacrificed in the duplicating process.

As displayed on an oscilloscope, traces of the tape-recorded scanner electrical signals have the appearance shown in Fig. 28. The figure parts include traces for each of the eleven video channels comprising the total spectral range of the scanner and one trace for the synchronizing signal. Approximately the same scene line scans are shown for each video display, and all of the views are in time phase relative to the scan sync. Time or scan angle is displayed along the horizontal axis (approximately 1.78 msec or 38.3 degrees per division, respectively); the vertical axis shows signal voltage (1 volt per division).

Although all video channels share one scan mirror and view the same set of radiation reference sources, these sources—taken individually—register differently for different spectral regions. The sky illumination reference (S) appears in all bands except the thermal one where it is absent because the opal glass is opaque to its wavelengths. Conversely, the thermal reference graybody plates (A, P_1 and P_2) appear only in the thermal band, since they radiate insignificant energy in the nonthermal bands. The calibration lamp source (L) appears only in the visible, near-, and mid-infrared bands because it is a point source directed into that portion of the scan mirror that reflects radiation to these particular detectors. (The ultraviolet and thermal infrared detectors receive radiation reflected from a different portion of the scan mirror.) The thermal detector receives radiation from the hot housing of this lamp just preceding graybody plate P_1 as shown in Fig. 281. Plate P_1 does not contrast sharply with the baseline as does P_2 because it happens to be set for ambient temperature (A). The view (C) external to the scanner registers radiation received from the ground for that particular spectral band. Several line scans were integrated in the display to obtain sufficient photographic exposure.

Figure 29 presents the scanner data format in a different way. In this figure, which illustrates the current data format, the scan plane is the paper and the angular position of the various radiation sources are referred to the scanner axes and the marker pulse position. For an illustration of the comparable format during the first year of M7 scanner system operation, refer to Fig. A.1 in Appendix A.

5.2 SCANNER VIDEO DISPLAYED ON FILM OR FILM-RECORDED DATA FORMAT

Although the original recording of all scanner data is on analog magnetic tape in the aircraft, the data users require that at least some of the spectral bands be printed on film for visual analysis. This is accomplished in the laboratory after a flight. Primary uses of this scanner film data are to document flight-line coverage and for manual editing of the imagery to select specific areas to be machine-processed. Indexing of the selected areas for processing is accomplished either by reference to the scan line count in the sync signal or to a visual display of the imagery.

The filmstrips of scanner imagery are reproduced at real-time rates, one track at a time, from the original analog magnetic tapes. The laboratory tape machine has associated electronics which provide operator selection of playback electronic bandwidths of from 10 kHz to 100 kHz. The reproduction bandwidth is selected to match the optimal information bandwidth of the various-size detectors used in the scanner. For instance, the large spatial resolution of the layered thermal detectors shows the best signal-to-noise at the lower bandwidth limit, and the small spatial resolution of the spectrometer in the visible region requires the upper bandwidth limit. Other electronics in the filmstrip reproduction facility provide clamping of the dc level of the signal to radiation references for dc restoration, and the registration of radiation reference quantities through sample gates. These reference quantities can be stored temporarily and, if desired, retrieved for reformatting of the data in analog form. Data "slant" for film labeling through direct exposure is also available.

The filmstrip of scanner data is made by photographing an intensity-modulated line scan on the face of a cathode ray tube (CRT). The intensity modulation is a direct function of voltage variation in the particular radiation detector output recorded on magnetic tape. Normally the 0- to 3-volt variation of the tape signal is transferred to the film as the total variation in gray scale. However, this transfer relationship is controlled by the operator. Other relationships may be selected, such as remaining in the linear portion of film sensitivity. Between runs, an equal-voltage-increment gray scale is printed on the film to establish the voltage-to-film tone calibration.

The filmstrip camera drives 70 mm film across the CRT face, perpendicular to the line scan, at rates proportional to the aircraft ground speed and absolute altitude. The camera film speed range includes absolute flight altitudes of from 1000 to 10,000 ft at a ground speed of 120 knots to provide an imagery scaling on film of the absolute flight altitude per inch of film. At the higher flight altitudes, several line scans are integrated in the film display because of overlap at the constant scan rate. At the lower altitudes, the imagery is barely contiguous (no overlap) for the small detector spatial resolution.

An example of multispectral scanner imagery reproduced on film is shown in Fig. 30 along with a section of a topographic map of the same scene. The scene is approximately a 2×5 mile portion of the Black Hills of South Dakota, showing the town of Deadwood. The large light-colored area to the left of the town is a relatively bare mountain slope which was burned over by a forest fire several years ago. The darker-toned areas are chiefly coniferous forests consisting primarily of ponderosa pine. Power line cuts through the forests are clearly discernible. There is no particular significance to the selection of this scene other than to show terrain appearance in the different spectral bands, or "colors." Nevertheless, by closely examining the scene and comparing contrasts of different features in different spectral bands,

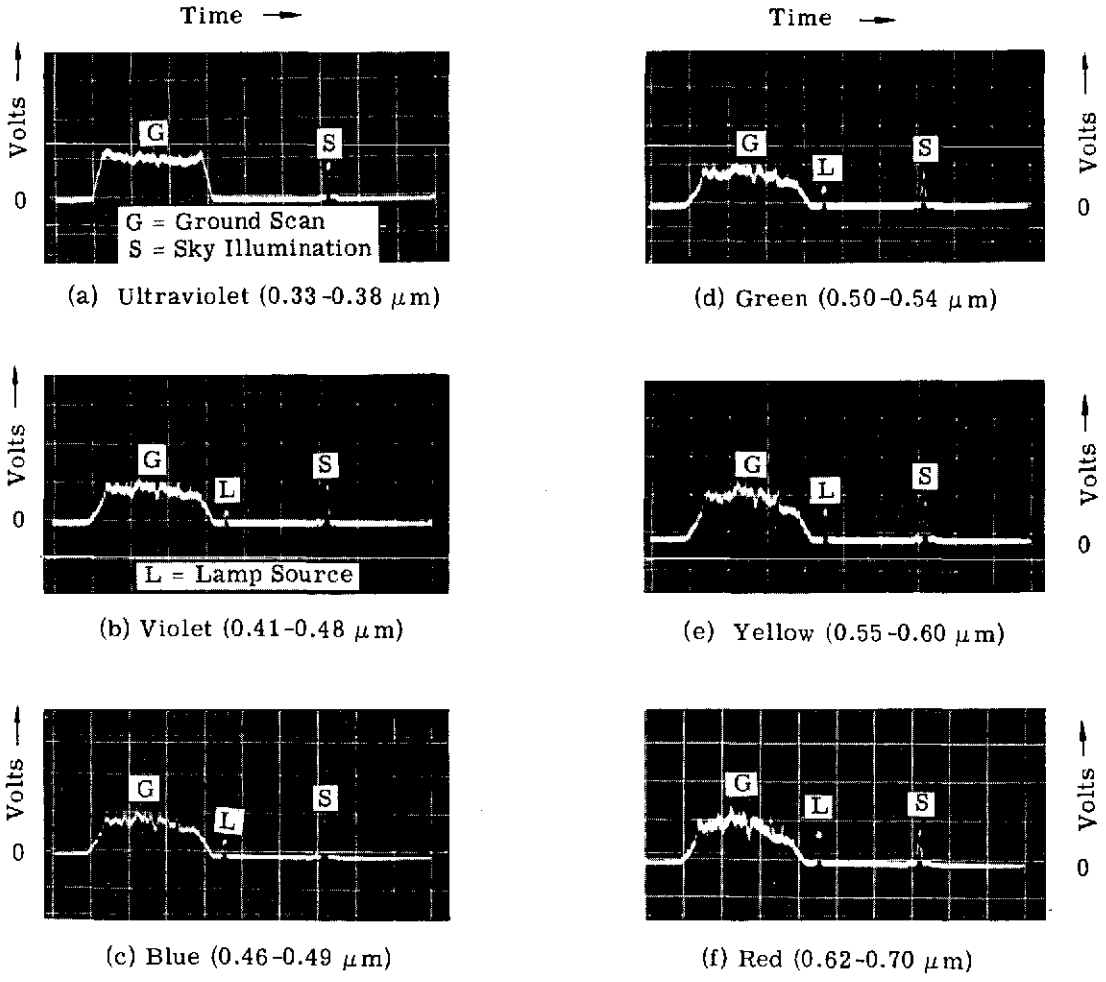

FIGURE 28. A-SCOPE PRESENTATION OF SELECTED SPECTRAL BANDS. Black Hills, South Dakota. Several line scans are integrated in each display.

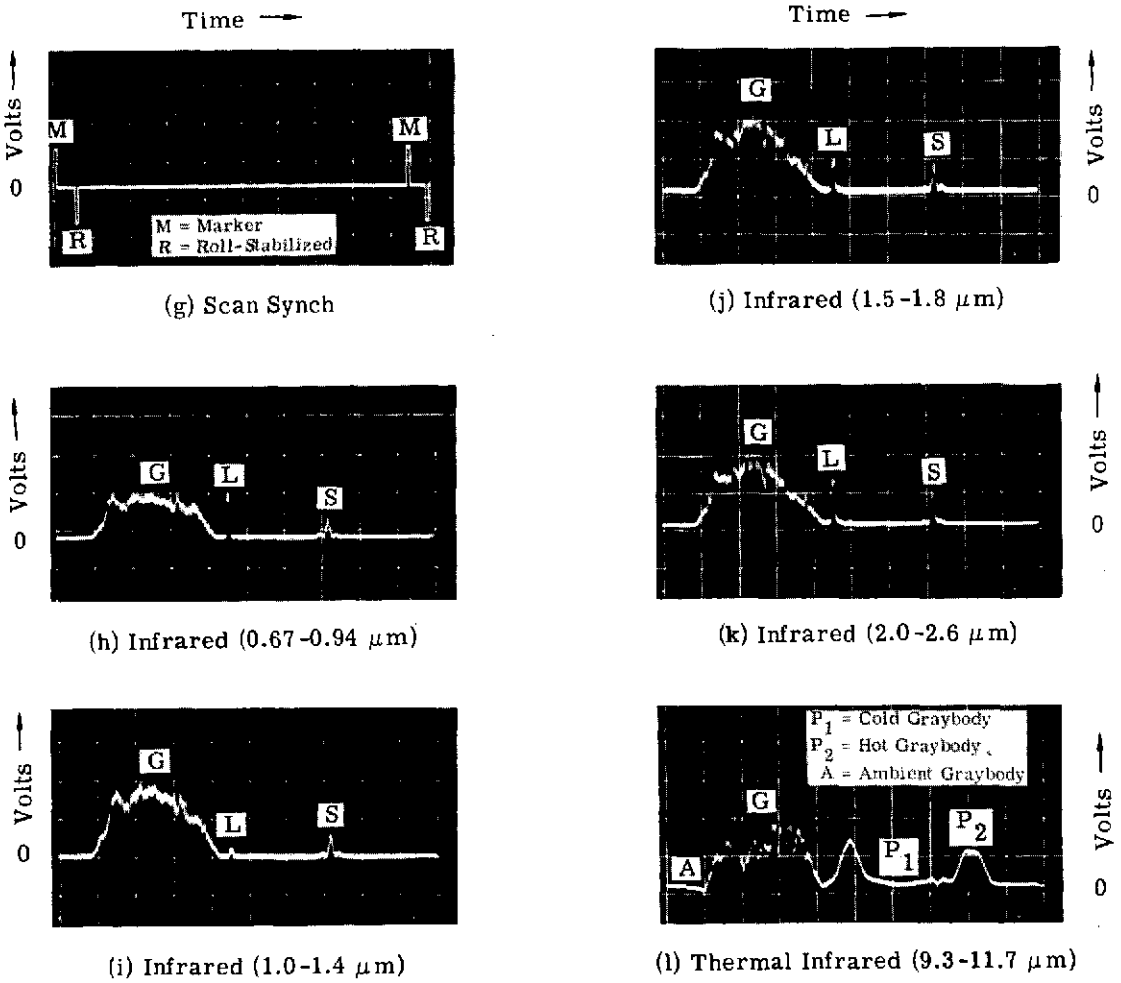

(g) Scan Synch

(j) Infrared (1.5-1.8 μm)

(h) Infrared (0.67-0.94 μm)

(k) Infrared (2.0-2.6 μm)

(i) Infrared (1.0-1.4 μm)

(l) Thermal Infrared (9.3-11.7 μm)

FIGURE 28. A-SCOPE PRESENTATION OF SELECTED SPECTRAL BANDS. Black Hills, South Dakota. Several line scans are integrated in each display. (Concluded)

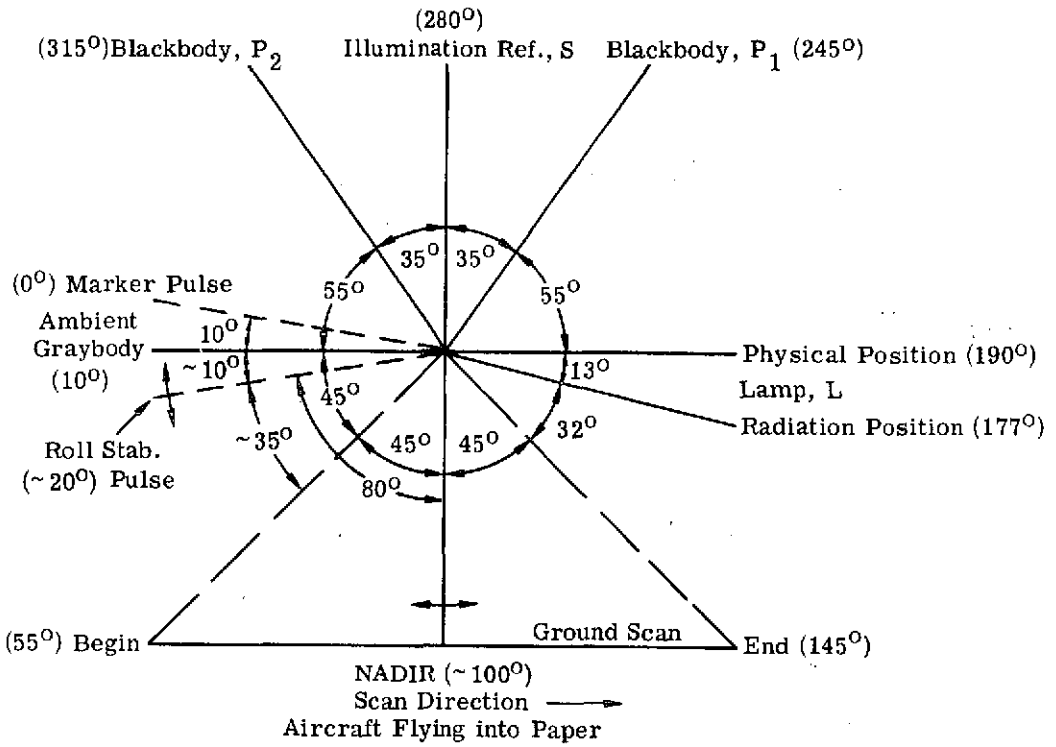

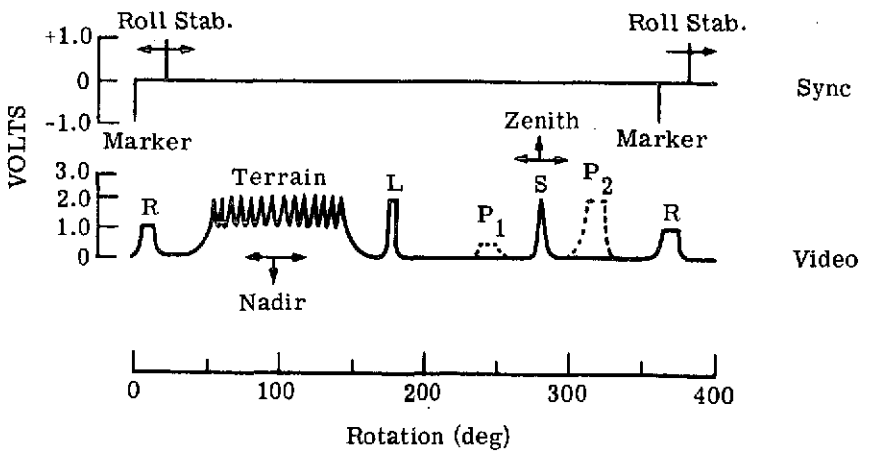

60 Scans/sec, 1° of Rotation = 46.3 μsec

FIGURE 29. RELATIVE ANGULAR POSITIONS OF SYNC AND RADIATION SOURCES

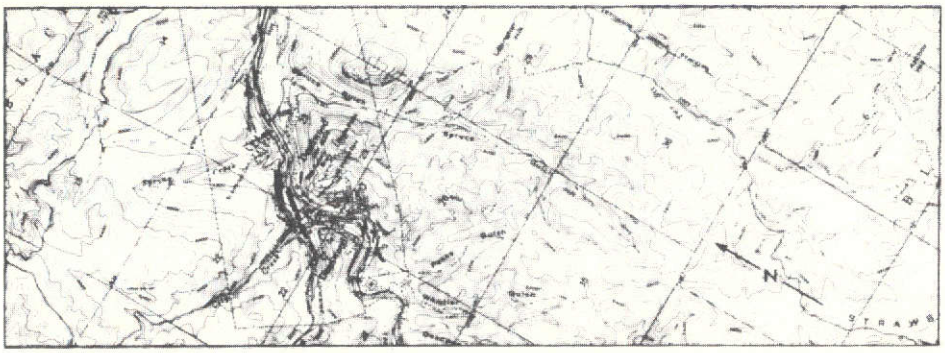

(a) USGS Topographic Map Section

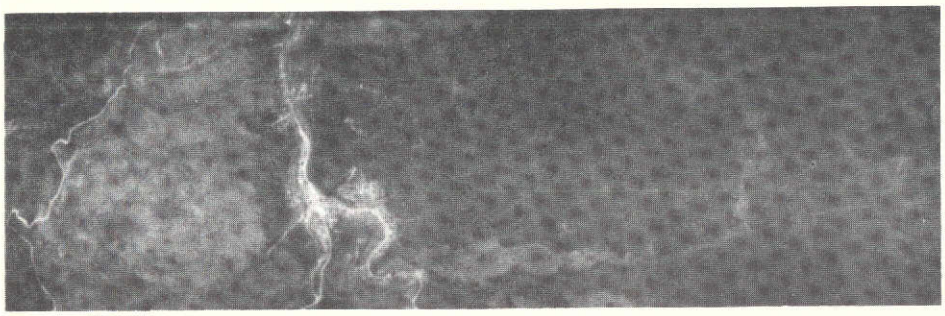

(b) Ultraviolet (0.33-0.38 μm)

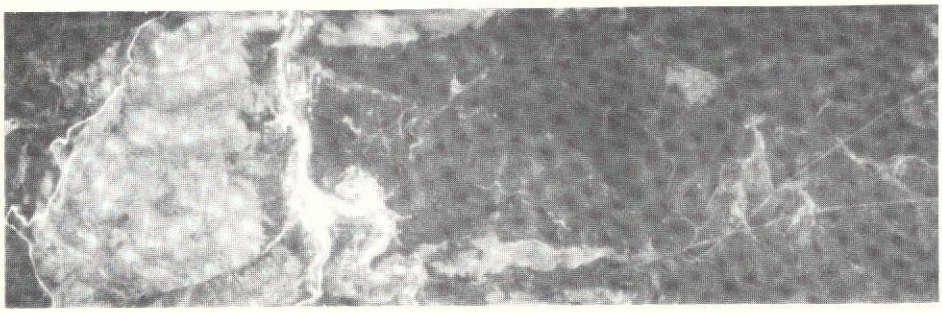

(c) Violet (0.41-0.48 μm)

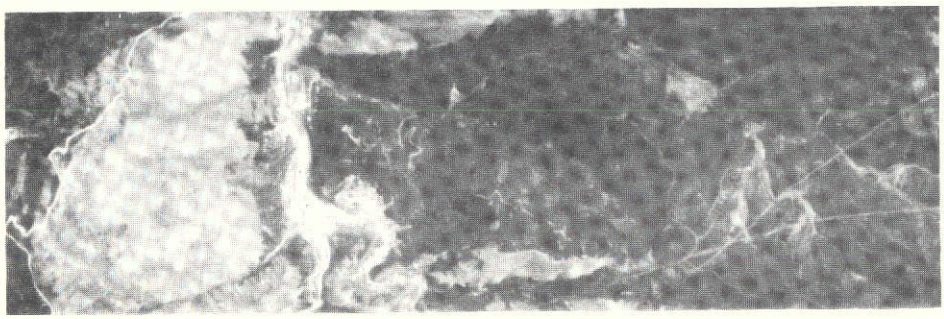

72IRO-9-579

(d) Blue (0.46-0.49 μm)

FIGURE 30. MULTISPECTRAL IMAGERY DISPLAY. Black Hills, South Dakota. 21 May 1972, 1100 hr 5000 ft altitude.

(e) Green (0.50-0.54 μm)

(f) Yellow (0.55-0.60 μm)

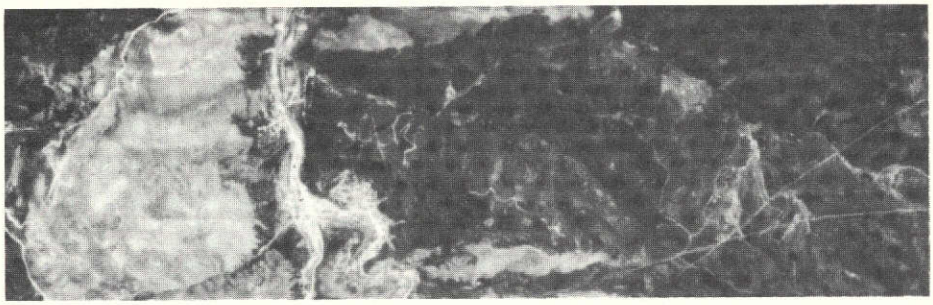

(g) Red (0.62-0.70 μm)

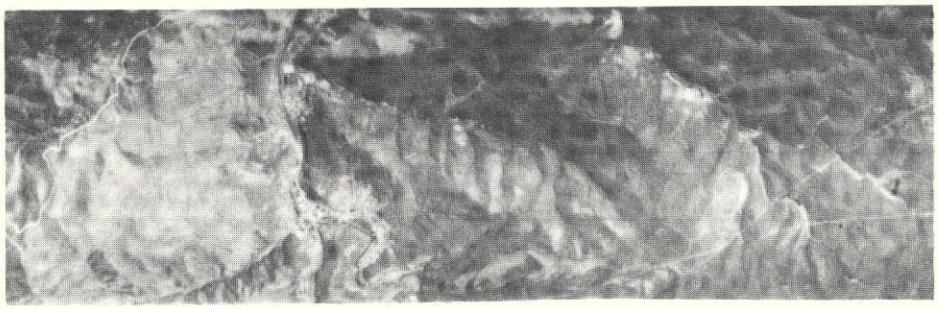

72IRO-9-579

(h) Near Infrared (0.67-0.94 μm)

FIGURE 30. MULTISPECTRAL IMAGERY DISPLAY. Black Hills, South Dakota. 21 May 1972, 1100 hr 5000 ft altitude.
(Continued)

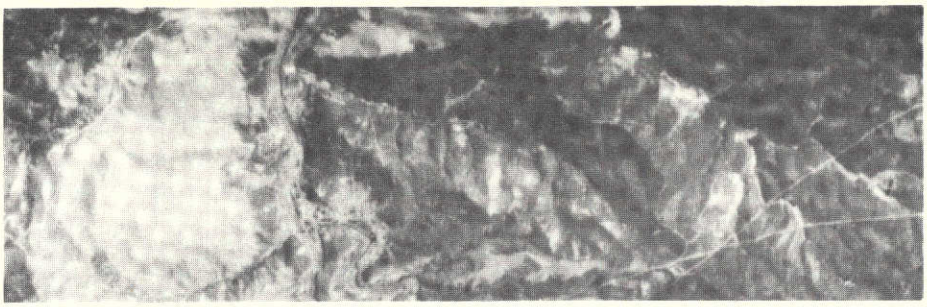

(i) Infrared (1.0-1.4 μm)

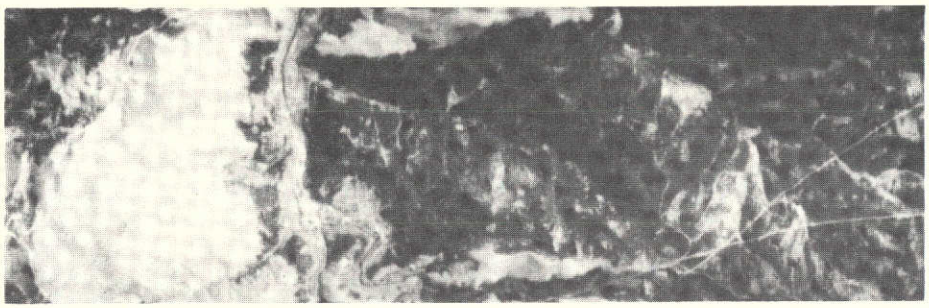

(j) Infrared (1.5-1.8 μm)

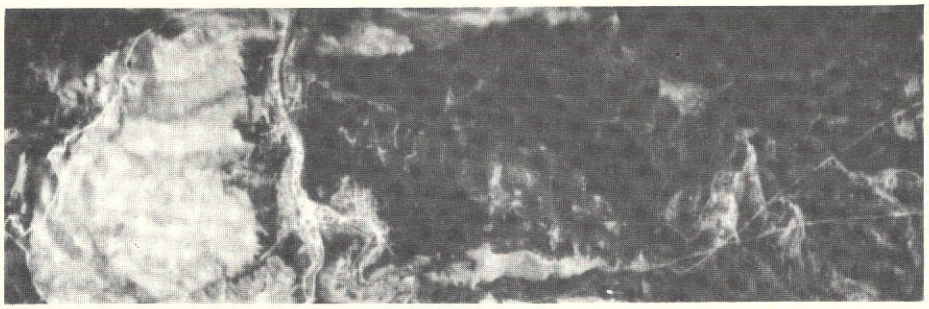

(k) Infrared (2.0-2.6 μm)

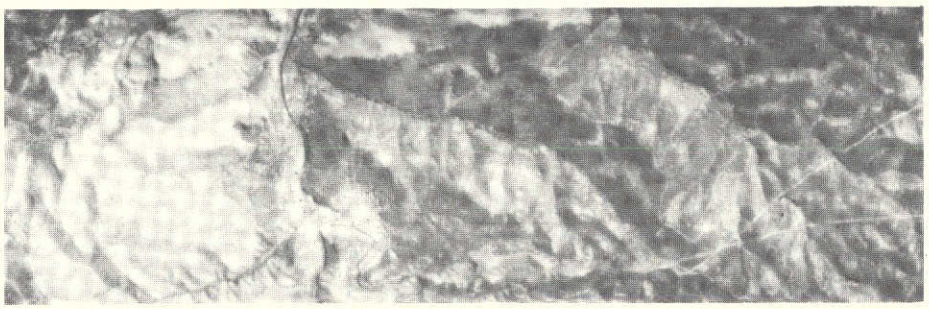

72IRO-9-579 (l) Thermal Infrared (9.3-11.7 μm)

FIGURE 30. MULTISPECTRAL IMAGERY DISPLAY. Black Hills, South Dakota. 21 May 1972, 1100 hr 5000 ft altitude. (Concluded)

one can begin to see and appreciate the possibilities in recognition based on subtle spectral differences.

Filmstrip displays of scanner imagery are not restricted to the mere printing of a particular tape channel on film. The electrical signals from the separate tape channels can be combined or processed in various ways before printing. Some of these functions are described further in Appendix B. Those most often used are level slicing and the mixing of spectral bands to simulate other instruments. An example of the latter is the simulation of ERTS-A spectral bands by controlled mixing of selected M7 scanner bands. The spectral response of each channel of the ERTS scanner was simulated by a weighted addition of appropriate M7 scanner channels. Figure 31 compares the actual and simulated ERTS-A channels; the solid line is the actual channel. Four different M7 scanner bands were used for simulation of ERTS channel 1: three bands for channel 2 and one each for channels 3 and 4.

5.3 DATA INDEXING AND SCALING

Airborne scanner data has been used historically without concern for spatial distortions or machine indexing of specific geographical areas in the imagery. However, as practical applications of scanner data become established, the need for accurate scaling and indexing becomes more apparent. Some of the more critical needs in this regard have already been implemented. Other such needs are well understood and can be implemented relatively easily upon allocation of necessary funds.

The indexing of data for geographical location and the accurate scaling of scanner data are dependent for the most part on additional sensors in the aircraft. These additional sensors must provide a continuous output of aircraft position, motion, and attitude for recording along with the scanner imagery. Standard aircraft equipment can provide this information for a price ranging from $15,000 to $150,000, depending on the degree of sophistication desired.

Currently, data indexing relies on the pilot's visual alignment with landmarks to guide the data collection and on the interpreter's visual recognition of landmarks in the imagery to establish precise location. The only scaling data recorded are the pilot's dead reckoning determination of ground speed, pressure altitude, and drift angle, based on weather service information regarding atmospheric conditions and the roll attitude of the aircraft as read from a vertical gyro unit. Information normally used in scaling and stabilizing the scanner imagery includes ground speed, absolute altitude, and roll attitude. In special cases, corrections can be made to remove average drift angle and nonlinear scan distortions. While scaling accuracy can be improved by trial-and-error matching of features in the imagery to Geological Survey maps of the same area, this is time consuming and expensive.

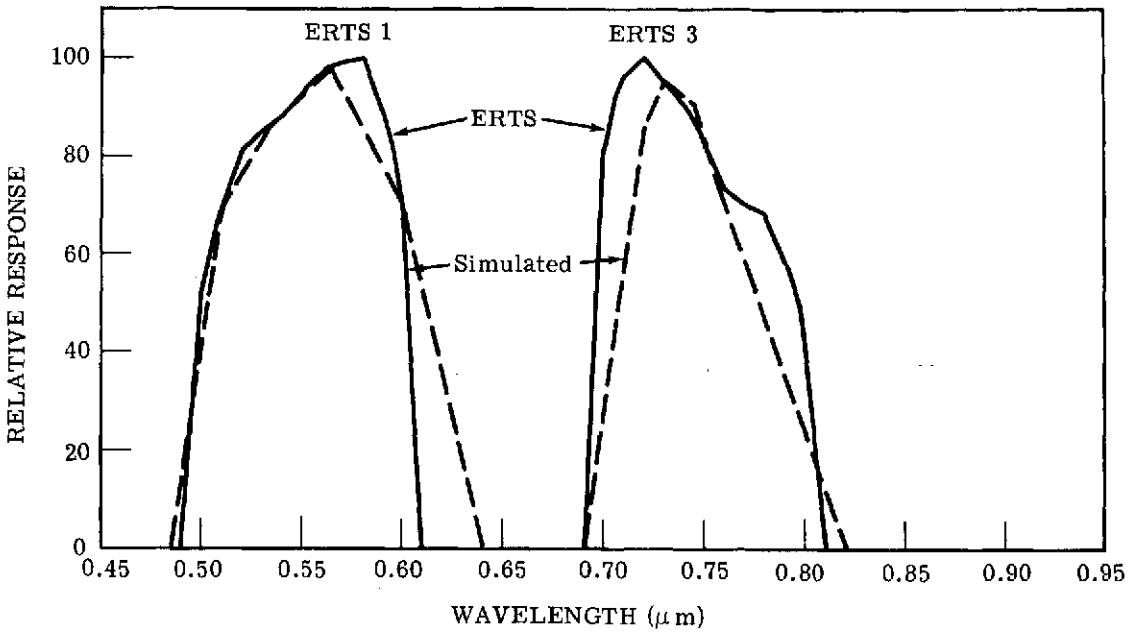

(a) ERTS Channels 1 and 3

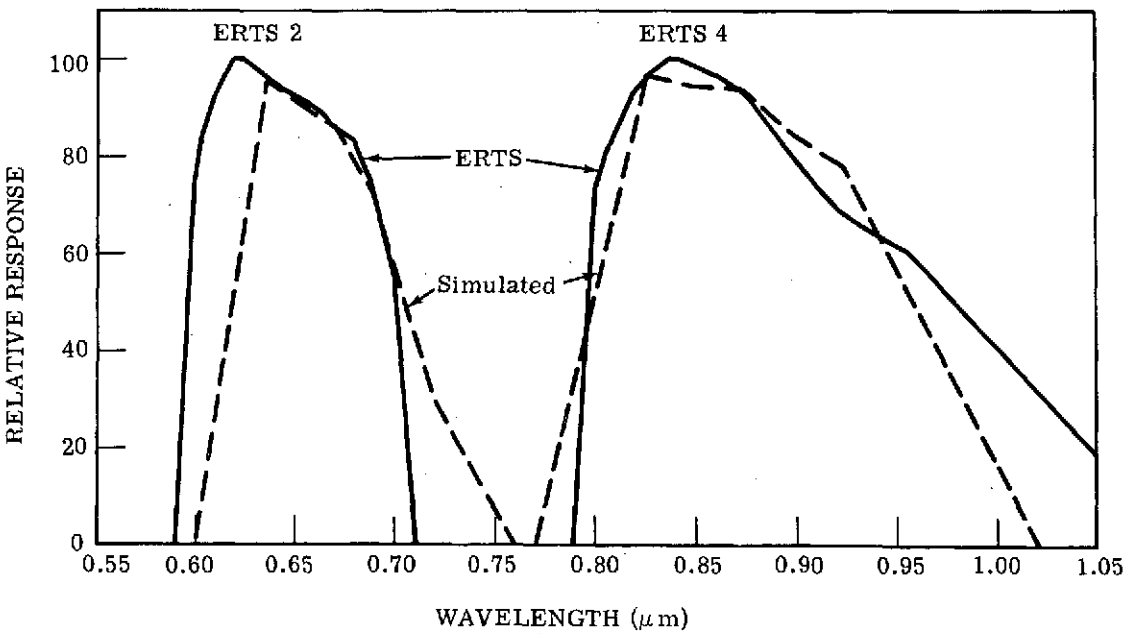

(b) ERTS Channels 2 and 4

FIGURE 31. ACTUAL AND SIMULATED ERTS SPECTRAL SENSITIVITY

The scaling and indexing capabilities of the M7 scanner system can be significantly improved by adding a commercial Doppler navigator to provide accurate ground speed and drift angle. These data, coupled with existing aircraft and scanner reference data and recorded on magnetic tape with the scanner imagery, could provide all of the essential information needed for scaling corrections in scanner imagery processing.

5.4 RADIOMETRIC AND SPECTRAL CALIBRATION

M7 scanner system performance is continuously monitored through reference to operator-controlled internal radiation sources. Several times per year, these secondary standards within the system are compared with primary standards in the laboratory. Documentation on these radiometric and spectral calibrations of the system is then made available to users of the multispectral data. Because only those users who have processing capabilities are normally interested in this data, it is not distributed widely. Currently, ERIM processes 95% of all multispectral data collected with the M7 system. Only Purdue University, South Dakota State University, NASA/Wallops, and NASA/JSC have also processed Michigan (WRL/ERIM) multispectral data. Users requiring the most recent primary calibration records associated with a particular multispectral data set should request that any raw data supplied them be accompanied by such records.

The Mission Report, issued with each site tape and film data set, documents the calibration of the system with regard to secondary internal standards. Here, spectral bands are defined at a nominal 10% of peak response limits, and radiation reference source outputs are noted from panel displays.

The panel display for the graybody references is a number readout relatable to temperature through a calibration curve for the temperature sensor. The temperature of the blackbody sources, including that of the one at ambient, can be determined to the nearest $0.1^{\circ}C$. For a more accurate calibration of the actual radiation temperature of these sources, the source emissivity and temperature differential from ambient must be taken into account. Usually, however, blackbody temperatures are close enough to ambient that this correction to the direct readout is unnecessary.

The readout of the calibration lamp source indicates lamp current to the nearest 0.1 amp. This readout must be referred to curves relating this lamp current to actual radiation in each of the defined spectral bands.

The sky illumination or "sun sensor" reference has at best a gross relative calibration. Its main use is to denote changes in incoming radiation from the sky since reflected radiation from the surface is proportional to changes in the general level of sky illumination. Thus this reference serves primarily as an operator aid in setting up the video gains to most advantageously

record the reflection of objects of interest based on a priori information. The panel readout tells the amount of attenuation inserted in the optical path for the reference. This attenuation is grossly relatable to surface reflection.

Because the M7 multispectral scanner system is still an experimental model under continual development, its configuration is often changed, our understanding of its performance is constantly improved, and its deficiencies are being progressively overcome. Documentation on these changes and improvements is recorded internally but seldom circulated externally because of limited interest. Therefore, users desiring precise and complete information on the M7 system's transfer function as it relates to their particular data set must personally visit ERIM to discuss their requirements.

5.5 FLIGHT RECORDS

These records direct the flight crew in performing a data collection flight and provide a way for them to document their observations during the flight. All auxiliary information associated with the sensor imagery recordings is noted manually in the flight records. One record is kept by the pilots, one by the test conductor, one by the scanner operator, and one by the camera operator.

The Aircraft Data Record kept by the pilot specifies the flight lines to be flown and under what limitations. On this record and also on an accompanying map, the pilot notes the lines actually flown and the gross atmospheric conditions at the time of flight.

The Flight Data Record, which also specifies the flight lines and limiting conditions, is kept by the test conductor. During the flight, he manually records the start and stop times of data runs and the magnetic tape assignment to runs. Further, he notes flight plan changes, instrument performance irregularities, and other information which may affect data quality or indexing. After the flight or mission is completed, the test conductor writes a narrative account of the flight operation with emphasis on the circumstances of data collection; this account is included with the Flight Data Record.

The Scanner Data Record is kept by the scanner operator; it specifies the configuration of the scanner system and the assignment of spectral bands to tape channels. During the flight, the operator records the gain settings for each video channel and the control settings for each radiation reference source. He also notes any peculiarities observed in the data set.

The Camera Data Record kept by the camera operator specifies the camera configuration, including film/filter combinations and framing intervals for specified overlap. During the flight he notes any configuration changes as well as light level readings, exposure settings, frame count, and film magazine assignment for each run. He also records any observations which may affect the photographic results.

The foregoing flight records are considered a part of the raw data set which also includes analog magnetic tapes and aerial camera film transparencies. Copies of these flight records are available to data users, but the Mission Report—which includes most of the same information in a more organized form—is normally used to distribute this data.

6
AIRBORNE SYSTEM PERFORMANCE

This section describes the various system performance tests, both optical and electrical, completed on the M7 scanner just before its operation in calendar year 1972. Table 5 summarizes the test results obtained as well as the general operating characteristics of the M7 scanner system. Implications of the test results with regard to overall data quality are discussed and some suggestions made for possible future improvements in data quality.

6.1 RADIATION CALIBRATION

6.1.1 VISIBLE AND NEAR-IR RADIANCE CALIBRATION (0.4-2.6 μm)

The task of trying to provide absolute radiance calibration in the visible and near-IR regions for any line scanner is difficult, to say the least. Much has been written about the theory behind such radiation calibrations, so no attempt will be made here to go into any great depth on the subject. This section provides, as background, a limited amount of theory on radiance calibration and describes the procedure and results of the tests.

6.1.1.1 Calibration Procedure

The scanner calibration lamp signal, as described in Section 4.4, is used basically as a transfer standard to obtain the apparent spectral radiance of terrain objects. Its main purpose is to account for scanner system responsivity changes that, in general, are almost impossible to monitor conveniently. The scanner components themselves are designed to respond linearly with increased radiance from the ground terrain—i.e., an increase in radiance gives a corresponding increase in detector signal. Hence the scanner detector voltage for each channel can be represented by the following general equation:

$$V_{T+p}(\lambda) = K[L_T(\lambda) + L_p(\lambda)] \tag{1}$$

where

$$L_T(\lambda) = \frac{\rho_\tau E_T(\lambda)}{\pi}$$

and

$V_{T+p}(\lambda)$ = scanner signal voltages* recorded by aircraft recorder

K = a constant dependent on system factors such as responsivity of detectors and photomultipliers, system transmission losses, gains, etc.

$L_T(\lambda)$ = radiance of target,* assuming a Lambertian surface

*In each scanner channel.

TABLE 5. PARAMETERS OF M7 SCANNER SYSTEM PERFORMANCE

Spectral Ranges	Spectral Sensor Bands (μm)	Calibration Reference Sources	Calibration Type	Noise Equivalent Data	Spatial Resolution (mrad)	Scan Angle Response	
						Degrees from Nadir	Percent Increase Relative to Nadir
Ultra-violet	0.33-0.38	None	None	Not Available	3	Not Available	
Visible	0.41-0.48	Quartz-Iodine Lamp	Radiance* $\left(\frac{\mu W}{cm^2 \cdot sr \cdot \mu m}\right)$	$\Delta L(\mu W/cm^2 \cdot sr \cdot \mu m)$ 31	2	30	+3
	0.46-0.47			65			
	0.48-0.51			52		45	+6
	0.50-0.54			59			
	0.52-0.57			44			
	0.54-0.60			69			
	0.58-0.65			125			
	0.61-0.70			115			
	0.72-0.92			205			
Near Infrared	1.0-1.4	Quartz-Iodine Lamp	Radiance* $\left(\frac{\mu W}{cm^2 \cdot sr \cdot \mu m}\right)$	27	2	30	0.0
	1.5-1.8			17			
	2.0-2.6			7		45	0.0
Thermal	8.0-14.0	3 Blackbody Reference Plates	Temperature (^oC)**	ΔT 0.11^oC	3	30	0.0
						45	0.0

*Section 6.1.1.

**Section 6.1.2.

TABLE 5. PARAMETERS OF M7 SCANNER SYSTEM PERFORMANCE
(Concluded)

Polarization Sensitivity at Nadir L-Vector from Scan Direction (deg) / Response Decrease Relative to Nadir	External FOV (deg)	Diameter Collector Optics	Effective f/No of Optics	Effective Collecting Area	Effective Bandwidth†
Not Available	90 (±45 from Nadir)	3-in. Diameter	f/3	6.18 in.^{2}	DC to 80 kHz (3dB)
45 ⟶ -10.6 90 ⟶ -36.8	90 (±45 from Nadir)	5-in. O.D. 3-in. I.D. Annulus	f/5	12.57 in.^{2}	DC to 80 kHz (3dB)
Not Available	90 (±45 from Nadir)	5-in. O.D. 3-in. I.D. Annulus	f/1.25	12.57 in.^{2}	DC to 80 kHz (3dB)
Not Available	90 (±45 from Nadir)	3-in. Diameter	f/1	6.18 in.^{2}	DC to 80 kHz (3dB)

†Tape recorder limited.

$L_p(\lambda)$ = path radiance produced as a result of scattering of radiation by molecular and aerosol particles in the atmosphere*

ρ_τ = object directional reflectance

At present, the radiance quantity $L_p(\lambda)$ is impractical to measure simultaneously with the airborne scanner imagery. But to make up for this, considerable effort is going into modeling the atmosphere so that the appropriate corrections can be made to the data during processing.

In terms of scanner radiance calibration, however, the individual terms of Eq. (1) are less important than the total radiance received at the scanner's aperture. Hence, the apparent target radiance (which includes the path radiance contribution) is a more appropriate quantity to measure. Simplifying Eq. (1), then, we get:

$$V_{T+p} = KL_{T+p}(\lambda) \tag{2}$$

$L_{T+p}(\lambda)$ = apparent radiance of target, $L_T(\lambda) + L_p(\lambda)$

Were it not for the fact that the constant K in Eq. (2) actually varies somewhat because of changes in the detector and its responsivity, the radiance calibration of a scanner would be easy. A quick look at a known radiance source such as a reflectance standard illuminated by calibrated irradiance standards would suffice. Since this "constant" does vary, however, a means to remove K from Eq. (2) becomes necessary.

The prime purpose of the lamp reference source, as stated earlier, is to remote the factor K. This is done by dividing the voltage obtained from the target by the lamp voltage. Hence, if the target voltage is given by Eq. (2) and the lamp voltage is given by

$$V_\ell = KL_\ell(\lambda) \tag{3}$$

then by dividing Eq. (2) by Eq. (3) we get

$$V_{T+p} = \frac{V_\ell L_{T+p}(\lambda)}{L_\ell(\lambda)} \tag{4}$$

The radiance calibration is performed in a similar manner, except that the target, instead of being a terrain object, is an object of known radiance. If the calibration target is flame-sprayed aluminum (a well measured and stable reflectance standard) illuminated by quartz-iodine lamps, then the voltage generated by the radiance standard is

$$V_{A\ell}(\lambda) = K' L_{A\ell}(\lambda) \tag{5}$$

where $L_{A\ell}(\lambda) = [\rho_{A\ell} E_{QI}(\lambda)]/\pi$

E_{QI} = spectral irradiance of quartz-iodine lamps

$\rho_{A\ell}$ = directional reflectance of flame-sprayed aluminum

K' = system constant which has varied from K in previous equation

Dividing Eq. (5) by the lamp voltage

$$V_{\ell'}(\lambda) = K' L_{\ell}(\lambda) \tag{6}$$

we get

$$V_{A\ell} = \frac{V_{\ell'} \rho_{A\ell} E_{QI}(\lambda)}{L_{\ell}(\lambda)\pi} \tag{7}$$

Substituting Eq. (7) back into Eq. (4) and rearranging, we have

$$L_{T+p}(\lambda) = \left(\frac{V_T}{V_\ell}\right)\left(\frac{V_{\ell'}}{V_{A\ell}}\right)\left[\frac{\rho_{A\ell} E_{QI}(\lambda)}{\pi}\right] \tag{8}$$

Equation (8) gives the apparent radiance of the target in terms of known or measured quantities. It is obvious from Eq. (8) that the accuracy of radiance calibration depends upon two factors: first, how well $\rho_{A\ell}$ and E_{QI} are known; and second, $L_\ell(\lambda)$ remaining spectrally constant. A complete error analysis of M7 scanner signal calibration is planned. Also, a more detailed explanation of radiance calibration and uses of the sun sensor is given in Ref. [1].

6.1.1.2 Tests and Results

The calibration fixture used to calibrate the M7 scanner is shown in Fig. 32. The lamps used as irradiance standards are 200W General Electric 6.6A/T42/1CL quartz-iodine lamps traceable to similar NBS standards. The reflectance panel was a sheet of flame-sprayed aluminum painted with 3M white paint. To obtain maximal accuracy, the 3M panel was not assumed to be a Lambertian reflector but instead its bidirectional reflectance characteristics were measured and actually integrated over the scanner view angles of interest.

1. Hasell, P. G., and L. M. Larsen, Calibration of an Airborne Multispectral Optical Sensor, Report 6400-137-T, Willow Run Laboratories, Institute of Science and Technology, The University of Michigan, Ann Arbor, Sept., 1968.

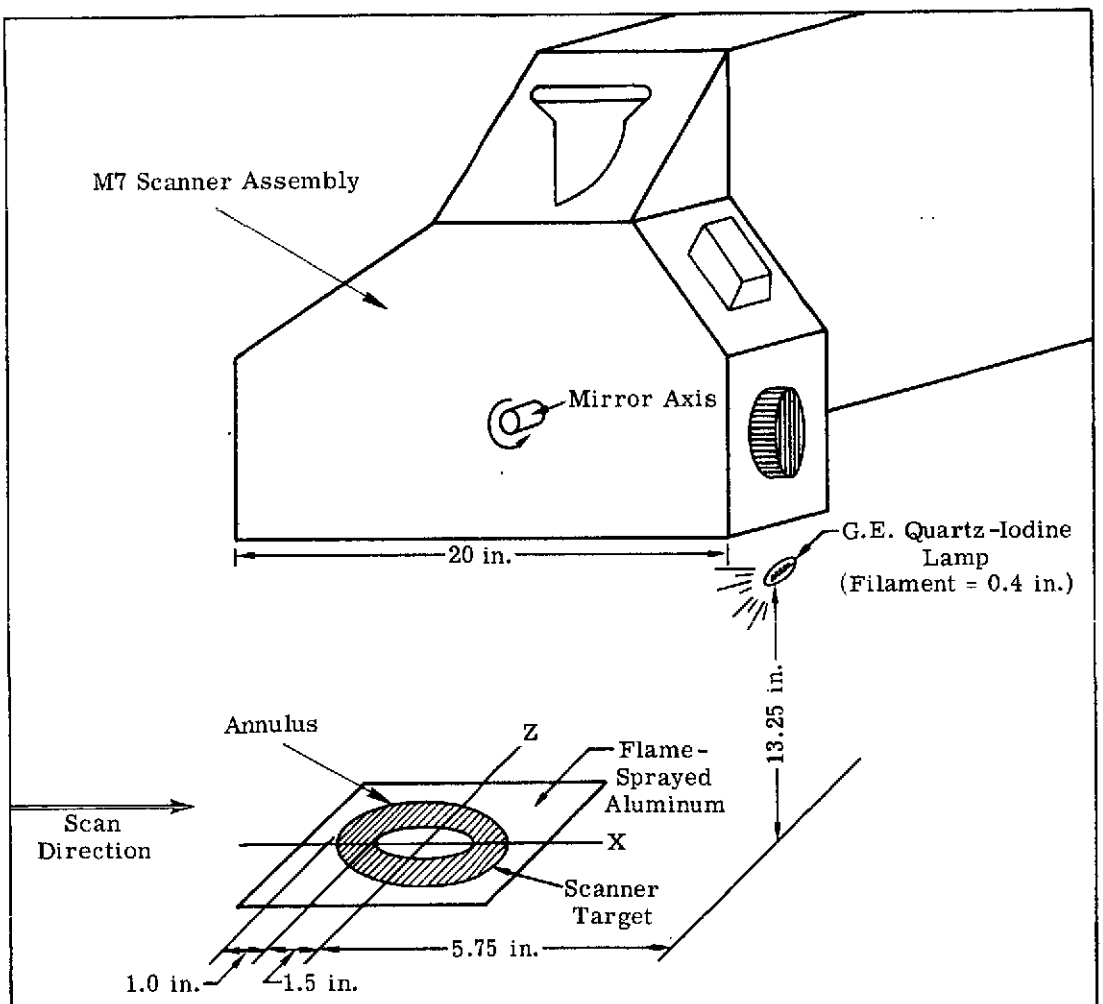

FIGURE 32. M7 SCANNER CALIBRATION FIXTURE

The dimensions shown in Fig. 32 were obtained by analytical methods to provide the maximum uniformity of illumination on the flame-sprayed aluminum panel, and also by the geometrical restraints imposed by the scanner.

Figure 33 shows the result of the integration of the lamp irradiance and panel bidirectional reflectance to give uniform radiance from the panel. In this figure, the average radiance value viewed by the scanner looking perpendicular to the panel was assigned a value of 100%, and contours of radiance differing by ±1% were plotted over the rest of the panel. The area between the two inner rings (shaded area) represents the area actually viewed by the scanner. The clear center portion is obscured by a mirror used for collecting thermal energy. As can be seen, the radiance varies by -4% and +2% about the average for a typical spectrometer channel. The total radiance [$L_{A\ell}(\lambda)$ in Eq. (5)] versus wavelength off the flame-sprayed aluminum panel is shown in Fig. 34.

The actual computation of the scanner calibration constant C involves the last two terms of Eq. (8), i.e.,

$$C = \frac{V_{\ell'}}{V_{A\ell}} [L_{\ell}(\lambda)] \tag{9}$$

where $V_{\ell'}$ = signal voltage of scanner calibration lamp for each channel
$V_{A\ell}$ = signal voltage of aluminum reference panel for each channel
$L_{\ell}(\lambda)$ = total radiance of aluminum reference panel viewed by scanner for each channel

However, the wide range of the calibration lamp currents encountered during data collection produces a series of constants C corresponding to several lamp currents. Hence Eq. (9) can actually be written:

$$C_i(\lambda) = \frac{V_{\ell' i}}{V_{A\ell}} [L_{\ell}(\lambda)] \tag{10}$$

where C_i = radiance calibration constant for lamp current i and wavelength λ

To obtain the radiance of a terrain object in channel n, the appropriate $C_i(\lambda)$ for channel n at lamp current i is found and multiplied by V_T/V_{ℓ}, i.e.,

$$L_T(\lambda) = C_i(\lambda) \left(\frac{V_T}{V_{\ell,i}} \right) \tag{11}$$

Several measurements of this constant $C_i(\lambda)$ have shown it to change whenever the scanner lamp housing is moved, as when the scanner is removed from the aircraft for periodic maintenance. For this reason, several $C_i(\lambda)$ curves are available, each of which applies to a certain

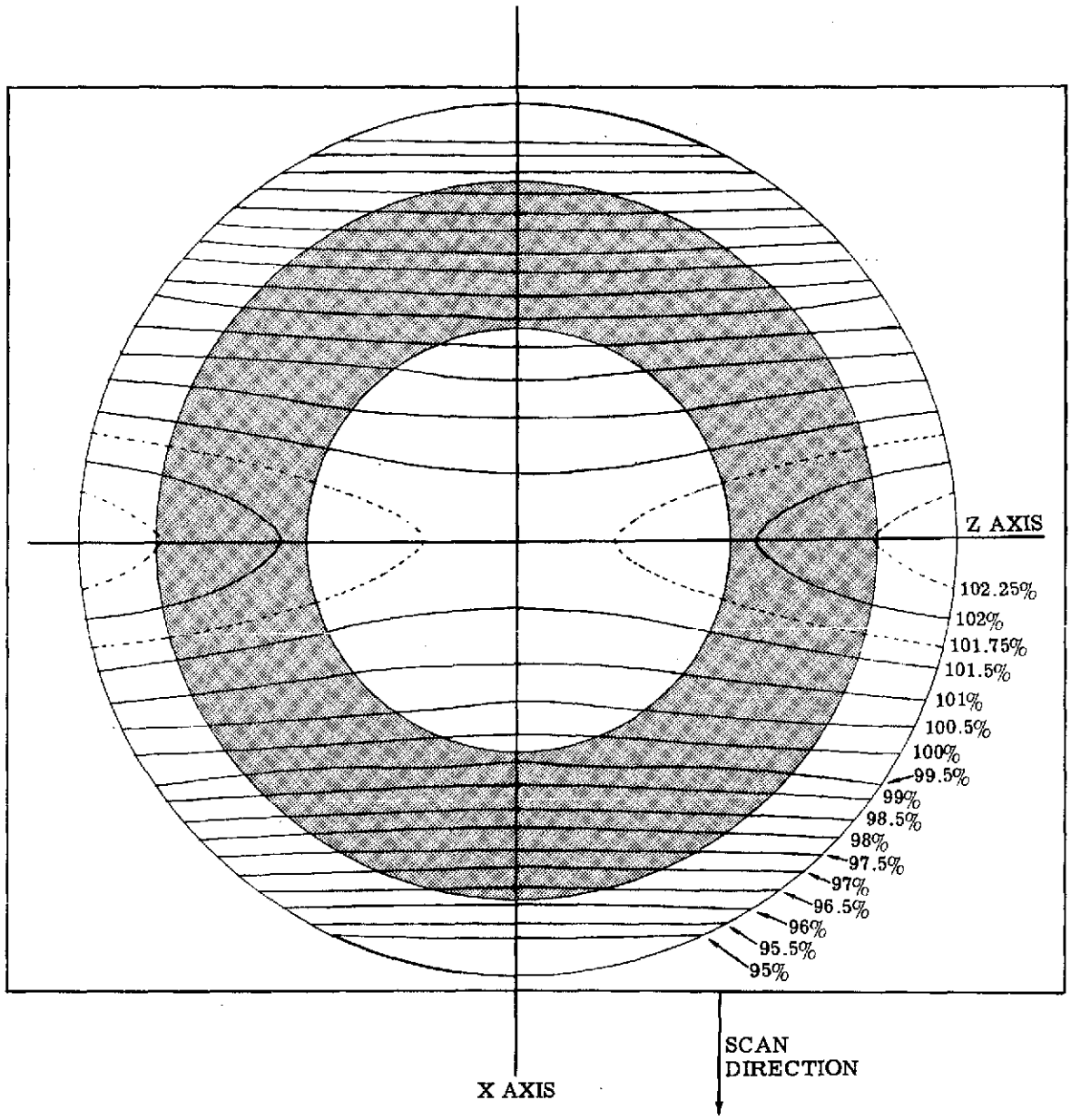

FIGURE 33. RADIANCE CONTOURS ON M7 SCANNER CALIBRATION REFERENCE PANEL.
View normal to panel as seen by scanner.

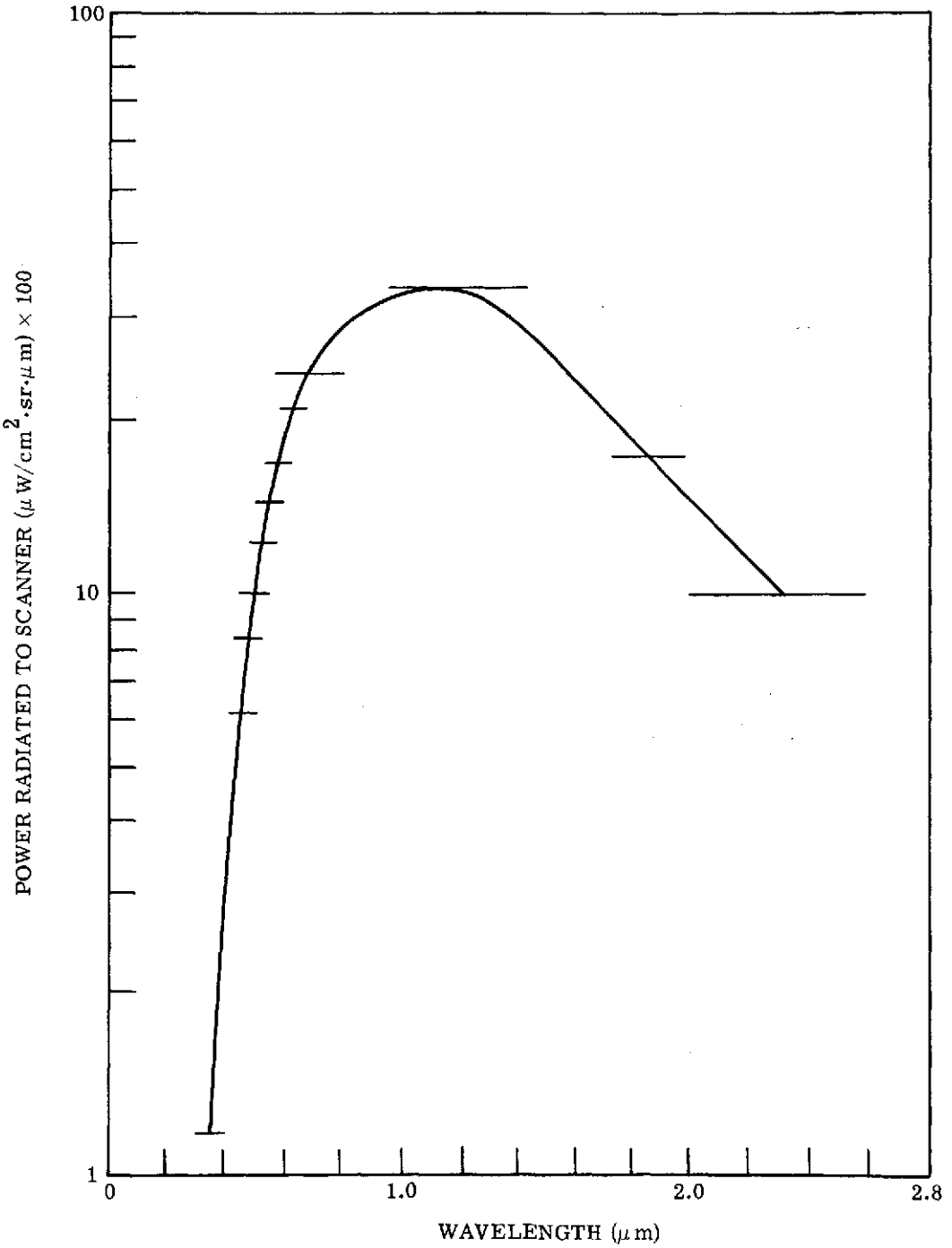

FIGURE 34. POWER RADIATED TO SCANNER VERSUS WAVELENGTH BANDS

time of the year. To include all of them in this report would serve no practical purpose, so only a representative set is shown in Fig. 35 parts a through k. The error flags on the curve are based on a standard deviation of ±1 as calculated by the digital computer, and represent the noise in the measurement, not the error in radiance calibration. No radiance calibration exists for the UV channel nor for any channel in Detector Position 1B, because the scanner lamp does not illuminate that portion of the scan mirror viewed by detectors in Position 1 However, a separate calibration lamp for visible detectors in this position will be implemented in the near future.

6.1.2 THERMAL REFERENCE SOURCE CALIBRATION (9.3-11.7 μm)

As described in Section 4.4, the reference sources for the thermal detectors in the M7 scanner consist of three blackbody plates viewed sequentially during each scan. Two of these plates are temperature-controlled while the third is allowed to vary with the ambient temperature. The purpose of these plates is to provide known sources of emitted radiation by means of which the temperatures of objects viewed on the ground by the scanner can be calculated. Unfortunately, a known radiation source alone is not enough to ensure accurate temperature determinations, since several other factors must be taken into account.

(1) Few objects have an emissivity near 1.0. This means that only apparent temperatures can be measured by an airborne scanner.

(2) The atmosphere through which the radiation from the ground is received absorbs and re-emits some of this radiation. Hence, unless atmospheric corrections are made, the apparent temperature measurements only apply at the receiving aperture of the scanner.

(3) Perfect blackbody reference sources are difficult to construct. This means that the reference sources themselves can be viewed only as sources of apparent temperature.

The remainder of this section outlines the steps taken to minimize outside influences (such as the atmosphere) on the apparent temperature calculations, and steps taken to document for future reference all calibration tests conducted on the thermal plates.

6.1.2.1 Temperature Calibration of Thermal Channel

Many models of atmospheric transmission in the thermal region from 4.0 μm to 15.0 μm have been formulated for various meteorological conditions in recent years. These permit reasonable corrections for thermal data obtained in any band in this region. However, to minimize the number of corrections needed to obtain temperature information, a 9.3- to 11.7-μm filter has been used on the thermal detectors to utilize the excellent atmospheric transmission in that region. For most purposes, negligible atmospheric corrections are needed in

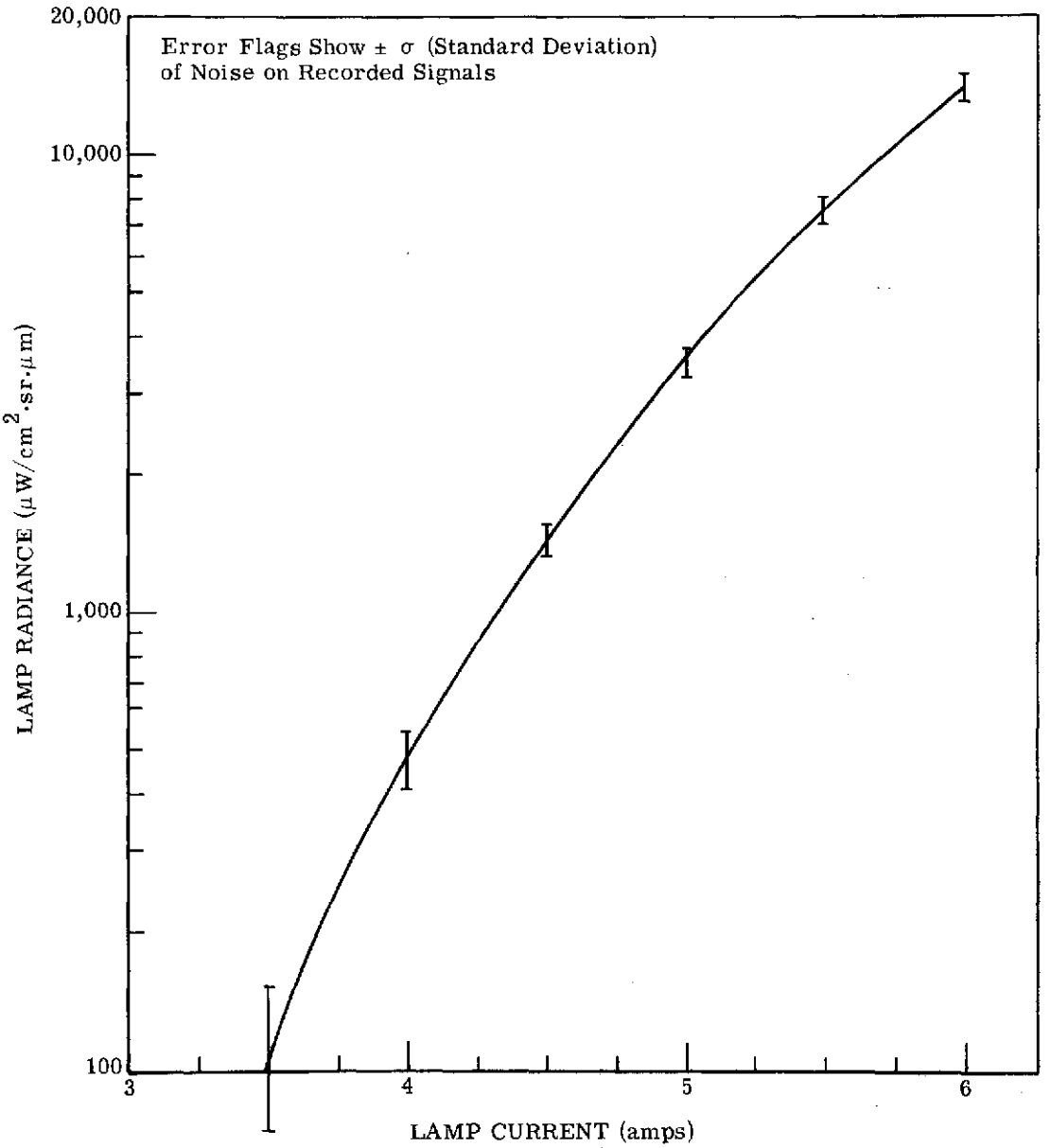

(a) Wavelength: 0.46 to 0.49 μm (C10)

FIGURE 35. INTERNAL LAMP TRANSFER STANDARD CALIBRATION 1 JUNE TO 30 DECEMBER 1972

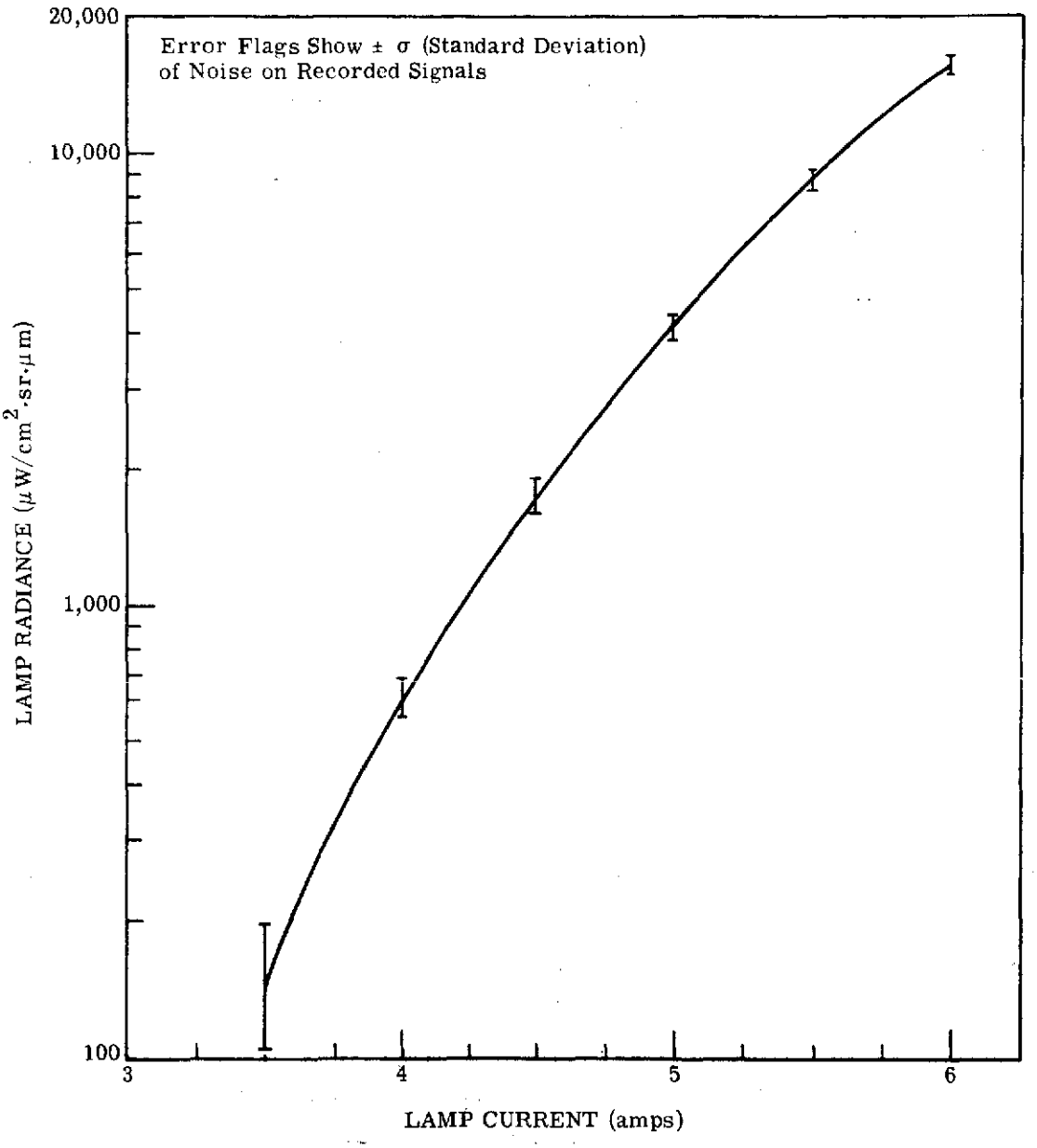

(b) Wavelength: 0.48 to 0.51 μm (C9)

FIGURE 35. INTERNAL LAMP TRANSFER STANDARD CALIBRATION 1 JUNE TO 30 DECEMBER 1972 (Continued)

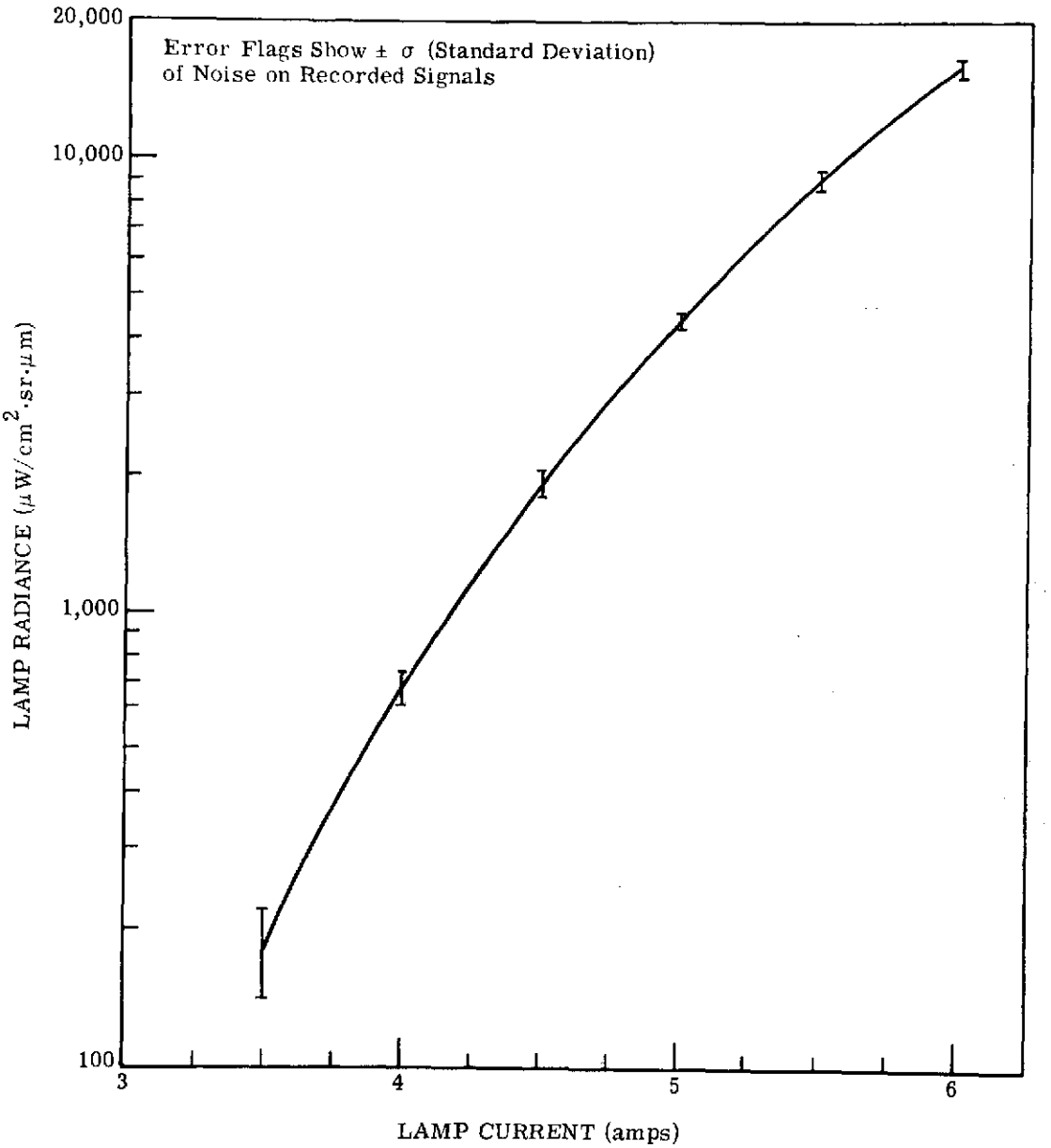

(c) Wavelength: 0.50 to 0.54 μm (C8)

FIGURE 35. INTERNAL LAMP TRANSFER STANDARD CALIBRATION 1 JUNE TO 30 DECEMBER 1972 (Continued)

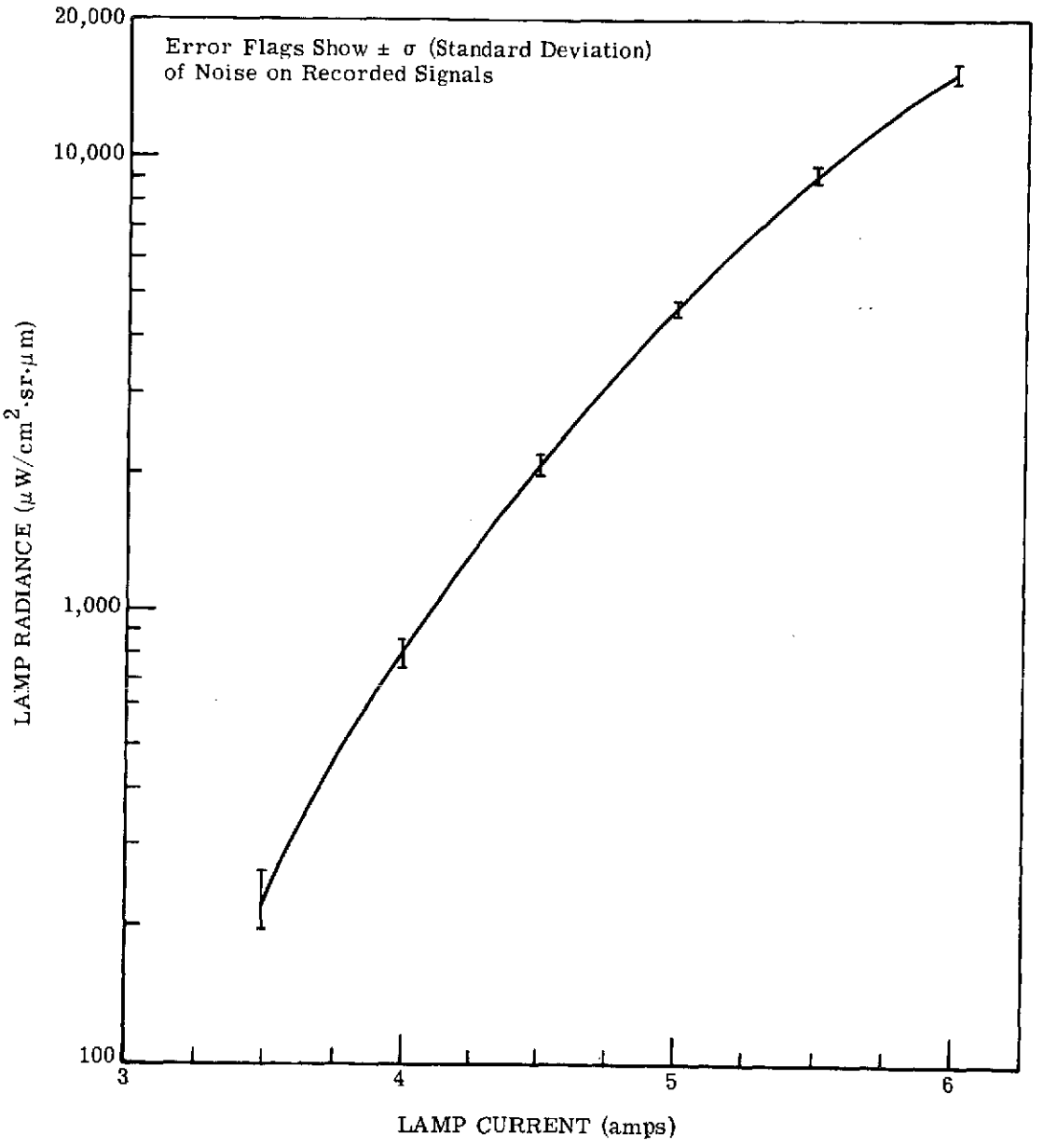

(d) Wavelength: 0.52 to 0.57 μm (C7)

FIGURE 35. INTERNAL LAMP TRANSFER STANDARD CALIBRATION 1 JUNE TO 30 DECEMBER 1972 (Continued)

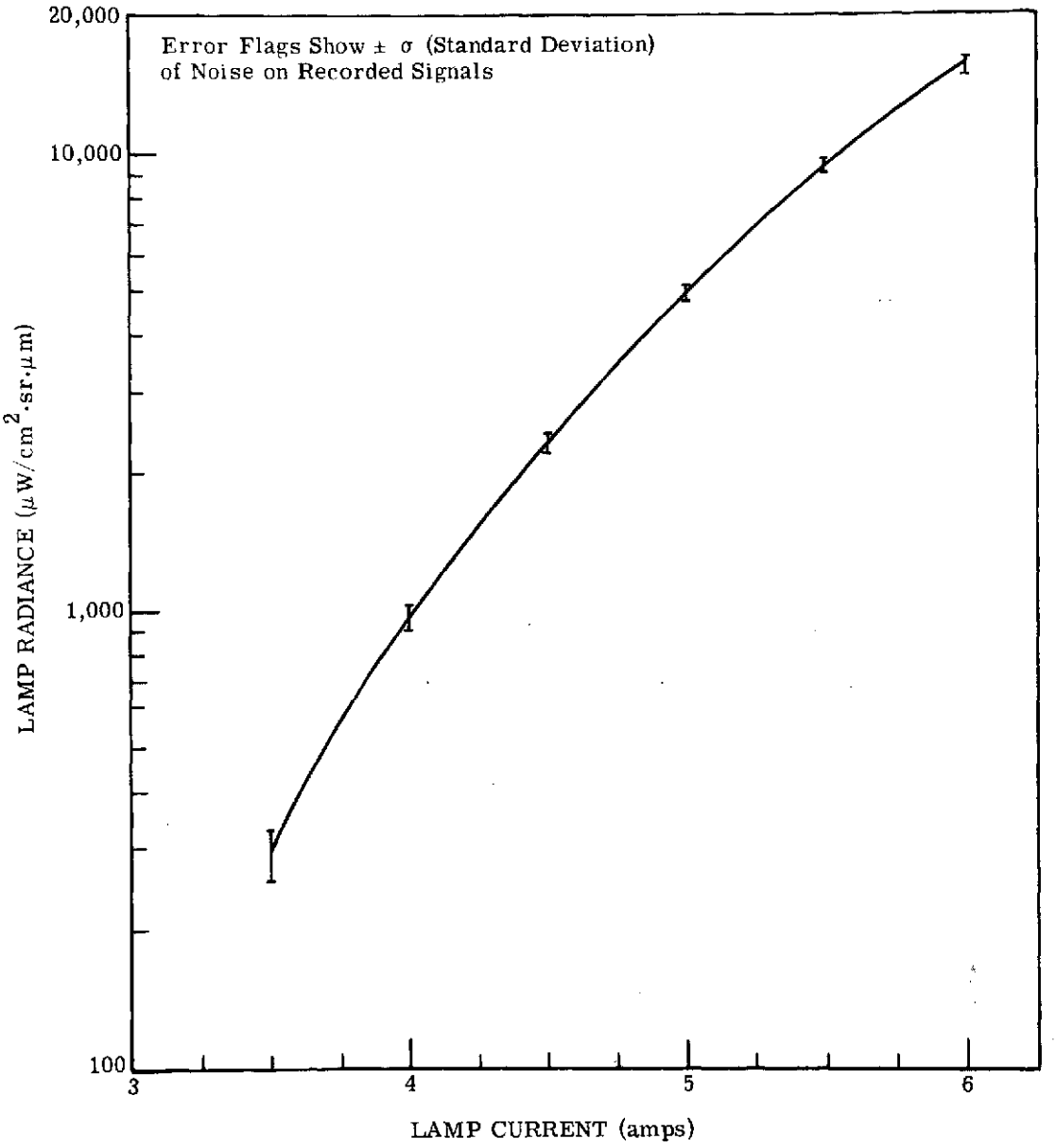

(e) Wavelength: 0.54 to 0.60 μm (C6)

FIGURE 35. INTERNAL LAMP TRANSFER STANDARD CALIBRATION 1 JUNE TO 30 DECEMBER 1972 (Continued)

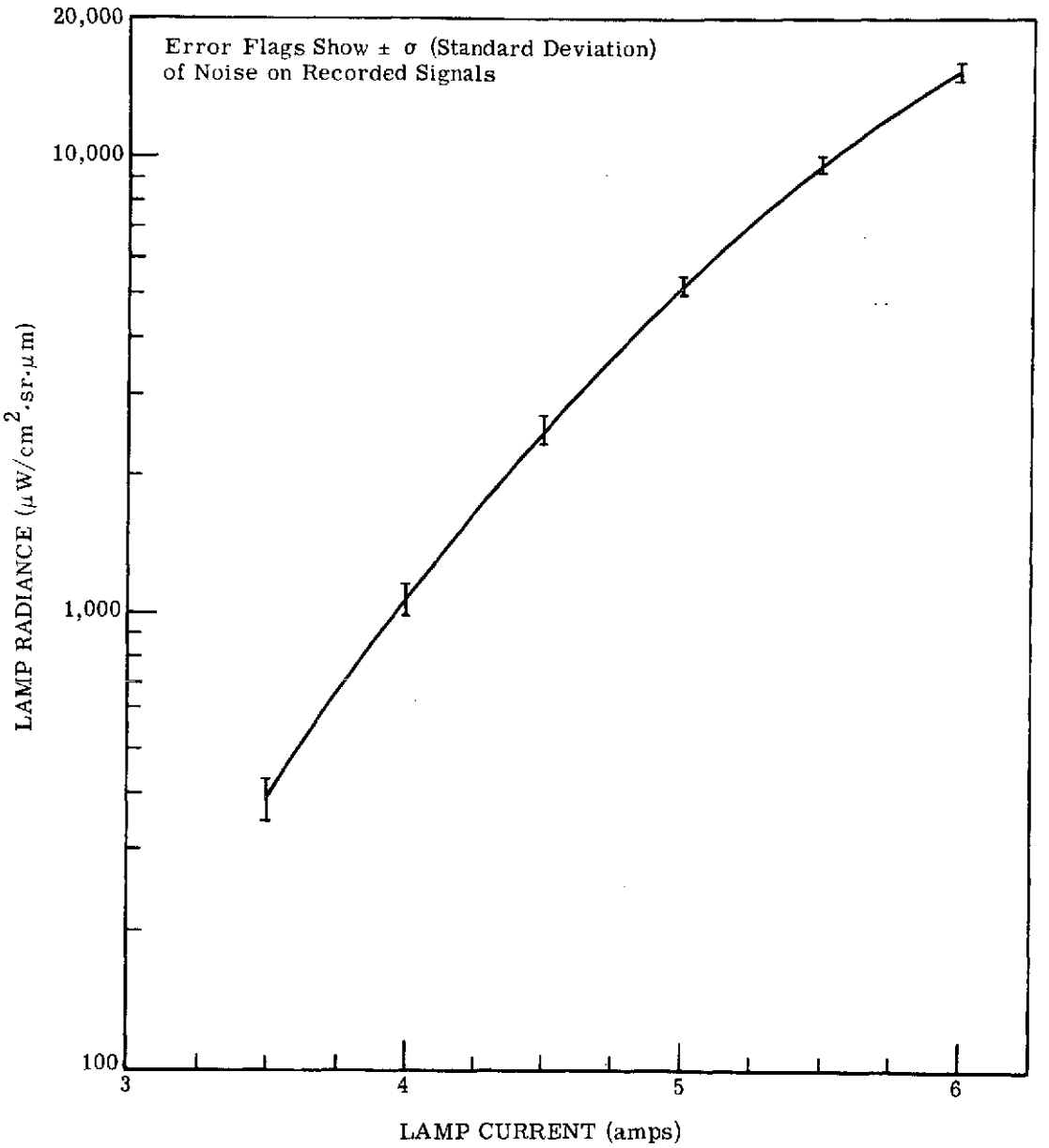

(f) Wavelength: 0.58 to 0.65 μm (C5)

FIGURE 35. INTERNAL LAMP TRANSFER STANDARD CALIBRATION 1 JUNE TO 30 DECEMBER 1972 (Continued)

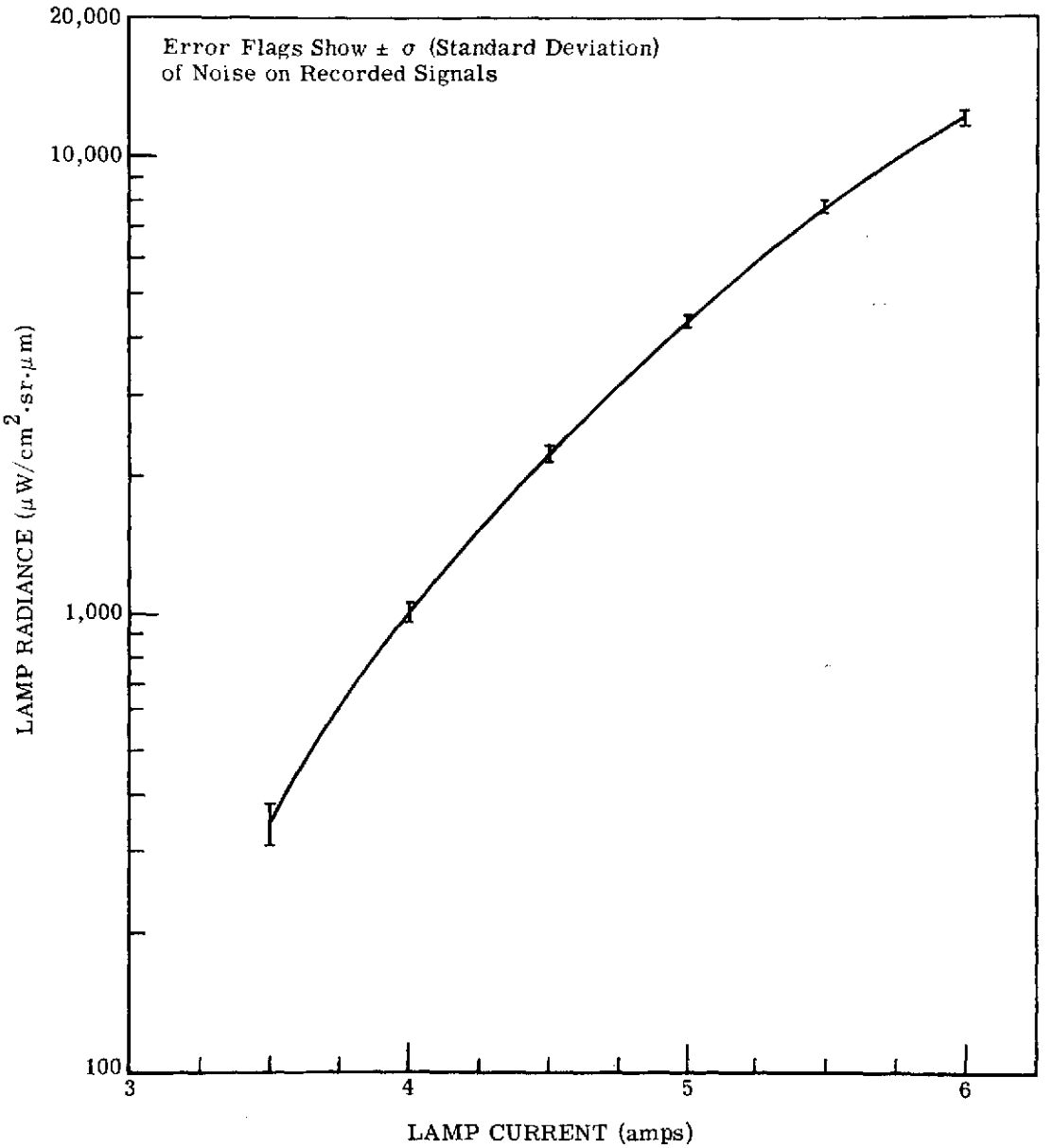

(g) Wavelength: 0.61 to 0.70 μm (C4)

FIGURE 35. INTERNAL LAMP TRANSFER STANDARD CALIBRATION 1 JUNE TO 30 DECEMBER 1972 (Continued)

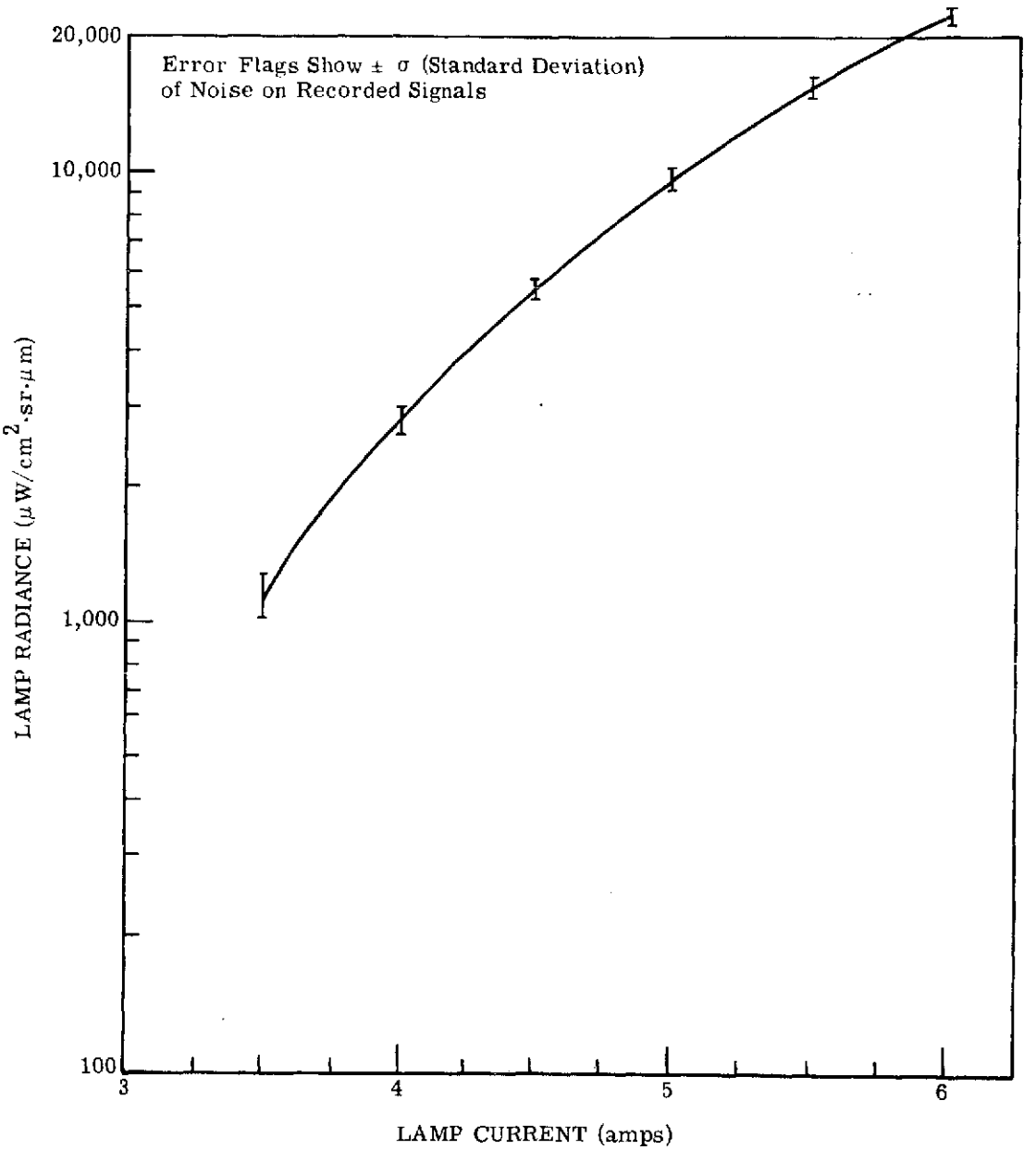

(h) Wavelength: 0.72 to 0.92 μm (C2)

FIGURE 35. INTERNAL LAMP TRANSFER STANDARD CALIBRATION 1 JUNE TO 30 DECEMBER 1972 (Continued)

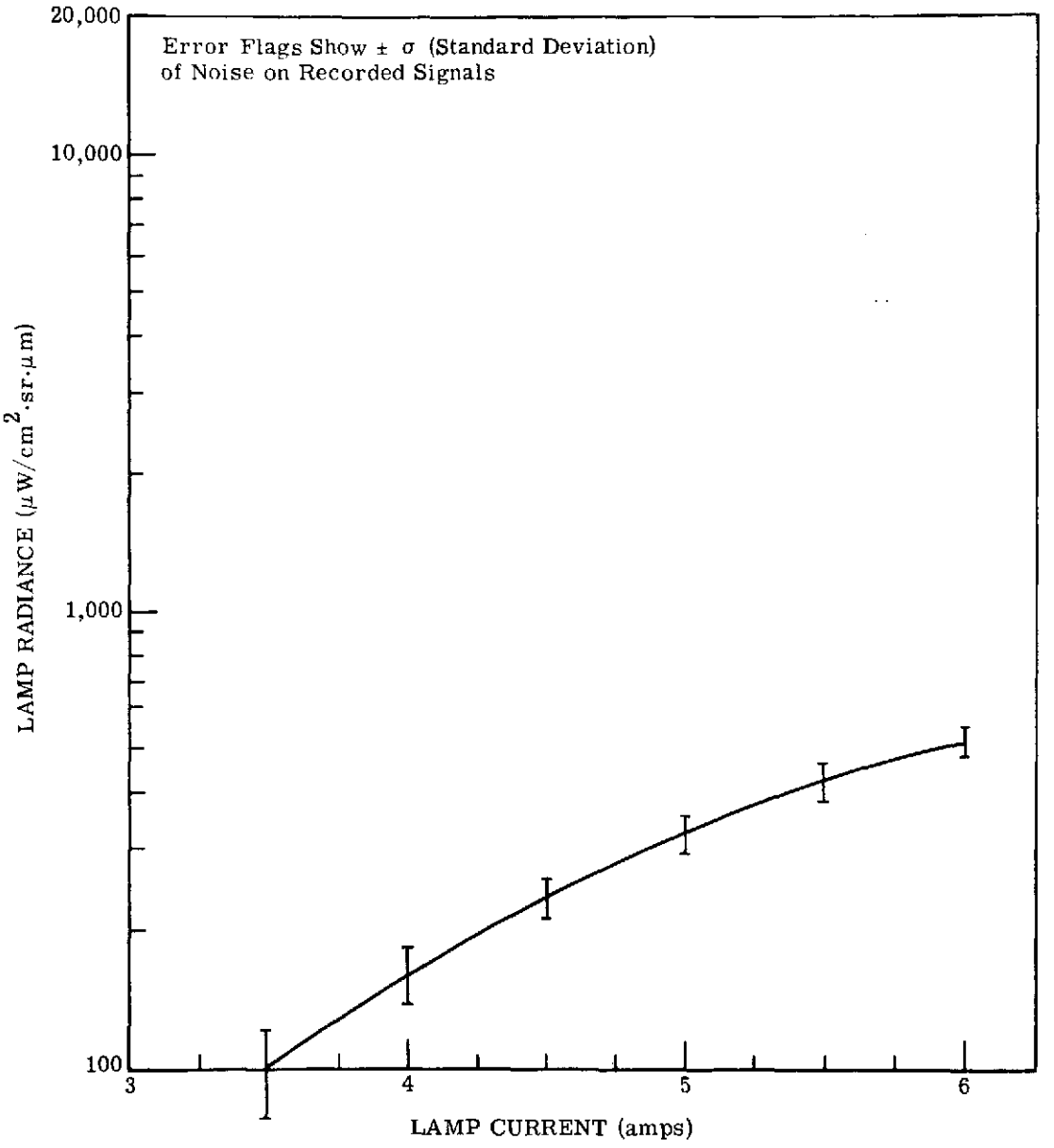

(i) Wavelength: 1.0 to 1.4 μm (D3)

FIGURE 35. INTERNAL LAMP TRANSFER STANDARD CALIBRATION 1 JUNE TO 30 DECEMBER 1972 (Continued)

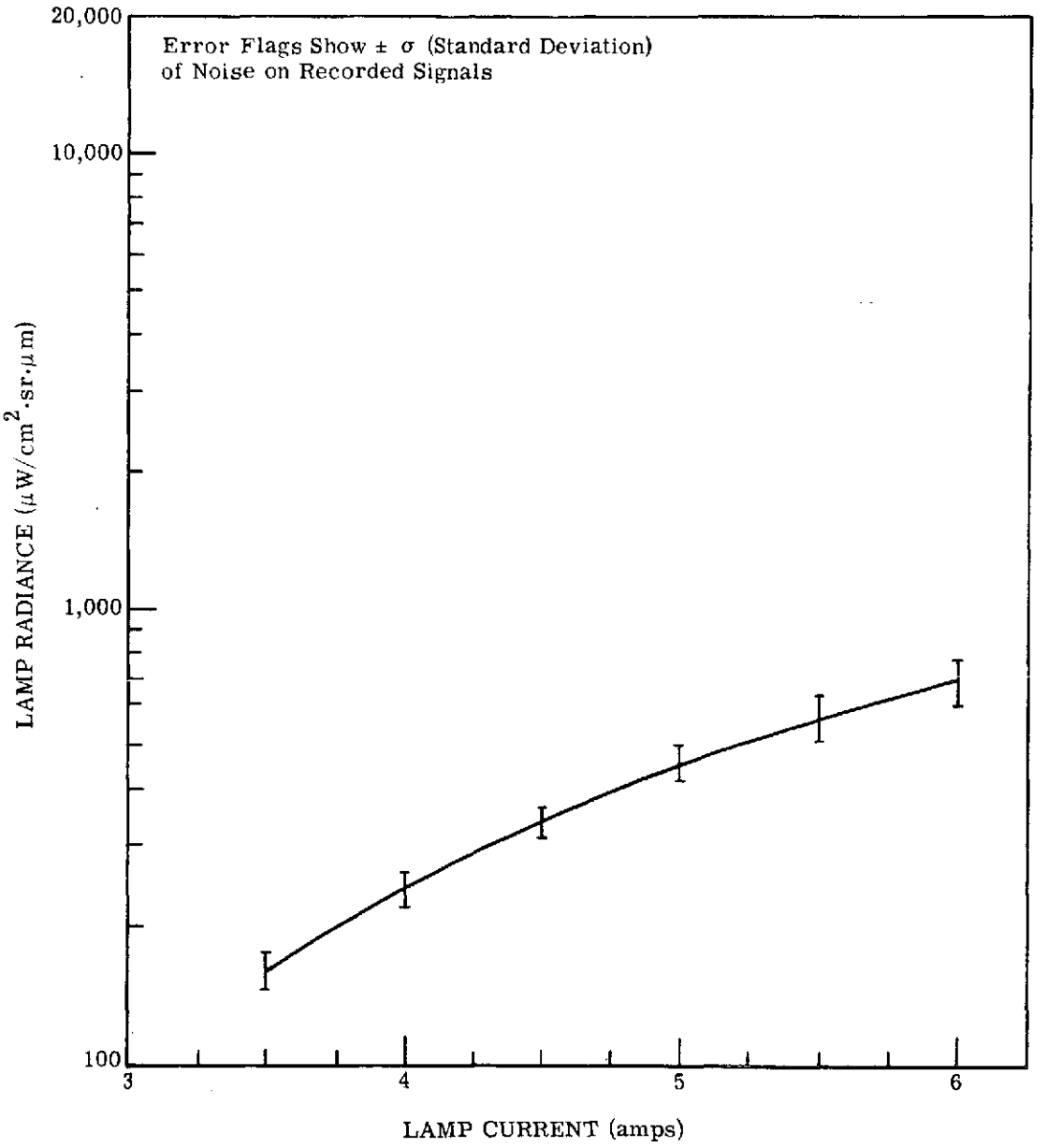

(j) Wavelength: 1.5 to 1.8 μm (D2)

FIGURE 35. INTERNAL LAMP TRANSFER STANDARD CALIBRATION 1 JUNE TO 30 DECEMBER 1972 (Continued)

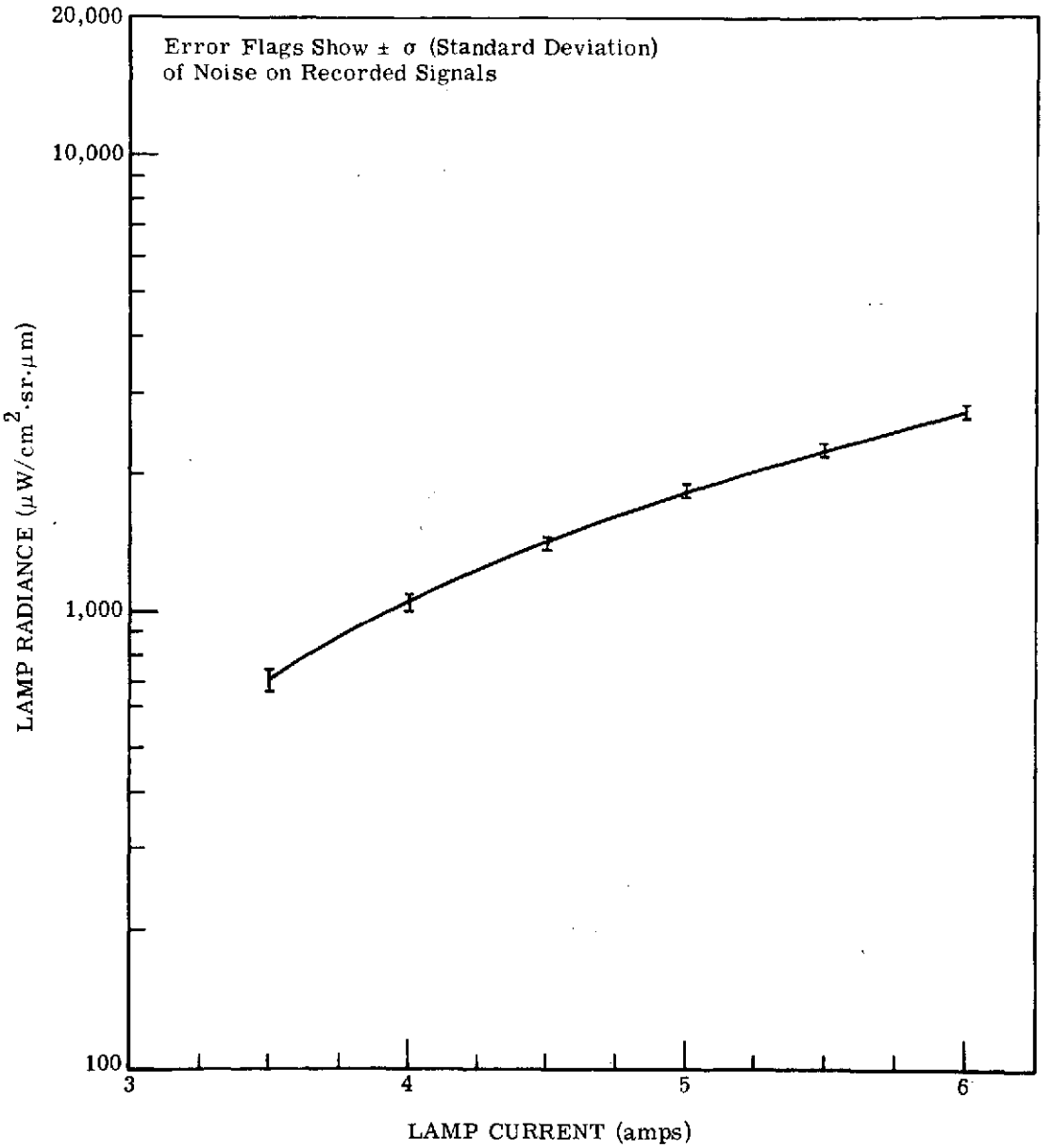

(k) Wavelength: 2.0 to 2.6 μm (D1)

FIGURE 35. INTERNAL LAMP TRANSFER STANDARD CALIBRATION 1 JUNE TO 30 DECEMBER 1972 (Concluded)

this band on dry days at the altitudes flown by the ERIM C-47 aircraft (i.e., 15,000 ft and below). No attempt was made to calibrate the reference plates at any band other than 9.3 to 11.7 μm.

The reference plates themselves, as described earlier, are copper plates which are thermoelectrically temperature controlled and spray-painted with a flat black paint. Although the surface temperatures are accurately controlled to within 0.1°C of the desired temperature by precision thermistors, these plates do not emit radiation as an ideal blackbody; this is primarily because of the emissivity of the flat black paint. Measurements made on this type of paint indicate an emissivity of approximately 0.94, which means that 6% of the radiation coming off a plate is reflected energy. Hence, for any plate temperature other than the surrounding ambient, the apparent plate temperature as seen by the scanner will be partly dependent on some reflected energy, and will not, in general, agree with the surface temperature as denoted by the thermistor.

Laboratory tests were made on the plates to measure the difference between surface temperatures and apparent temperatures. Strictly speaking, these measurements apply only to the ambient temperature conditions existing in the laboratory (approximately 22°-23°C) at the time of the measurements. However, the apparent temperature of the plates for any surface temperature can be calculated if the ambient temperature in the scanner housing is known. This is the prime reason for having an ambient plate as a reference.

Our measurements utilized YSI (Yellow Springs Instrument Company) precision thermistors imbedded in each plate to control the temperature through a feedback loop. These thermistors are calibrated to ±0.1°C over the range -50°C to +100°C. Calibration data giving the temperature vs. resistance relationship is shown in Table 6. The radiometric temperatures were obtained from a 20° FOV radiometer (Barnes PRT-5) calibrated against high emissivity (0.99) conical blackbodies. The result, shown in Fig. 36, is plotted as dial setting vs. plate temperature, where

$$\text{dial setting} = \frac{\text{thermistor resistance (in ohms)}}{100}$$

The dashed curve is the surface temperature as calculated from the thermistors, and the solid and dotted black curves are the apparent temperatures of the two plates. As can be seen, the reference plates are not perfect blackbodies; some correction for their emissivity is needed. The surface temperature curve does not cross the apparent curve at the ambient temperature existing in the lab (≈22°C), but instead crosses at approximately 35°C. This is because the radiometer head, being much warmer than the surrounding walls, increases the ambient temperature seen by the plates. The emissivity of the plates as indicated in Fig. 36 is approximately 0.95.

TABLE 6. TEMPERATURE VERSUS RESISTANCE FOR YSI PRECISION THERMISTOR

TEMPERATURE VERSUS RESISTANCE -50°C to +100°C									
TEMP (°C)	RES (Ohms)	TEMP (°C)	RES (Ohms)	TEMP (°C)	RES (Ohms)	TEMP (°C)	RES (Ohms)	TEMP (°C)	RES (Ohms)
-50	201.1K	-20	29.13K	+10	5971	+40	1598	+70	525.4
49	187.3K	19	27.49K	11	5692	41	1535	71	507.8
48	174.5K	18	25.95K	12	5427	42	1475	72	490.9
47	162.7K	17	24.51K	13	5177	43	1418	73	474.7
45	151.7K	16	23.16K	14	4939	44	1363	74	459.0
45	141.6K	15	21.89K	15	4714	45	1310	75	444.0
44	132.2K	14	20.70K	16	4500	46	1260	76	429.5
43	126.5K	13	19.58K	17	4297	47	1212	77	415.6
42	115.4K	12	18.52K	18	4105	48	1167	78	402.2
41	107.9K	11	17.53K	19	3922	49	1123	79	389.3
-40	101.0K	-10	16.60K	+20	3748	+50	1081	+80	376.9
39	94.48K	9	15.72K	21	3583	51	1040	81	364.9
38	88.46K	8	14.90K	22	3426	52	1002	82	353.4
37	82.87K	7	14.12K	23	3277	53	965.0	83	342.2
36	77.66K	6	13.39K	24	3135	54	929.6	84	331.5
35	72.81K	5	12.70K	25	3000	55	895.8	85	321.2
34	68.30K	4	12.05K	26	2872	56	863.3	86	311.3
33	64.09K	3	11.44K	27	2750	57	832.2	87	301.7
32	60.17K	2	10.86K	28	2633	58	802.3	88	292.4
31	56.51K	-1	10.31K	29	2523	59	773.7	89	283.5
-30	53.10K	0	9796	+30	2417	+60	746.3	+90	274.9
29	49.91K	+1	9310	31	2317	61	719.9	91	266.6
28	46.94K	2	8851	32	2221	62	694.7	92	258.6
27	44.16K	3	8417	33	2130	63	670.4	93	250.9
26	41.56K	4	8006	34	2042	64	647.1	94	243.4
25	39.13K	5	7618	35	1959	65	624.7	95	235.2
24	36.86K	6	7252	36	1880	66	603.3	96	229.3
23	34.73K	7	6905	37	1805	67	582.6	97	222.6
22	32.74K	8	6576	38	1733	68	562.8	98	216.1
21	30.87K	9	5265	39	1664	69	543.7	99	200.8
								100	203.8

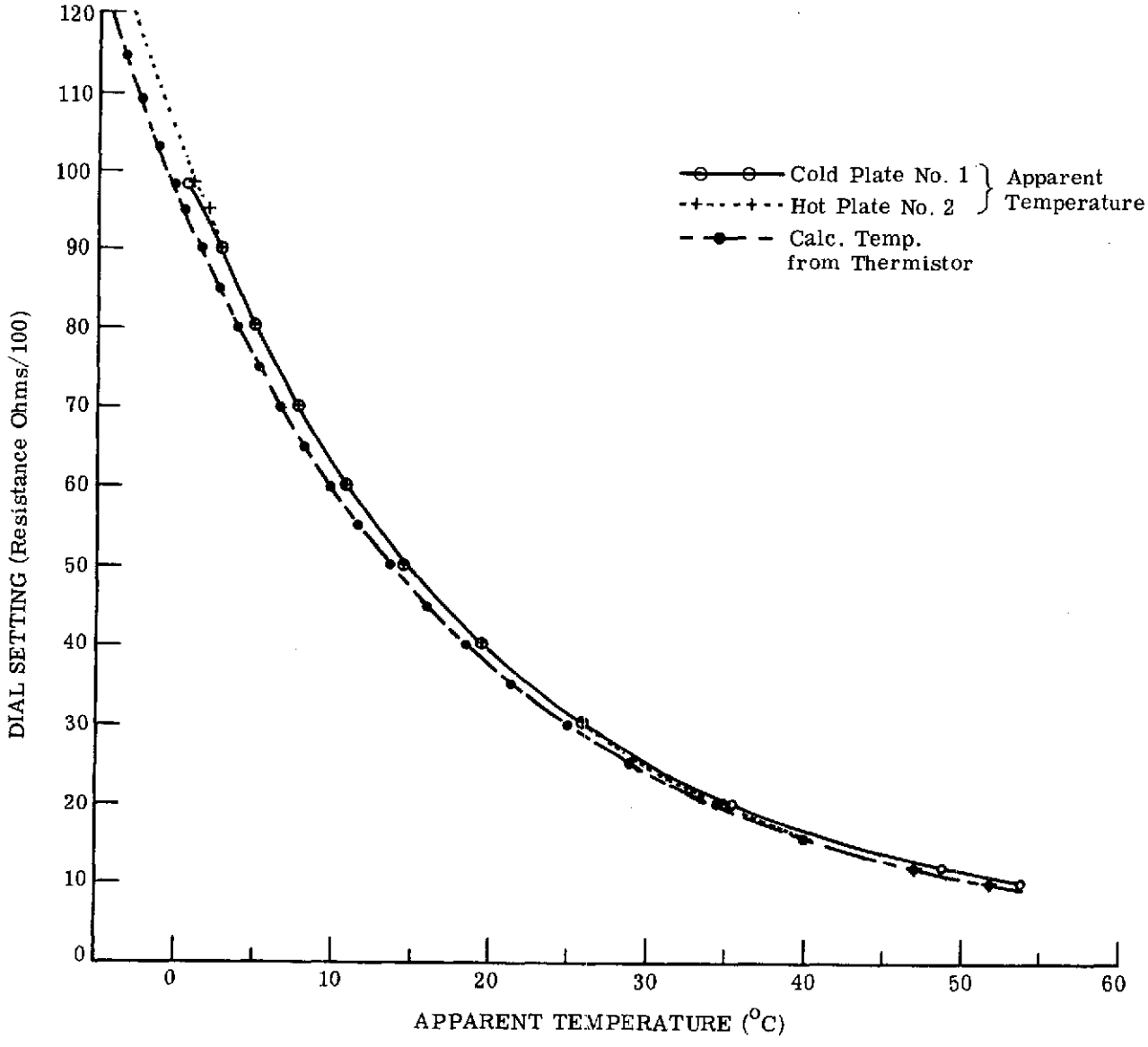

FIGURE 36. CONTROL PANEL SETTING VERSUS APPARENT TEMPERATURE (JANUARY 1972)

To a first approximation and, more exactly, for ambient housing temperatures around 35°C, the curve shown in Fig. 36 can be used to obtain the apparent plate temperature calibration points for any given thermistor control dial setting. Normally, the two temperature-controlled plates are adjusted, via oscilloscope display, to bracket the range of terrain signals viewed by the scanner. Terrain temperatures are then extracted later by interpolation between the apparent plate temperatures. Care must be taken, however, where there are plate temperature differences of more than 20°C because although the interpolation used is a linear procedure, the temperature vs. radiance relationship is not linear in the thermal region. Figure 37 shows this relationship at X = 10.5 μm. As can be seen, a linear approximation is possible over a range of 20°C, but larger errors would appear at ranges greater than 20°C.

For scanner housing temperatures other than 35°C, a correction to the apparent temperatures shown in Fig. 36 can be made. However, for most temperatures in the housing, the error in not making this correction is most likely to be not more than 0.5°C to 1.0°C. The housing's actual ambient temperature is calculated from the ambient plate, which has imbedded in it a YSI precision thermistor identical to the ones in the controlled plates. Because the controlled plates are tilted at an angle of 45° to nadir, the ambient temperature — as determined from the ambient plate — does not really indicate the true ambient radiation reflected by the controlled plates. Some radiation from the ground also is reflected off the plates and contributes to the ambient radiation coming from the inside surfaces of the scanner housing; its influence is small, however, and the effort required to measure it too great. So for all practical purposes the temperatures determined from the ambient plate are sufficient to make the necessary corrections.

6.1.2.2 Accuracy Test of Plate Calibration Temperature

As a check on the plate calibration performed in the laboratory, a test utilizing hot and cold water baths was devised to measure the scanner's overall temperature sensitivity and accuracy. Separate plastic ice chests containing heated and cooled water were placed side by side underneath the aircraft. The temperatures of these water baths were monitored constantly by both a thermometer and a PRT-5 radiometer. With the scanner running, water temperatures were also determined from the reference plates. These three results were compared for closeness.

Figure 38 shows an oscilloscope trace obtained in one of these tests. The important parameters and results of this temperature test are shown in Table 7.

As can be seen, the agreement between calculated and measured temperatures is excellent. Note that no corrections were made for the ambient housing temperature, since it is fairly close to the laboratory test conditions of 35°C and the atmosphere influence is negligible. Under

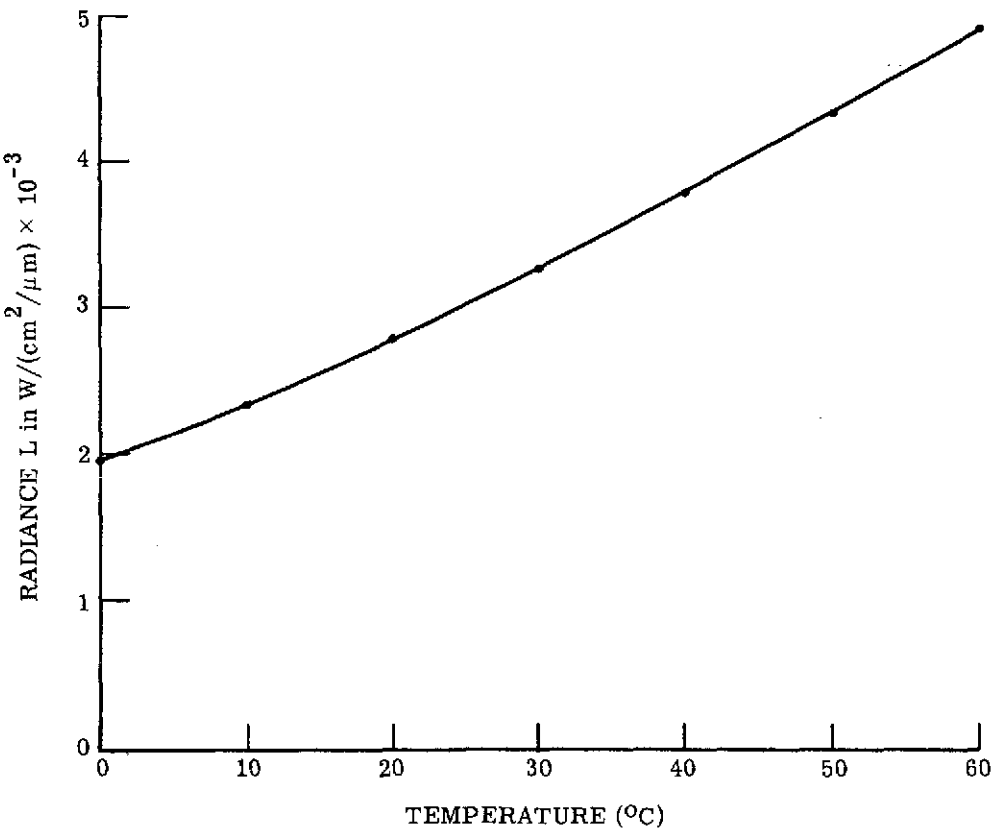

FIGURE 37. BLACKBODY TEMPERATURE VERSUS BLACKBODY RADIANCE (10.5 μm)

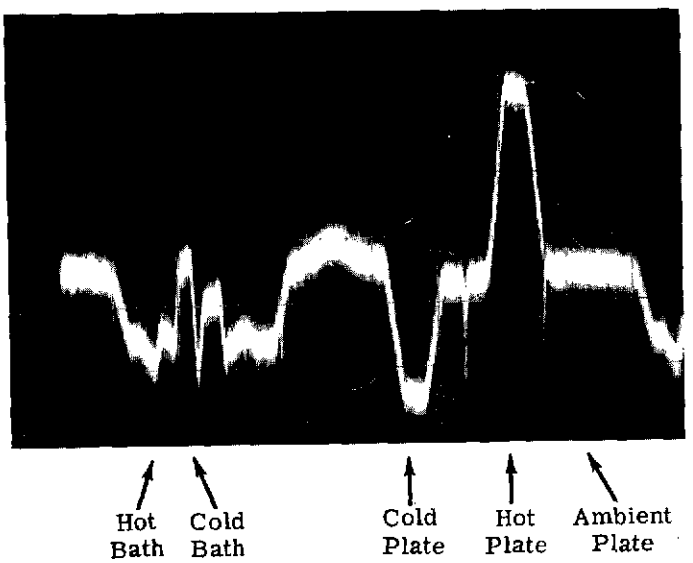

FIGURE 38. OSCILLOSCOPE TRACE OF 9.3 to 11.7 μm BAND IN M7 SCANNER DURING THERMAL CALIBRATION

TABLE 7. RESULTS OF THERMAL CALIBRATION TESTS IN 9.3-11.7 μm BAND

Cold plate ref. temp. = 24.1°C*
Hot plate ref. temp. = 33.7°C*
Ambient plate ref. temp. = 28.5°C*

	Thermometer	PRT-5	Scanner
Hot bath	28.3°C	28.3°C	28.4°C
Cold bath	27.2°C	26.9°C	27.2°C
Ambient plate	--		28.1°C

*Obtained by thermistor measurement.

actual flying conditions, however, both of these effects would have to be considered to obtain anything approaching the accuracy shown above.

6.1.2.3 Noise Equivalent Temperature Measurements

NEΔT information was also obtained from the data gathered in the previously described experiment. Generally speaking, NEΔT is defined as the temperature difference required by the thermal detector to obtain an RMS noise voltage to signal voltage difference ratio of unity. Experimentally, this is obtained according to the following relationship:

$$NE\Delta T = (T_2 - T_1)\left(\frac{V_{N,RMS}}{V_{T_2} - V_{T_1}}\right)$$

where T_2 = temperature of plate 2

T_1 = temperature of plate 1

V_{T_2} = signal voltage of plate 2

V_{T_1} = signal voltage of plate 1

$V_{N,RMS}$ = RMS noise voltage of either plate 2 or plate 1

The noise value $V_{N,RMS}$ is, of course, dependent on the electronic bandwidth of the system. More specifically, it varies inversely with the square root of the bandwidth for a flat spectral density condition. For the test case depicted in Fig. 38, the bandwidth was preamplifier-limited to approximately 240 kHz. However, in most cases the system is tape-recorder-limited to approximately 96 kHz. Hence, the actual NEΔT encountered in normal operation is found (from Fig. 38) to be

$$NE\Delta T = 9.6^{\circ}C \times \frac{0.015\ V}{0.80\ V} \times \frac{\sqrt{96}}{\sqrt{240}}$$

$$NE\Delta T = 0.11^{\circ}C$$

It should be mentioned that the noise voltage, $V_{N,RMS}$, was obtained from the peak-to-peak noise voltage by assuming a Gaussian noise distribution and a peak factor of 8 dB (which corresponds to peak/RMS ratios of 2.6).

6.2 SPECTRAL CALIBRATION

Any attempt to identify an object by its spectral characteristics obviously requires an accurate description of the spectral throughput of the measuring instrument. In the case of the M7 scanner, only the 12-channel spectrometer lends itself easily to this kind of measurement. The detectors used in the other two positions, i.e., near-IR and thermal, use bandpass filters which are an integral part of the detector. Once the filter-detector characteristics are deter-

mined (they are well-documented upon purchase), there is little need to measure the spectral characteristics unless, of course, some type of trouble is suspected, such as light leakage, etc. The 12-channel spectrometer, on the other hand, uses light pipes on the output of a dispersing prism to obtain the required bandpasses, and is considerably more subject to vibrations, misalignment, etc. Primarily for this reason, considerable effort is made to maintain an up-to-date spectral calibration.

The spectral calibration of the 12-channel spectrometer was accomplished by mounting the whole scanner assembly, including spectrometer, on a collimator (Fig. 39a). The collimator consists of a large, 20-in.-diameter parabolic mirror with a 100-in. focal length. The exit slit of a monochromator, serving as a source of known wavelength, sits at the focus of the spherical mirror. The collimated beam is then directed to illuminate the aperture of the scanner. We found that the image of the monochromator exit slit filled the entire scanner aperture. But because this image did not fill the instantaneous field of view, calibration became necessary with the scanner operating so that the collimated beam was scanned across the field of view which was thus filled on the average.

For this calibration, the entrance slit of the monochromator was illuminated by the image of a quartz-iodine lamp. The wavelength scale of the monochromator itself had been calibrated using mercury, potassium, sodium, cadmium, and cesium spectral lamps, a helium-neon laser, and various narrowband filters.

The relative spectral response of the 12-channel spectrometer is shown in Fig. 39b. Unless otherwise noted, all wavelength bands are described by their 10% response points.

6.3 SPATIAL RESOLUTION AND REGISTRATION

Spatial resolution measurements were performed on the M7 scanner using the collimator described in Section 4.2 and pictured in Fig. 17. Purposes of these measurements were not only to verify the spatial resolution against its calculated value but also to provide an overall check on the alignment of the components in the optical system, including registration in all detector positions. The targets placed near the focal plane of the collimator were blackened panels, each with three rectangular holes near its center.

A number of such targets were constructed with the widths of the holes and spacing between them varied to provide 0.5, 1, 2, 4, 10, and 20 mrad targets for imaging in the detector plane of the scanner. For a 100-in. focal length parabolic mirror and a 2-mrad target, calculations show that a hole width and spacing of 0.2 in. is needed. All the other targets were dimensioned proportionately.

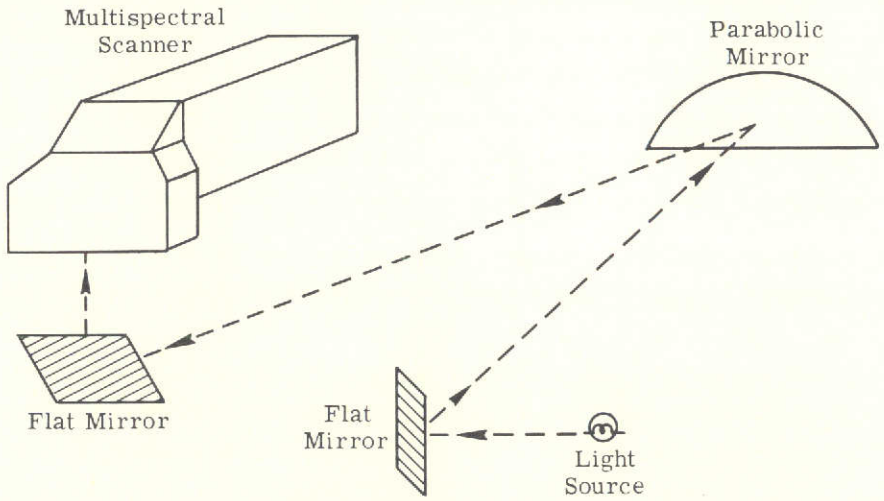

(a) Schematic of Collimator Assembly

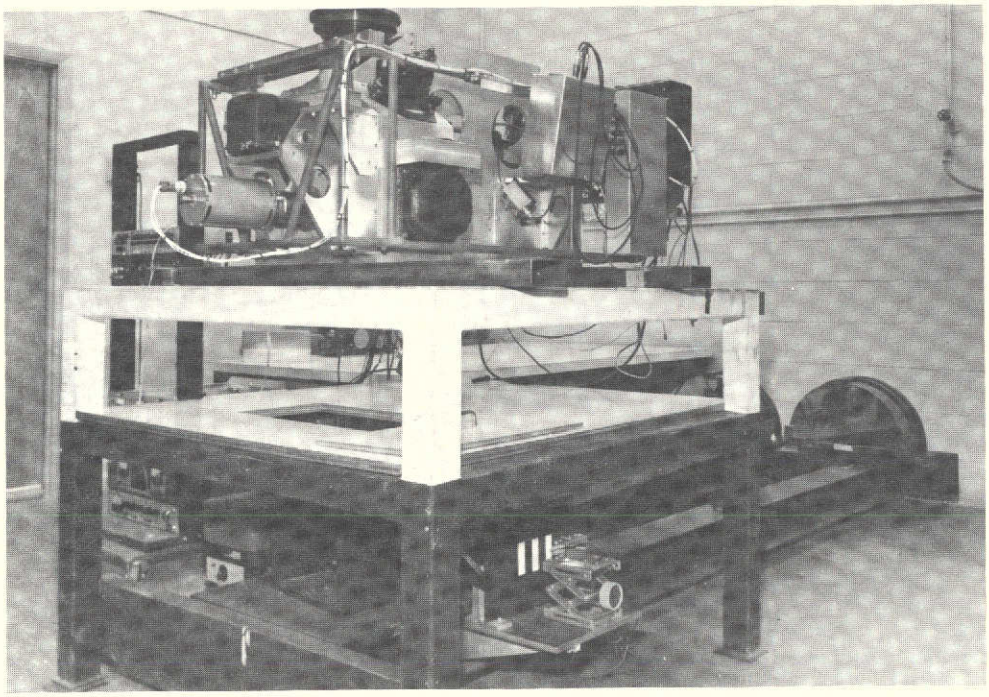

(b) Laboratory Collimator

FIGURE 39. COLLIMATOR FOR SPECTRAL CALIBRATION OF THE 12-CHANNEL SPECTROMETER

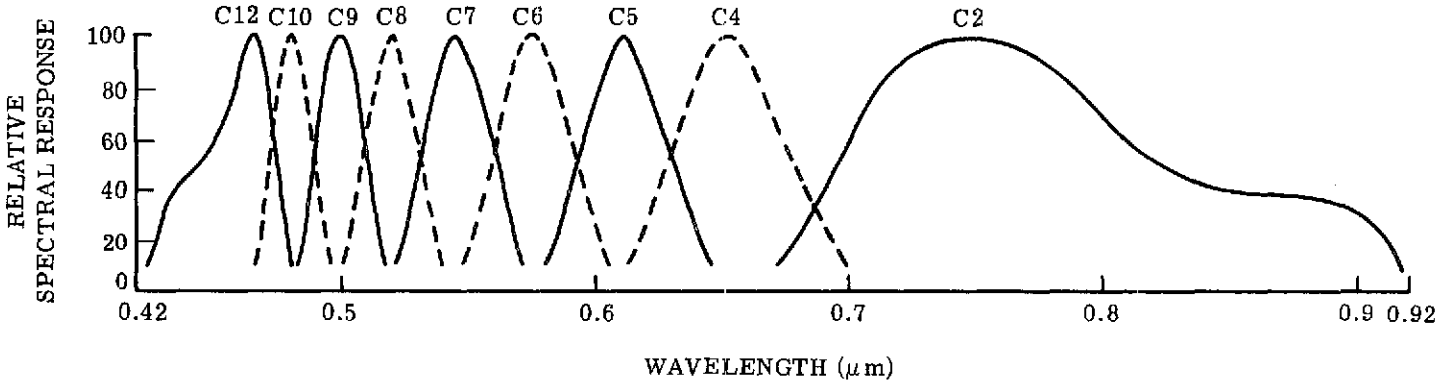

(c) Relative Spectral Response of M7 Spectrometer

FIGURE 39. COLLIMATOR FOR SPECTRAL CALIBRATION OF THE 12-CHANNEL SPECTROMETER
(Concluded)

In the actual measurements, the targets were not placed in the focal plane but 0.5 in. from it, so that the target images appeared to be at 1650 ft from the scanner rather than at infinity. An extended source was placed behind the targets to illuminate the holes, although, as may be noticed in the figures which follow, the holes are not always illuminated uniformly.

The pictures shown in Fig. 40 were obtained with a scope bandwidth of 100 kHz and amplifier bandwidths ranging between 100 kHz and 500 kHz. Hence the resolution shown represents primarily the optical resolution, although the associated electronics have some marginal effect. This is not the resolution, however, that one could expect from data recorded on a tape machine, since in many cases the bandwidths in recording and playback are considerably less than those described above (see Section 5.1). These more stringent bandwidth limitations would have to be accounted for before an overall resolution could be assigned to the imagery. Since the main objective was to determine overall performance of the optical system, the performance evident in Fig. 40a, b, and c is perfectly satisfactory for our purposes.

As well as can be determined from the photographs, a resolution of approximately 2 mrad is obtained from the spectrometer and near-IR detectors, while the HgCdTe 1-3 thermal detector has a resolution of approximately 3 mrad.

Ideally, for a system with an optical resolution of X mrad, an X mrad target would appear as a triangle of half-width X mrad. Of the three detector resolutions shown, only that in Fig. 40a, which is representative of all nine spectrometer channels, appears to be almost perfectly triangular. The other two show some rounding off at the peaks and valleys, indicating a modular transfer function of less than 100%. Their resolutions can be approximated from the photographs, however, and are as given above. The amplitude unevenness discernible in Figs. 40a and b is attributable to a nonuniform extended source.

The different detectors available and their resolutions are listed in Table 2 (Section 2). The prime criteria in determining spatial resolution (neglecting optical aberration and electronic bandwidth limitations) are (1) the focal length of the detector position and (2) detector size. This can be shown from the lens equation and Fig. 41.

The resolution of the optical system pictured in Fig. 41 is defined as the angle θ.

For θ very small (as is usually the case for most scanners),

$$\theta = \frac{D'}{h} \tag{12}$$

From the lens equation,

$$\frac{1}{f} = \frac{1}{h} + \frac{1}{i} \tag{13}$$

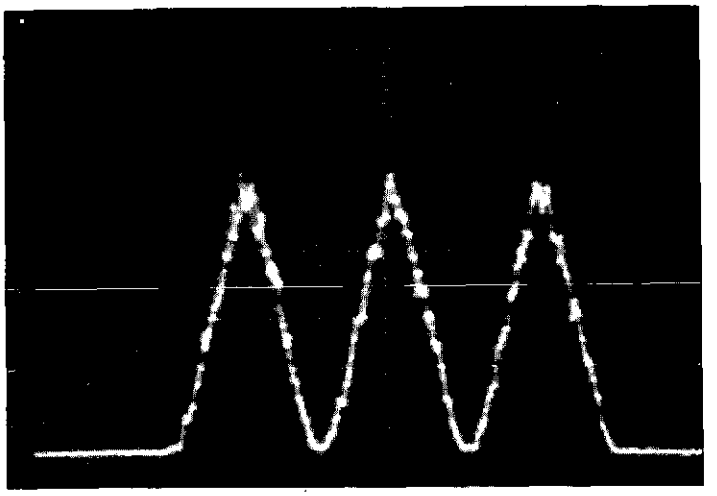

5 μsec/cm^2
2 mrad Target

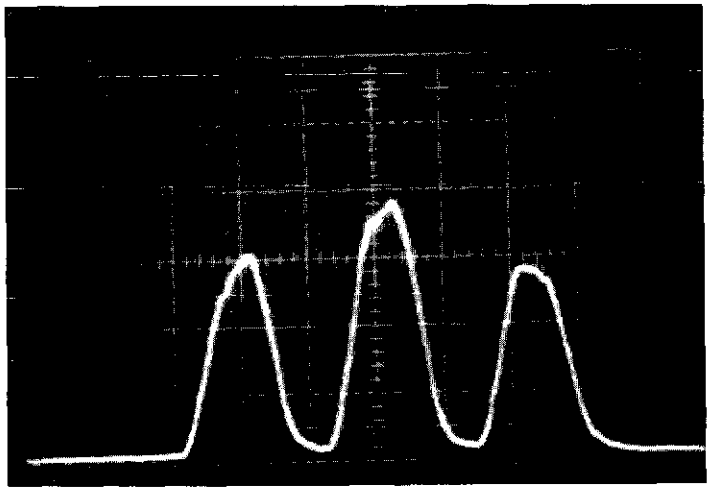

10 μsec/cm
4 mrad Target

(a) Channel 4, 0.52 to 0.57 μm, 100 kHz Bandwidth

FIGURE 40. OSCILLOSCOPE TARGET RESPONSES

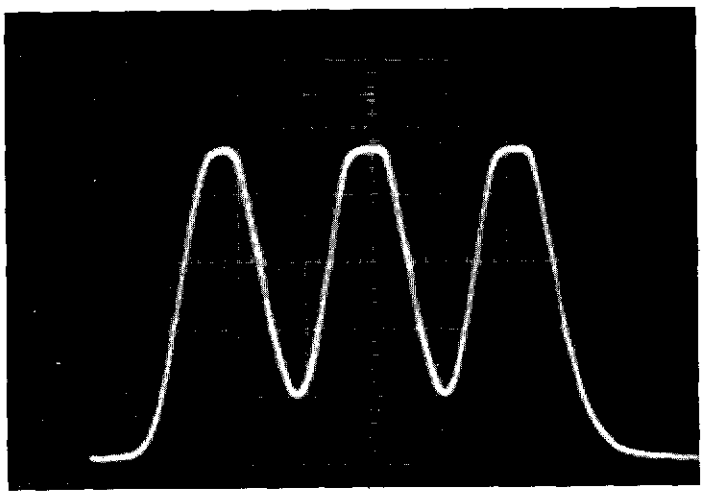

5 μsec/cm
2 mrad Target

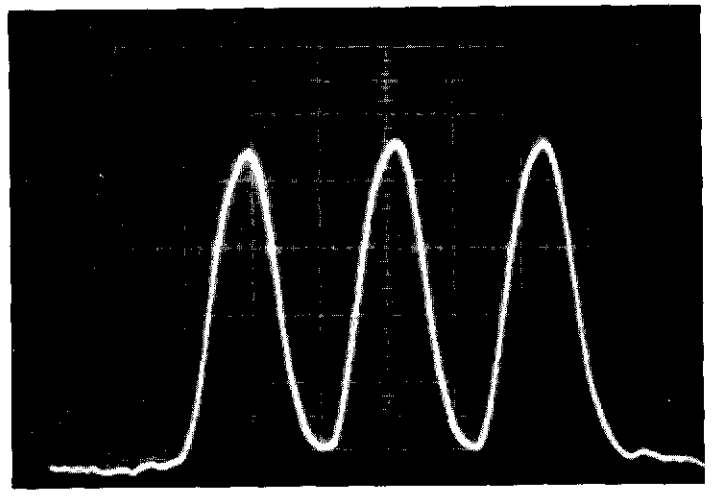

10 μsec/cm
4 mrad Target

(b) HgCdTe 1-3, 9.3 to 11.7 μm, 100 kHz Bandwidth

FIGURE 40. OSCILLOSCOPE TARGET RESPONSES (Continued)

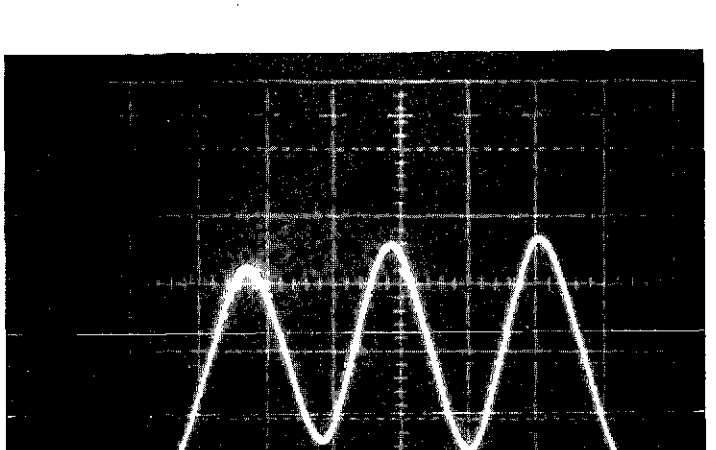

5 μsec/cm
2 mrad Target

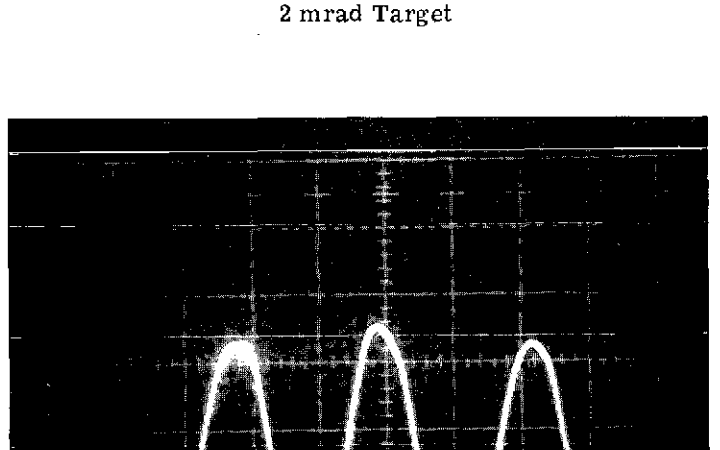

10 μsec/cm
4 mrad Target

(c) InSb 3-6, 2.0 to 2.6 μm, 100 kHz Bandwidth

FIGURE 40. OSCILLOSCOPE TARGET RESPONSES (Concluded)

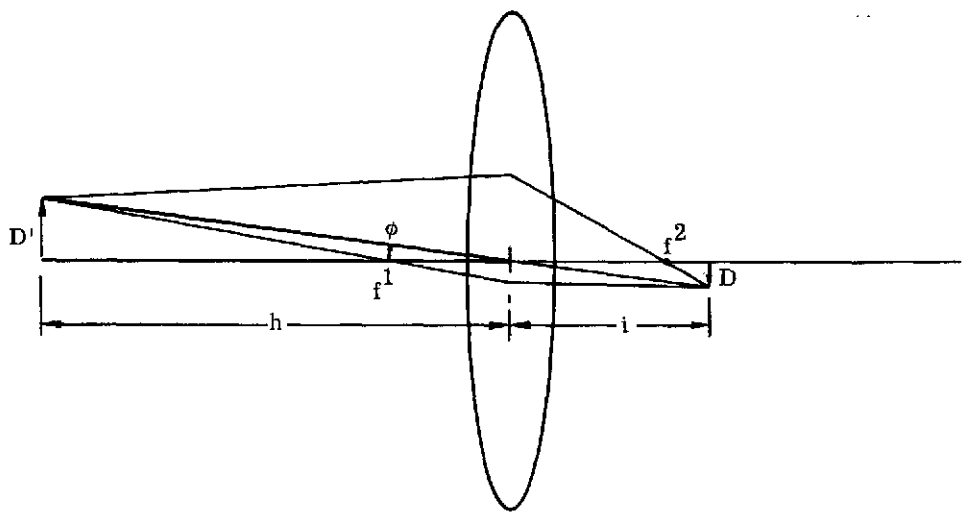

FIGURE 41. SIMPLIFIED SCANNER OPTICAL SYSTEM. Detector (D) and image of detector (D') on ground at height (h).

it can be shown that the magnification of D is given by

$$m = \text{magnification} = \frac{-D}{D'} = \frac{-i}{h} \tag{14}$$

However, for most scanning systems, $0 \gg i$ and from Eq. (13), we get

$$\frac{1}{f} = \frac{1}{h} + \frac{1}{i}, \quad \therefore i \simeq f$$

Re-writing Eq. (14)

$$\frac{-D}{D'} = \frac{-f}{h} \tag{15}$$

Re-arranging Eq. (15) and combining with Eq. (12), we get

$$\theta = \text{optical resolution} = \frac{D}{f} \text{ (in radians)} \tag{16}$$

where f = focal length of lens system

D = detector size

For example, the spectrometer in the M7 scanner (at Position 3) has a 20-in. focal length and 0.040-in. × 0.040-in. detector elements. Using Eq. (16), we get

$$\text{optical resolution} = \frac{0.040 \text{ in.}}{20 \text{ in.}} = 0.002 \text{ radians} = 2 \text{ mrad}$$

Hence, the resolution of the spectrometer should be 2 mrad × 2 mrad, which is also the value obtained experimentally. In general, as the detectors get larger in a fixed-focal-length system, the optical resolution also increases. The three detectors mentioned earlier are used most often, however, and represent the typical spatial resolutions to be expected from the M7 scanner. Figure 42 shows the superposition of these detector images on the ground at the nadir.

6.4 SCAN ANGLE AND POLARIZATION RESPONSE

Ideally, the M7 scanner's throughput should be independent of both scan mirror orientation and target signal polarization. From a practical standpoint, however, such independence is not simple to obtain since the number and variety of different components in such a complex and tightly toleranced optical system as a scanner preclude the assumption. Yet on the other hand, reliable application of data processing techniques to any earth resources problem requires that all systematic errors in the data be removed or, at a minimum, be documented for later removal. For this reason, we made an effort to measure system performance with respect to these two parameters. Results of these tests are discussed below.

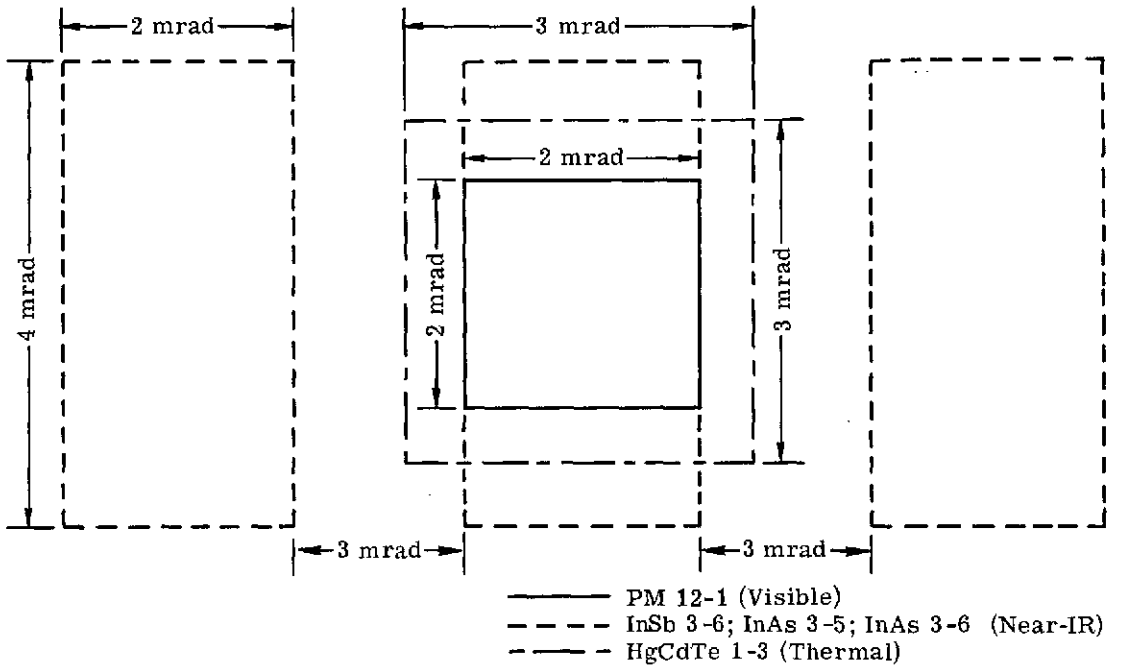

FIGURE 42. SUPERPOSITION OF RESOLUTION ELEMENTS AT NADIR FOR THREE DETECTORS IN M7 SCANNER

6.4.1 ANGULAR RESPONSE

The angular responsivity of the scanner was measured by means of the test fixture depicted in Fig. 43a and b. The scanner views a diffuse reflector (in this case a flame-sprayed aluminum plate) illuminated in an approximately uniform manner by two quartz-iodine lamps (identical to the type used as NBS standards) positioned out of the direct view of the scanner (Fig. 43c). Analyzing this configuration, we derived an expression for the illumination at any one spot on the panel; lamp geometry was then optimized to produce a maximum nonuniformity of less than 1.0% across the panel between lamps. Measurements were also taken to make sure that unpolarized light was being reflected off the surface (see Section 6.4.2). The test rig enabled the illuminated surface, which filled the entire field of the scanner, to be moved along an arc of constant radius from the scan mirror axis, permitting the response of the scanner to be measured as a function of scan mirror angle. The track for the light source dolly is shown in Fig. 43d. For this particular test, the scanner was mounted in its normal position so that nadir was located at 0°. All subsequent angle measurements were made with respect to nadir.

The output of a given detector was recorded as a time-exposed picture of an oscilloscope trace specially calibrated such that 1 cm on the abscissa represents a 20° interval in scan angle. Each channel was normalized to the same signal strength at 0° and filtered with a bandpass filter of 1 kHz. All nine spectrometer channels in Detector Position 3 (Fig. 4) and two near-IR channels in Position 2 were measured in this manner. Detector Position 1 was measured with a thermal detector and an electrically heated black plate substituted for the flame-sprayed aluminum panel and lamps. Results of these measurements are presented in Fig. 43e. Since any angular variation in responsivity should be associated with primarily geometric effects in the detector and associated optics, we did not investigate all available detector channels, filters, and positions.

As can be seen from Fig. 43e, the maximum increase in response of approximately $\pm 4\%$ occurs in the spectrometer position (Position 3) at any scan mirror angle between -45° and -50°. Variation is negligible from the right side to approximately 30° on the left in all nine spectrometer channels. Detector Positions 1 and 2 show a practically constant radiation throughput as a function of mirror angle.

6.4.2 POLARIZATION SENSITIVITY

Measurement of the M7 scanner's sensitivity to the polarization of incoming radiation is not a straightforward task, since the orientation of the irradiation electric vector for maximum scanner responsivity can be a function of scan angle. Moreover, the scanner's sizeable collecting aperture (5 in.) presents problems in providing a uniformly polarized source large enough to entirely fill the scanner's field-of-view. These problems were solved, for the most

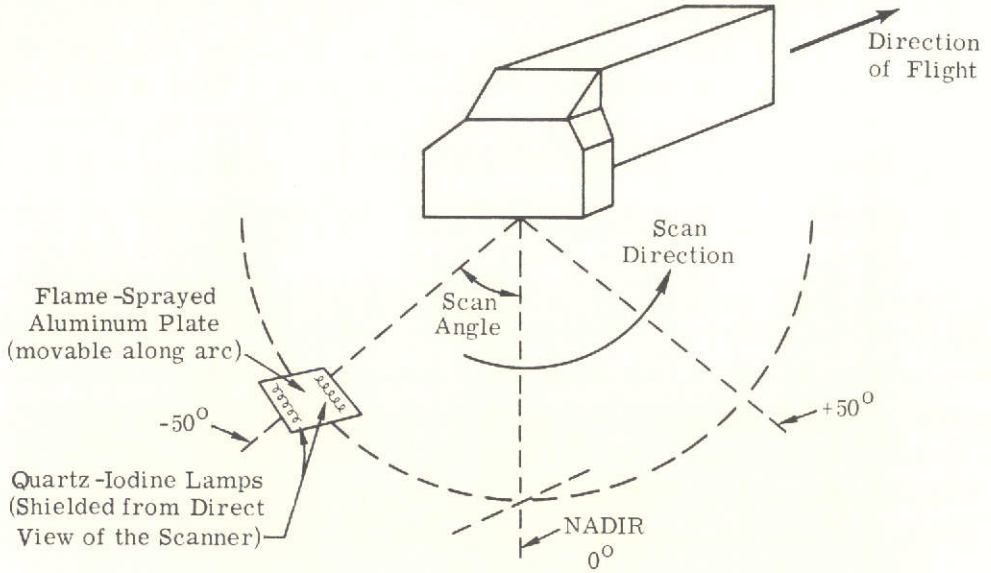

(a) Schematic of Angular Response Test Fixture

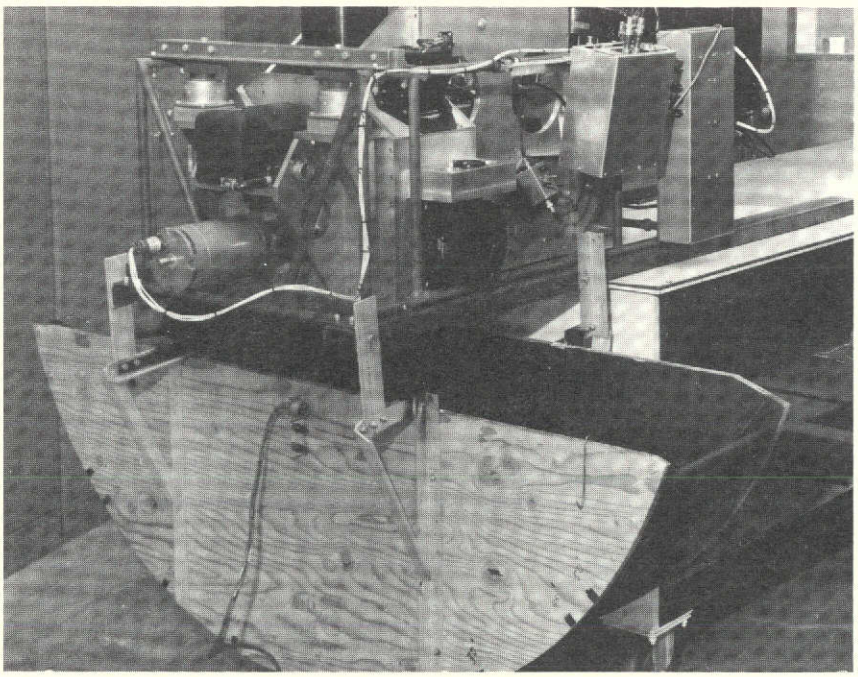

(b) Photograph of Actual Test Fixture

FIGURE 43. MEASUREMENT OF ANGULAR RESPONSIVITY

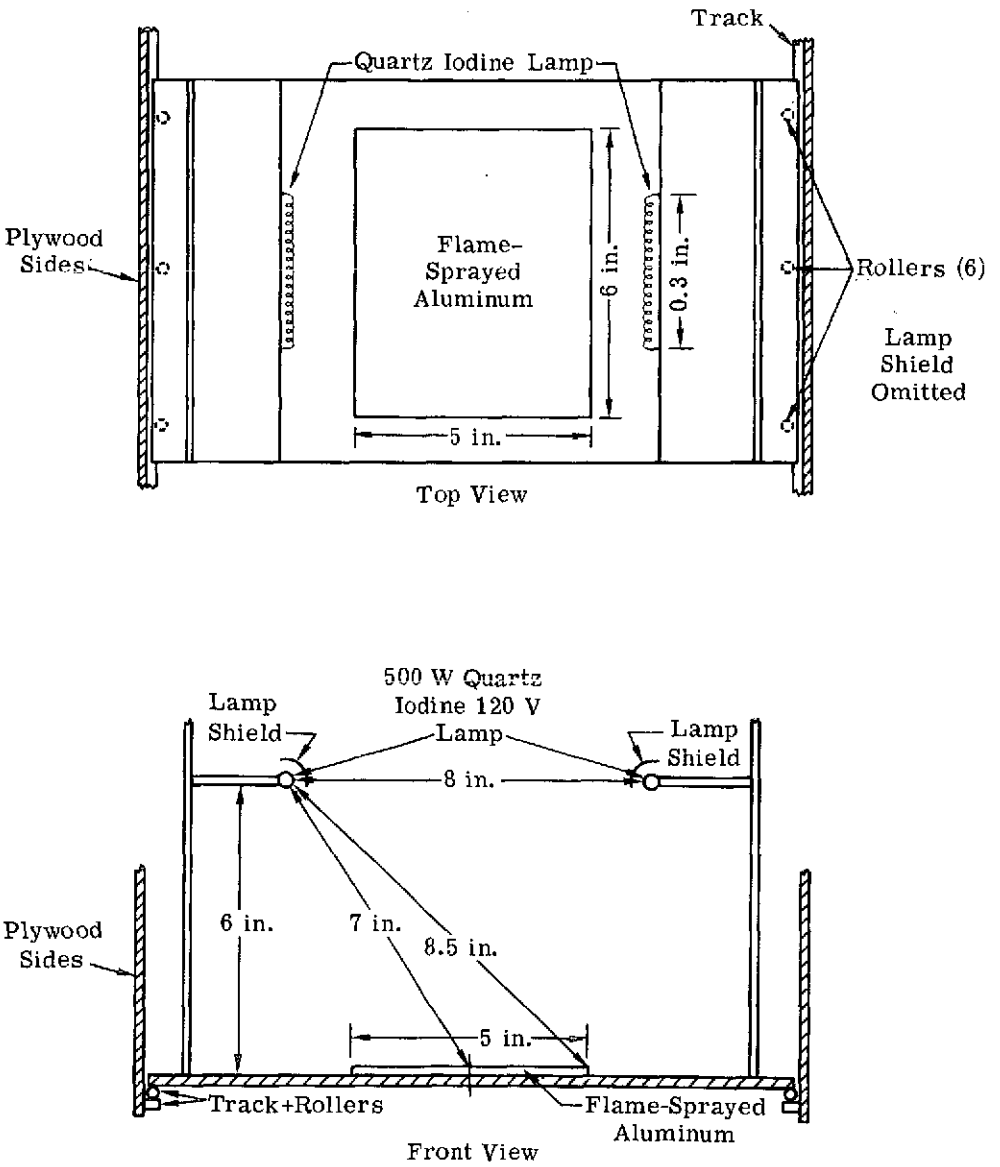

(c) Light-Source Carriage

FIGURE 43. MEASUREMENT OF ANGULAR RESPONSIVITY (Continued)

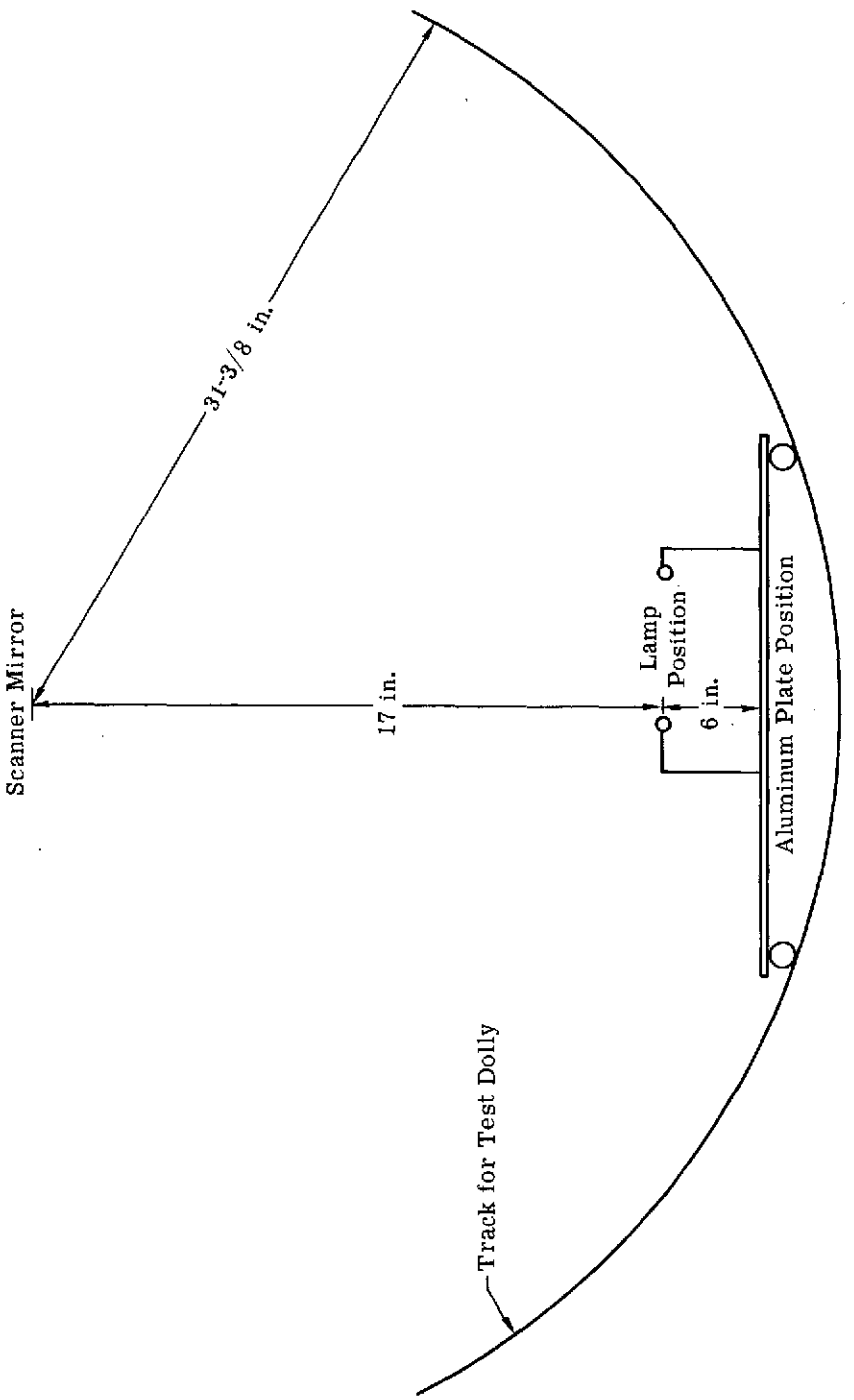

(d) Track for Light Source

FIGURE 43. MEASUREMENT OF ANGULAR RESPONSIVITY (Continued)

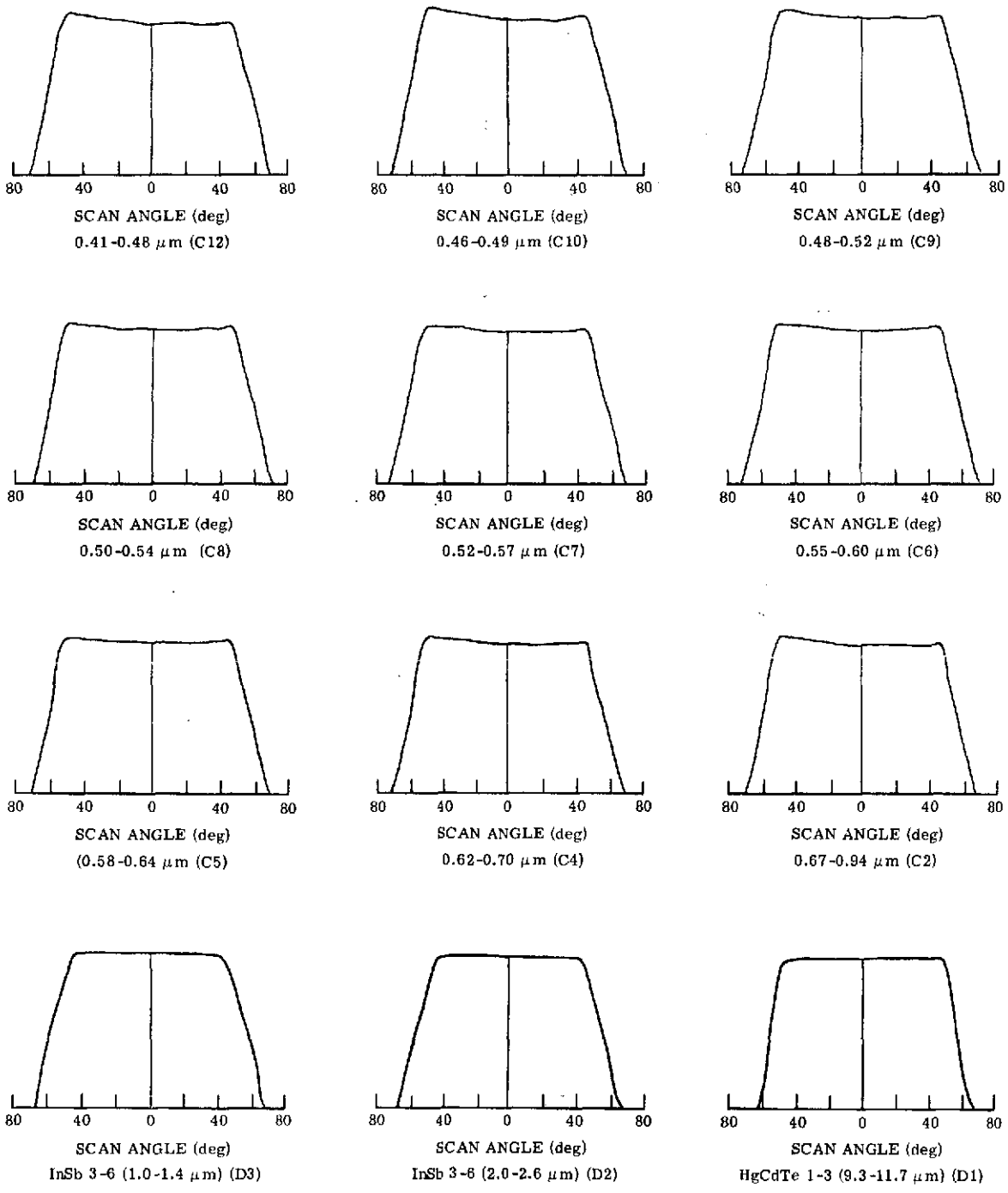

(e) Channel Responses

FIGURE 43. MEASUREMENT OF ANGULAR RESPONSIVITY (Concluded)

part, by using the jig constructed for the angular responsivity tests reported in Section 6.4.1. An adaptor was made (see Fig. 43a) to fit between the flame-sprayed aluminum panel and the scanner. This linearly polarized the light reflected off the panel and, at the same time, shielded the scanner from any stray radiation. Conventional 12 × 12-in. sheets of Polaroid types HN22 and HN7 polarizing material were used in the tests. Type HN22 is a neutral-color linear polarizer having a total luminous transmittance of 22% for white light and an extinction ratio of better than 10^{-4} in the region 0.45 to 0.75 μm. Type HN7 is a medium-dark-green linear polarizer having a total luminous transmittance of approximately 10% for white light; it provides substantial polarization in the region 0.7 to 0.9 μm. By rotating the polarizing sheet and swinging the panel, we were able to measure a linearly polarized signal of any orientation perpendicular to the scanner's line-of-sight up to a maximum swing angle of $\pm 45^{\circ}$ from nadir.

To make sure the light reflected off the flame-sprayed aluminum panel was initially unpolarized (so that polarizer rotation would not change the intensity of the light reaching the scanner), we ran a quick check. Using an unmounted photomultiplier tube with a small piece of linear polarizing material taped over its face, we rotated the tube 360° at a fixed height above the panel while recording tube output as a function of rotation angle. Results of this check showed few variations and proved the panel to be initially more than 99% unpolarized. This meant that any scanner signal variations observed while rotating the polarizing material could be assumed to have their origin internal to the scanner.

Initial tests of polarization sensitivity were conducted at discrete scanner view angles of 0°, -15°, -30° and -45°. The type HN22 polarizer was employed in four channels in the region from 0.41 to 0.70 μm, while the type HN7 was used in one band covering the region 0.67 to 0.94 μm. At each view angle our procedure was to rotate the polarizer 360° to find the position (if any) of maximum signal. After noting this orientation and its associated signal amplitude, we rotated the polarizer another 90°, and recorded the minimum signal. The rotation of the polarizer was always in a plane perpendicular to the scanner's line-of-sight. For orientation purposes, the E vector was arbitrarily assigned the 0°-180° position when it was perpendicular to the scan plane. Hence the 90°-270° position defines when this vector is in the scan plane. Table 8 summarizes these data.

As can be seen from the data, the radiation throughput of the M7 scanner varies between 15% and 30% with the polarization of the incoming radiation. In fact, the angle of maximum throughput rotates in the same manner and direction as the scan mirror itself, which indicates that the source of this nonuniform response to polarization is in a fixed plane internal to the scanner's optical system. A moment's consideration of all the optical components casts suspicion upon the dense flint dispersing prism as the most likely culprit. This is consistent

TABLE 8. M7 POLARIZATION SENSITIVITY

View Angle	Wavelength Band*	Sum of Min. and Max. Signals	Min./Max. Signal Ratio	Orientation of Max. E
0°	0.41-0.48 μm	17.1 mV	0.71	0°-180°
15°	0.41-0.48 μm	19.65 mV	0.74	345°-165°
30°	0.41-0.48 μm	19.7 mV	0.745	330°-150°
45°	0.41-0.48 μm	19.8 mV	0.75	315°-135°
0°	0.46-0.49 μm	20.5 mV	0.78	0°-180°
15°	0.46-0.49 μm	22.1 mV	0.826	345°-165°
30°	0.46-0.49 μm	21.7 mV	0.824	330°-150°
45°	0.46-0.49 μm	21.4 mV	0.799	315°-135°
0°	0.50-0.54 μm	30.5 mV	0.822	0°-180°
15°	0.50-0.54 μm	30.5 mV	0.822	345°-165°
30°	0.50-0.54 μm	31.0 mV	0.824	330°-150°
45°	0.50-0.54 μm	31.25 mV	0.812	315°-135°
-45°	0.50-0.54 μm	30.75 mV	0.81	45°-225°
0°	0.62-0.70 μm	107.75 mV	0.866	90°-270°
15°	0.62-0.70 μm	104.0 mV	0.84	345°-165°
45°	0.62-0.70 μm	107.0 mV	0.784	295°-115°
0°	0.67-0.94 μm	114.0 mV	0.916	0°-180°
15°	0.67-0.94 μm	117.5 mV	0.895	345°-165°
30°	0.67-0.94 μm	120.0 mV	0.86	330°-150°
45°	0.67-0.94 μm	120.0 mV	0.805	315°-135°

*10% response points

with Fresnel's Equations, which—for the geometry of interest—predict variations of about 20% resulting from polarization effects. A smaller effect is caused by reflection of mirrors.

In later tests we took time-exposed pictures of this polarization sensitivity as the reference panel was swung from $+45^{o}$ to -45^{o}, much as in the earlier angular responsivity tests. These pictures are shown in Fig. 44 for four fixed orientations of the linear polarized light in the 0.50 to 0.54 μm band. In future tests we plan to use polarizers for the near-IR channels. Hopefully the associated detectors will not display such polarization sensitivity, since this radiation does not pass through the dispersing prism in the spectrometer position (Position 3).

6.5 SIGNAL HANDLING PERFORMANCE

This section describes the airborne video electronics supporting the M7 scanner system and its performance. It does not discuss generation of synchronization pulses, time code, or reference frequencies for control track operation.

6.5.1 VIDEO ELECTRONICS

Figure 26 is the functional block diagram of the M7 airborne video electronics to be described. Components include the various detector combinations available for the M7 scanner detector, preamplifiers, M5 amplifiers, operator console postamplifiers, and tape recorder electronics.

6.5.1.1 Thermal and Near-IR Detectors and Their Pre-Preamplifiers

The M7 scanner is configured with four unique detector positions spanning the electromagnetic spectrum from 0.3 to 14.0 μm. Two of these four positions use detectors that require special preamplifiers tailored to that particular detector for best performance. Those detectors requiring special preamplifiers are the mercury cadmium telluride, indium arsenide, and indium antimonide. Table 9 gives performance data on these detectors.

6.5.1.2 Spectrometer and M5 Amplifiers

Detectors used in the UV and visible region (0.33 to 0.94 μm) are photomultiplier electron tubes with spectral responses corresponding to either the S-1 or S-20 curves. Twelve specific bands of radiation from 0.42 to 0.94 μm are coupled to an equal number of photomultiplier tubes by means of fiber optics. The output of each photomultiplier tube is coupled to the M5 amplifier. (This 12-channel amplifier was originally designed for the older M5 scanner and retained in the M7 scanner without modification.) The M5 amplifiers consist of 12 identical Burr-Brown 1607B operational amplifiers having inverting input only and closed loop gains at X1, X3, and X10. Nominal input impedance is 3.4KΩ and the closed loop output impedance less

TABLE 9. DETECTOR AND PREAMP CHARACTERISTICS

Parameter	InAs 3-5			InAs 3-6			InSb 3-6		
Spectral band 50% points (μm)	1.07-1.28	1.52-1.87	2.12-2.56	1.10-1.27	1.58-1.88	2.02-2.48	1.03-1.25	2.08-2.40	4.46-5.45
Spectral band 10% points (μm)	0.90-1.38	1.37-2.02	2.03-2.63	1.04-1.44	1.45-1.99	1.87-2.65	0.90-1.35	2.00-2.75	4.17-5.74
Size (in. × in.)	.01 × .02	.01 × .02	.01 × .02	.01 × .02	.01 × .02	.01 × .02	.01 × .02	.01 × .02	.01 × .02
Preamp card identification	PC-7	PC-9	PC-12				PC-5	PC-12	
Response time 10 to 90% rise time (μsec)	1.4	1.5	20				1.4	1.4**	
Approximate upper -3dB bandwidth (kHz)	210	200	15				210	210**	
$D^*(\lambda max, 20kHz) \times 10^9$, cm $Hz^{1/2}W^{-1}$	90	140	220	2000†	1100†	1300†	33	214	
Status (as of June 30, 1972)	Operational	Operational	Operational, but limited performance	Detector not tested	Detector not tested	Detector not tested	Operational	Operational	Not operational in present scanner config.

†At 900 Hz.

**Assumed response for channel, since GaAs diode emission at 0.9μm was not measurable with present lab equipment.

TABLE 9. DETECTOR AND PREAMP CHARACTERISTICS (Concluded)

HgCdTe 1-2	HgCdTe 1-3	HgCdTe 1-5	HgCdTe 2-2		HgCdTe 3-1			HgCdTe 2-3	
7.4 14.0	5.2- 10.9	5.8- 11.7	7.1 10.1	9.8- 11.2	5.7- 8.8	9.4- 10.4	10.4- 13.8	1.0- 1.9	1.9- 2.5
1.0 15.0	1.0 12.0	1.0- 12.0	1.0 10.9	9.4- 12.1	2.0 9.2	8.7- 10.8	9.8- 14.0		
.02 × .02	.0096 × .0087	.0097 × .0098	.063 × .084	.063 × .063	.06 × .06	.06 × .06	.06 × .06	.013 × .013	.013 × .013
PC-13 or 14	PC-13 or 14		PC-16	PC-15	PC-17	PC-18	PC-19		
.2	1.6		<2	<2	1	1**	1**		
1500	190		>150	>150	300	300**	300**		
2.7	68		9.4	5.8	3.4	2.4	1.0		
Poor D* performance due to probable damage during repair	Operational	Not tested	Operational	Operational	Operational	Operational	Operational	Detector on order	Not operational at this time

FIGURE 44. POLARIZATION ANGULAR RESPONSIVITY. Channel 3 response from 0.50 to 0.54 μm (Nadir at center).

than 1 ohm. Worst-case upper frequency response is 0.70 MHz in the X10 position with a slewing rate of 45 volts/μsec at this same gain setting. Nominal upper frequency response is in excess of 6 MHz in the X1 position and 2 MHz in the X3 position. The average noise figure at the preamplifier is 76.4 dB below one volt in the X10 position.

6.5.1.3 Operator Console Postamplifiers

Outputs from the 12-channel M5 amplifier are routed to an operator console and fed to the inputs of a 12-channel postamplifier. This postamplifier is of a new design used for the first time with the M7 scanner system. To maintain wide bandwidth with the required sine wave full-power response, the postamplifier has two stages of Burr-Brown 3341/15C inverting FET amplifiers. This type of Burr-Brown operational amplifier is designed for wideband, fast-slewing, very fast settling, and to drive low-impedance or capacitive loads. The first stage has a closed-loop gain of X1 or X10; its input impedance is 1 K ohm. Four of the twelve postamplifiers have a 5 K offset resistor in parallel with the input resistor used to offset the HgCdTe, InSb, and InAs detector outputs. First-stage output is direct-coupled to the second stage. Second-stage input impedance is also 1 K ohm. There are four fixed closed-loop gain settings at X1, X2, X5, and X10 associated with the second stage, plus an in-series variable gain which can multiply the fixed gain position up to a maximum of X2. Included in the feedback circuit of the second stage is a complementary transistor limiting circuit designed to hard-clip voltage levels in excess of ±3.6 volts peak. Worst-case upper frequency bandwidth is 200 kHz at a gain of X100 and slewing rate of 5 volts/μsec. At unity gain the upper frequency bandwidth is 800 kHz with a slewing rate of 19 volts/μsec.

6.5.1.4 Tape Recorder Electronics

The twelve postamplifier outputs are routed out from the operator console to twelve channels of FM record electronics. The FM record units are Model GOV-3 Voltage Controlled Oscillators, designed by Data Control Systems, Inc. In normal practice the record electronics are adjusted so that the offset voltage is zero and the gain of the system is X1. However, since the photomultiplier video output voltage swings only in one direction (negative) from ground potential, the best means to maintain full dynamic range of the FM record process is to offset the resting carrier frequency (216 kHz) of the FM record unit to the appropriate maximum deviation end + 30% = 280 kHz). Maximum deviation is then defined as 60% carrier shift (down to 151.2 kHz) for a 3-volt peak signal. Voltage gain is still maintained at X1, within the limits of drift specified by the manufacturer.

The VCO output carriers are fed into a 14-channel Mincom PC500 tape recorder and recorded direct at 60 ips. Direct record bias and record level are adjusted for best signal-to-noise ratio of the demodulated FM signal.

The playback signals from the Mincom PC500 are switched three channels at a time for display on a 4-channel Tektronix oscilloscope. The FM playback units are Model GFD-8 Demodulators, also designed by Data Control Systems, Inc. The fourth channel on the oscilloscope is reserved for display of sync signal and line count pulses.

The VCO modulator and FM demodulator combination have an 80 kHz bandwidth (5 μsec rise time with very little overshoot) and 0.5 volt/μsec slew rate. Worst-case S/N ratio for the PC500 FM record/playback system is -29 dB.

6.5.2 THROUGHPUT PERFORMANCE

Figures 45a-e illustrate the throughput performance of the airborne video electronics from M5 amplifier input through output of FM discrimination, including record and playback on the Mincom PC500 tape recorder. The sine wave response with gain of X1 at 80 kHz is 3 dB down from that at 1 kHz and the response at 100 kHz is 7 dB down. Figure 45a shows the slewing rate of the system to be 0.5 volt/μsec. Figures 45b and 45c show the throughput square wave response, indicating good rise time and very little overshoot. Figures 45d and 45e illustrate the overload response and hard limiting action of the postamplifier and the resultant response of the recording system to large signal input.

6.5.3 CONCLUSIONS

The airborne video signal conditioning electronics has a flat frequency response from dc to 65 kHz. The upper 3 dB rolloff point is 80 kHz and the rolloff slope is 12 dB/octave. The limiting factor here is the FM playback response. Although the upper frequency response of the system electronics is down 7 dB at 100 kHz, this is sufficient to resolve one resolution element of a 2 mrad detector. The system slewing rate is 0.5 volt/μsec, limited primarily by the VCO and FM discriminator combination. Maximum system gain is 200, or 66 dB. System noise at low gain settings is limited by tape recorder noise and at high gain settings by detector/preamplifier noise.

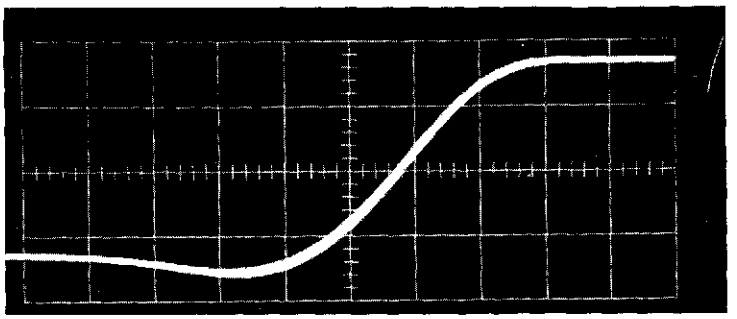

HORIZONTAL DEFLECTION 2 μsec/cm

(a) Transient Response
Input 3 V p-p, 10 Hz Sq. Wave
Slew rate = 0.5 V/μsec, Rise time = 6 μsec

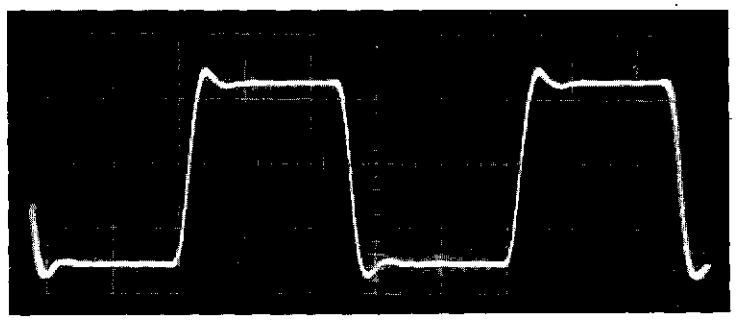

HORIZONTAL DEFLECTION 20 μsec/cm

(b) Transient Response
Input 3 V p-p, 10 kHz Sq. Wave

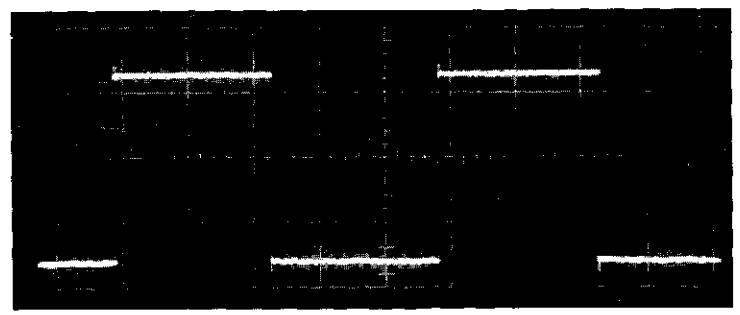

HORIZONTAL DEFLECTION 2 msec/cm

(c) Transient Response
Input 3 V p-p, 100 Hz Sq. Wave

FIGURE 45. THROUGHPUT RESPONSE

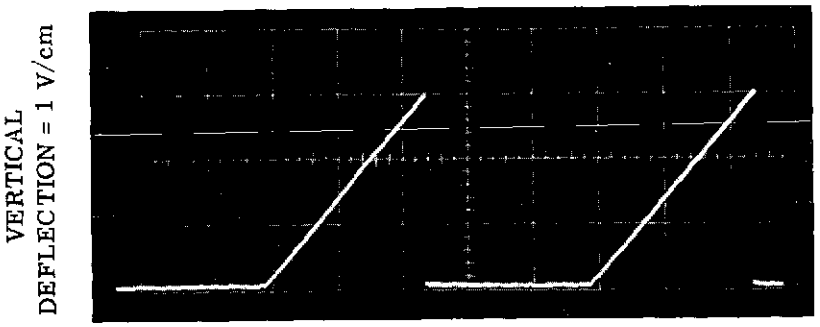

HORIZONTAL DEFLECTION 2 msec/cm

(d) Response on Overload
Input = 3V peak, 100 Hz Ramp

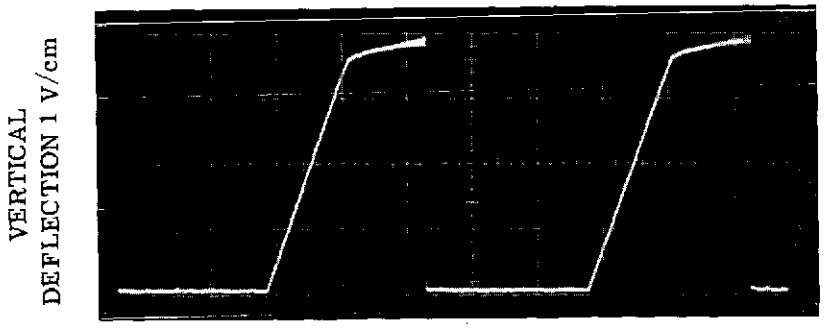

HORIZONTAL DEFLECTION 2 msec/cm

(e) Response on Overload
Input 8V peak, 100 Hz Ramp

FIGURE 45. THROUGHPUT RESPONSE (Concluded)

Appendix A
ORIGINAL M7 SCANNER CONFIGURATION

When the M7 multispectral scanner system was first put into operation in June 1971, many components of the M5 system being retired were used temporarily. The resulting initial M7 scanner configuration differed from the one described in the foregoing report. This appendix summarizes some notable design compromises in the earlier model; these resulted in certain differences among data collected with the M7 scanner during 1971.

A.1 DATA FORMAT

Initially, radiation reference sources from the M5 were used with the M7 scanner. The physical shape of these references required that the graybody thermal plates be located just before and just after the ground scan, as they were in the M5 system. The sky illumination reference was established at the zenith of the scan plane, and the calibrated lamp source was located between the thermal plate and the sky port following the ground scan. The scan reference marker pulse source was located 100° ahead of nadir for the level scanner position. The roll-stabilized reference pulse followed the marker pulse by approximately 30°.

This configuration is illustrated in Fig. A.1. The angular orientation of references in the scan plane is shown as well as a time (or angle) sequence of the electrical appearance of the reference synchronizing pulses and the scanner video signal. With reference to nadir in the level scanner position, one graybody thermal reference registered 90° before and one 90° after; the lamp registered 145° after; and the sky illumination 180° after.

In 1972, the M7 reference sources were incorporated into the system coincident with a resulting change in the data format. The sky illumination reference remained in the same position, but both the thermal plates and the lamp were relocated as described above. The reference marker pulse source remained in the same location relative to nadir, but the roll-stabilized pulse was positioned 20° after the marker (instead of 30°) to allow time for insertion of a scanner line count code between reference pulses.

The radiation characteristics of the original M7 system's reference sources were essentially the same as those for the M5 system. The change consisted merely of repackaging and selection of components with better reliability.

A.2 VIDEO AMPLIFIERS

When the M7 scanner system was first used operationally in June, 1971, the new video electronics that were eventually to be part of the system were not yet complete. So video amplifiers from the original M5 multispectral scanner were used temporarily. The only change was to add another operational amplifier stage with a fixed gain of 10 to reduce the

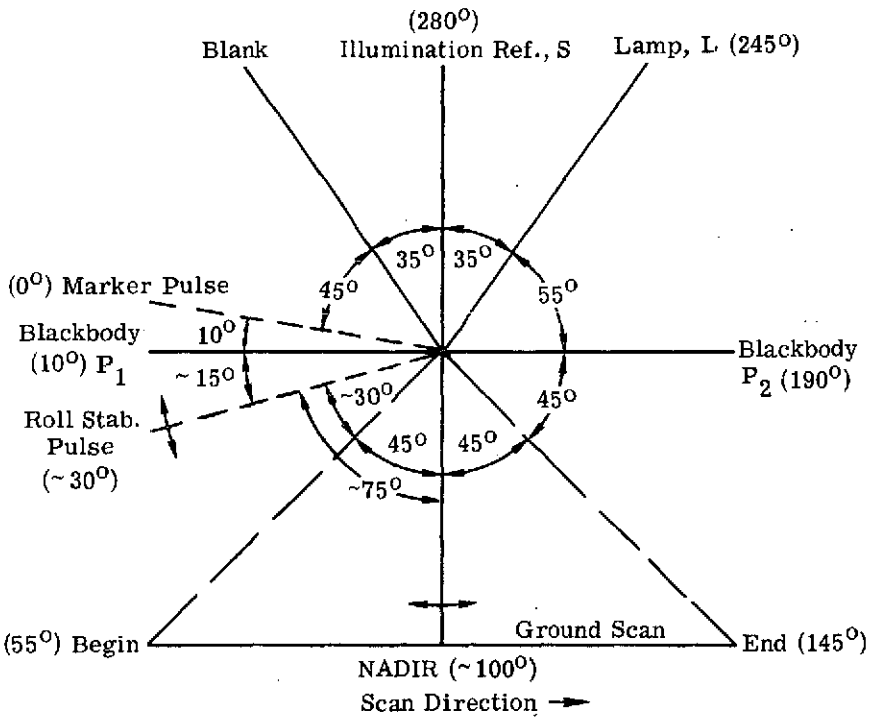

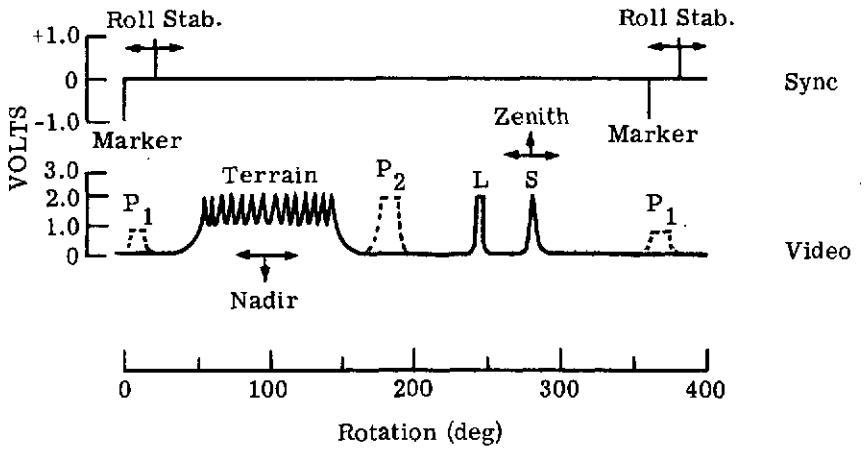

For 60 scans/sec, 1^{o} of rotation = 46.3 μsec

FIGURE A.1. 1971 RELATIVE ANGULAR POSITIONS OF SYNC AND RADIATION SOURCES, M7 SCANNER

maximum gain required in the final stage and to invert the signal. The signal inversion was desirable because of the change from tape recording on an Ampex FR1300 to the Mincom PC500 with DCS FM units. The polarity of FM deviation for the two tape machines was different, and having all data tapes with common polarity was considered best. Since the PC500 system would be recording twice the bandwidth of the FR1300, higher gain settings in the operational amplifiers would limit the bandwidth of the recorded signals. (The operational amplifiers were gain × bandwidth limited.)

Figure A.2 diagrams the video amplifier chain in use with the M7 system during June-October, 1971. The only significant shortcoming of this video link as compared to the eventual one was the lack of both variable gain and clipping of signals over +3.5 volts. During this period of operation we learned that the FM modulation units became nonlinear in response when driven beyond +4 volts. And in reversing the signal polarity into the final stage of video amplification, we inadvertently overlooked the fact that these amplifers were designed to limit or clip only negative-going signals. Later, during data analysis, we found that strong positive-going signals in excess of +4 volts were coming through the FM modulation and demodulation with negative gain—that is, the stronger the signal, the less was its amplitude. Of course these levels were then confused with the legitimate signals of less than 4 volts. Fortunately, very little data collected during this time period was at signal levels exceeding 4 volts.

The M7 postamplifier assembly was completed in the fall of 1971 and used with the version of the M7 video amplifier system shown in Fig. A.3 for the period from October 1971 through April 1972. This postamplifier package supplied the necessary clipping levels to prevent the non-linearities in gain experienced previously, and it also contained the needed additional gain stage and variable gain control. This configuration differed from the final M7 video amplifier configuration only in the preamps for the cooled IR detectors. The M5 preamps were eventually replaced with M7 types which provided improved signal-to-noise.

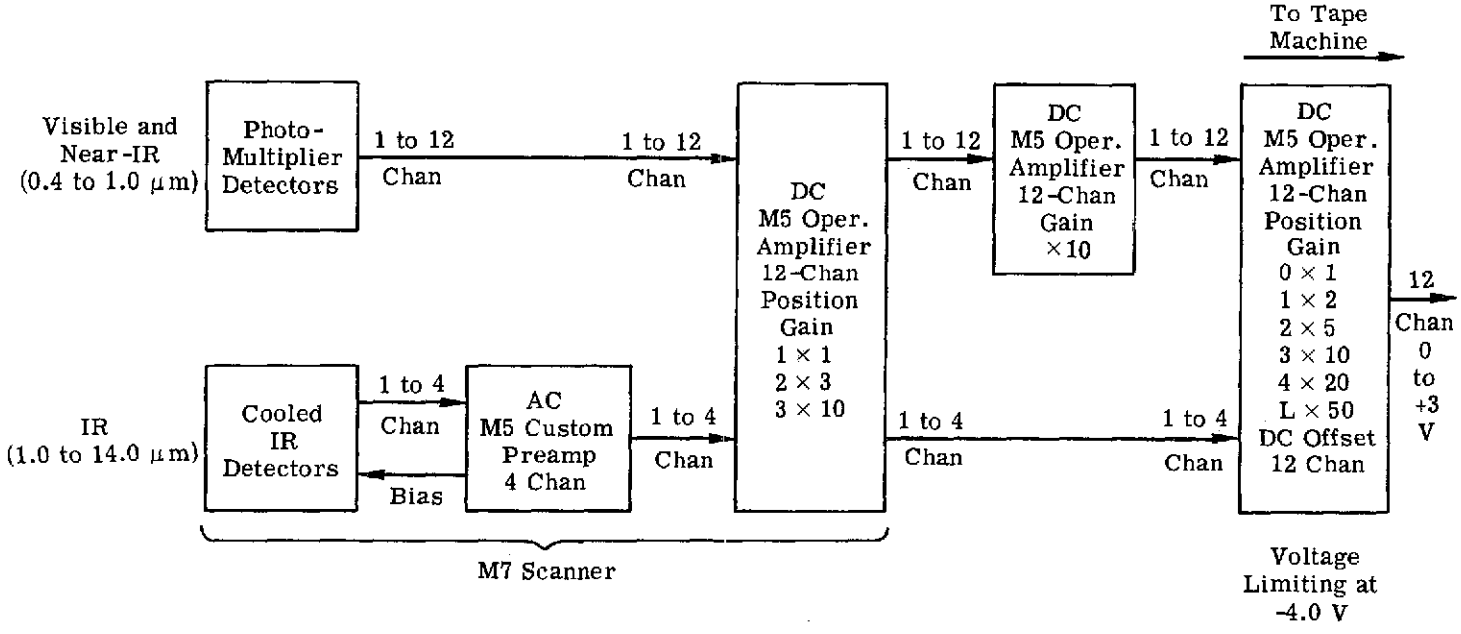

FIGURE A.2. BLOCK DIAGRAM: VIDEO AMPLIFIERS FOR JUNE-OCTOBER 1971

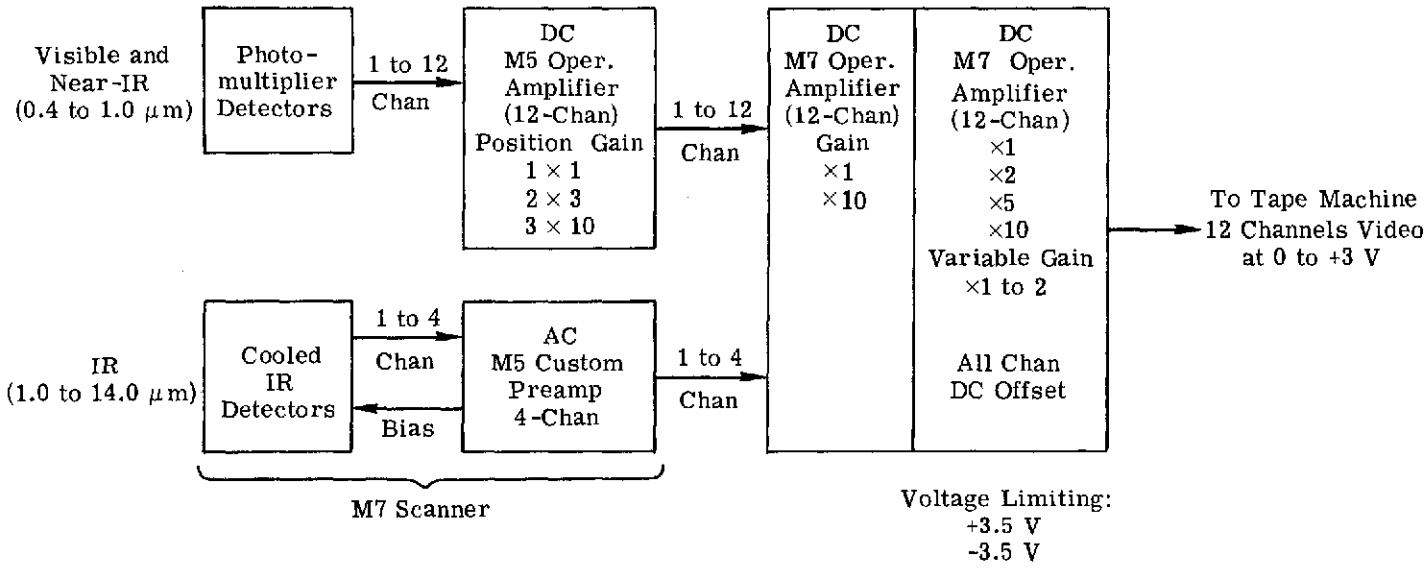

FIGURE A.3. BLOCK DIAGRAM: VIDEO AMPLIFIERS FOR NOVEMBER 1971-APRIL 1972

Appendix B
MULTISPECTRAL DATA PROCESSING AND ANALYSIS AT ERIM

While most techniques described herein apply to the processing of scanner data recorded on analog magnetic tape, they will also apply to ERTS and SKYLAB satellite data. In the satellite case, it is necessary, of course, to generate analog or digital tapes from data supplied.

Type I processing techniques described below are generally, though not always, applied to single-channel data. For ERTS and SKYLAB data processing, many of the imagery production and false-color film techniques mentioned will probably be implemented by NASA. The more sophisticated Type II techniques discussed in Section B.2 will be of primary interest to data users.

B.1 TYPE I PROCESSING

B.1.1 PREPARATION OF IMAGERY

Preparation of imagery from tape-recorded video information is one of the most basic forms of processing. This process displays video information on 70mm filmstrip negatives in a form which can be correlated with photography and other images. In all continuous filmstrip imagery produced at ERIM, a calibrated relationship is established between the video signal voltage from the magnetic tape and the film tone; this is done by periodically introducing a 16-step linear voltage scale in place of the video signal. There are several processing options, as described below.

B.1.1.1 Normal Tape Voltage to Film Tone Print

In the normal reproduction of filmstrip imagery, the lightest film gray-scale tone is clamped electrically to the signal representing the darkest or coldest reference source in the video signal, and the voltage gain is adjusted to place the signals representing the brightest or hottest objects of interest at the level of the darkest film gray-scale tone. This provision takes full advantage of the film dynamic range, but places the signal extreme in the nonlinear portion of the film transfer characteristics.

B.1.1.2 Special Tape Voltage to Film Tone Print

For calibration purposes, the video signal level can be clamped electrically to the signal representing the darkest (or "coldest") reference source. The video voltage can then be shifted in dc level and adjusted in gain to produce any preselected range of film gray-scale tone. Calibration reference levels, usually set to match the expected signal extremes, may be lost in the film print. To avoid this, the signal levels of interest (including calibration sources) can be

placed within the linear region of the film grayscale. Or, for ease of data analysis, small signal variations can be expanded over a wide gray-scale range.

B.1.1.3 Mixed Video Filmstrip

The video signals from two or more video channels may be mixed before the imagery is printed—provided that such signals are in registration. Since the signals may be mixed in any proportion, color film, false-color IR film, or ERTS-A spectral channels may be simulated. After mixing, the signal may be printed with either normal or enhanced grayscale, as discussed above.

B.1.1.4 Amplitude Gating of Tape Voltage to Film Tone Print

As an aid in data analysis, either an upper or lower voltage threshold level, or both, can be set in playback after electrical clamping so that signals outside these limits will not be printed on film. Again, some calibration information may be lost since the reference sources are usually adjusted to match the signal extremes.

B.1.1.5 False-Color Films

As an alternative to black and white imagery, false-color films may be produced to portray, in color, information from three bands. The process is similar to the color reversal process of color photography. Individual imagery separations are first converted to positive transparencies, which are then printed on color ozalid material in the three subtractive colors: yellow, magenta, and cyan. To produce the color film, the three sets of ozalid material are overlaid. Because there is no restriction on the type of data set which may be combined to produce the false-color print, imagery from the nonphotographic regions may be included to enhance certain data aspects.

B.1.1.6 Correction of Yaw and Scanner Geometry Distortions

All scanner imagery has distortion in it caused by the constant angular rate at which the scanning process covers the ground. Since imagery is produced with a simple, linear sweep on the printing CRT, the resultant image is compressed at the edges relative to a display in which ground feet per inch of film is constant.

This problem may be overcome by a nonlinear sweep of tan ϕ form, where ϕ is the angle of scan relative to nadir. Circuitry to implement the tan ϕ function is now in operation and can be used to generate partially rectified imagery—that is, imagery from which the scan-induced distortion has been removed.

Yaw distortions in the data can be similarly removed by special purpose circuitry. The correction removes dc-yaw or "crab-angle" distortion from the data. It is accomplished by first measuring the yaw angle from a piece of normally produced imagery, and then correcting for the yaw by rotating the CRT trace with respect to the film. The success of this technique depends on a priori knowledge—from a topographic map or photography—of scene compositional characteristics.

Roll corrections are made in all scanner imagery by generating and recording a roll-corrected sync pulse in the aircraft, and then using this pulse in data playback.

B.1.2 CONTOURING AND QUANTIZATION

Both contouring and quantization are single-band processing techniques that display data to an interpreter in a form slightly different from conventional imagery. In quantization, the data are displayed as a set of gray levels on film, each level corresponding to equal ranges of input signals as defined by the operator. In contouring, signal amplitude may be color-coded to enhance contrast.

B.1.2.1 Quantization

As a further processing step, individual signals may be subjected to quantizing. By breaking the signal range into any number of discrete levels, a black and white filmstrip can be produced having a finite number of gray levels. By noting at which levels calibration information appears, the range of each level can be calibrated. The widths of quantizing intervals may be as small as the noise level on the data, although this frequently leads to more levels than can be conveniently printed on film. (The eye can easily distinguish as many as 16 levels on a conventional filmstrip.) The main use of quantized filmstrips is to obtain a calibrated display of data without resort to densitometry. Accomplished by analysis of the electrical video signal before it is printed on film, quantization avoids the need to deal with nonlinear film and CRT transfer characteristics.

B.1.2.2 Contoured Separations

The method of producing contoured separations is similar to that of producing quantized data. But instead of printing out a series of gray steps on film corresponding to video signals within certain quantizing intervals, only video signals present in a particular quantizing interval are printed out as black on a clear film background. By setting the width of a quantizing interval equal to the noise on the signal and then printing data in all quantizing levels sequentially on film, nearly all of the information about a scene can be extracted from a series of black and clear filmstrips having the same scale as the video filmstrip. Calibration information

registered in the quantizing intervals permits calibration of each interval in terms of temperature, voltage, and radiance.

B.1.2.3 Color-Coded Contouring

Once the contour separations have been made, color coding may be added to accentuate radiance or temperature differences. The color coding is accomplished by printing each separation on a different colored ozalid foil. This step produces colored separations which may be overlaid to yield a color-coded contour display. The number of ozalid colors available and their contrast on the film upon which the ozalid overlay is photographed limit the number of data levels that can be meaningfully displayed to about 8 or 10; these may be chosen from any portion of the contouring separations.

Since all levels remain calibrated in the color-coding process, each color in the final display may be tied to a range of temperatures or radiances.

B.1.3 ANALOG TAPE DUPLICATION AND DIGITAL TAPE PREPARATION

All multispectral data are recorded in the aircraft on 1-in. magnetic instrumentation tape. Frequently, users who have access to data processing facilities request either duplicate analog tapes of data or digitized data for their own analysis. Properties of these two data formats are discussed below.

B.1.3.1 Duplicate Analog Tapes

The duplicate analog tape is simply a copy of the original data tape. All channels are commonly transferred from the original to the duplicate. The video and synchronizing data are recorded in IRIG* standard FM with 216-kHz center carrier (at 60 ips) and ±30% deviation. The synchronizing signal consists of two pulses of opposite polarity and close proximity, the first pulse being the non-roll-corrected sync, while the second is the roll-corrected sync. Since all tapes are supplied wound fully forward, they must be completely rewound before playing. Unless specifically noted, all channels on the duplicate correspond to the same channels on the original.

B.1.3.2 Digital Tapes

Digitized data suitable for digital computer processing may be supplied in one of two formats. All data are digitized to 9-bit accuracy (8 bits plus sign). Flexible control of the A/D conversion process allows sampling of the data once every resolution element, once every

*Inter-Range Instrumentation Group

other resolution element, and so on. Also, scan lines of data may be skipped. Unusual sampling formats may also be accommodated. Normal formats are as follows: sample each resolution element twice; sample each resolution element once; sample every other or every fourth resolution element. Any number of lines up to nine may be skipped.

Of the two formats available, the one commonly used for all processing at ERIM consists of the following information written as 48-bit words on 7-track (six bits and even parity), 1/2-in. digital tape. The first record is the binary title record containing the title (in standard alphanumeric form) and three numbers denoting, respectively, the number of data channels, the number of points per scan line, and an integer that tags the data as bipolar or unipolar. The second record is a binary record consisting of all the data from the first digitized scan line. These data are packed in words,with the first three octal digits (9 bits) corresponding to the value of the first channel at the first point. The next three octal digits denote the value of channel 2 at point 1. This process is continued until all the channels have been covered for point 1; then the process is repeated for point 2. Point 2 data starts where point 1 data ends, which may be in the middle of a word. The number of words per record is then

$$N = \frac{16}{3} N_{chan} \times N_{ss}$$

where N = total words per record

N_{chan} = number of channels

N_{ss} = number of points per scan

Note that the two numbers N_{chan} and N_{ss} are stored in the title. At the end of the digitized data, an "end of file" is written. In the event that a file continues over more than one tape, "end of tape" is written at the end of each tape.

The second format available at ERIM is similar to the first with two important exceptions: data are organized in card image format on the tape (short records); and data at 200 or 556 bpi can be supplied. The first two records of this format are the title and other numerical information written in binary coded decimal (BCD). The remaining records are binary records containing the data. Eighty-one 48-bit words are written in each record. The first word is a control word. Thus, each scan line of original data is covered in several records. A new record always begins with a new scan line. The numbers N_{chan} and N_{ss} serve to straighten out the packing. Further, each 81-word, 48-bit record may be converted into a 108-word, 36-bit record via relatively simple machine language programming. End-of-file and end-of-tape conventions are the same as for the first format.

Consultation with data-processing personnel at ERIM is recommended before specifying which format is to be used. This will assure format compatibility with a particular machine.

Areas to be digitized can be specified by marking data locations on a print of scanner imagery. Facilities will soon be available to put scan line numbering information on the filmstrip so that a precise specification of areas to be digitized (in terms of starting and stopping line number) will be possible. Data normally digitized include calibration and dark level information, which will be supplied in bipolar form unless otherwise specified. A graymap printout of video data alone will also be supplied. Line and point numbers on the map correspond to line and point numbers on the tape.

B.2 TYPE II PROCESSING

Type II processing comprises the more sophisticated analysis and pattern recognition operations usually applied to simultaneous multispectral data. These operations may be further divided into (1) signature analysis and calibration and (2) multispectral recognition.

B.2.1 SIGNATURE ANALYSIS AND CALIBRATION

This work, dealing with the extraction and analysis of signatures as a preparatory step before multispectral recognition, has four general categories: reflectance panel signature extraction, signature extraction of scene objects, analysis to determine optimum channels for multispectral recognition operations, and analysis of data to determine the presence of angle effects.

B.2.1.1 Reflectance Panel Signature Extraction

Standard 20 × 40 ft canvas reflectance panels are usually deployed during flight missions to permit calibration of the data collected in terms of equivalent directional reflectance. In order to calibrate scanner data in this manner, the voltage signatures of the panels are first extracted, and curves of scanner voltage versus reflectance are plotted for each spectral channel. Then voltage statistics of the area to be calibrated are obtained, and the curves generated previously are used to convert the voltage signature to a reflectance signature. Because of panel size and scanning system spatial resolution, useful panel signatures cannot be obtained at flight altitudes above 1000 ft.

B.2.1.2 Extraction of Signatures from Scene Objects or Areas

Signals received from various objects and materials on the ground exhibit spectral reflectance and emittance variations for a variety of reasons. Thus, in many applications, it is desirable for analysis purposes to obtain statistical descriptions of these multispectral signals

and their variations. Facilities exist at ERIM for obtaining such descriptions from scene objects or areas selected for detailed study.* The following types of information can be digitally computed:

(1) mean signal in each spectral channel and the corresponding variances for (a) each selected scan line that contains the material of interest, (b) each scan angle at which the material is observed and sampled, and (c) all samples considered as a group
(2) covariances and correlations between signals in the various spectral channels
(3) eigenvalues and eigenvectors of each variance/covariance matrix or distribution
(4) weighted combinations of statistics from several objects or areas
(5) measures of the amount of separation between such distributions for any set of spectral channels

The data computed have the following features:

(1) corrections are first made for scan-angle-dependent variations introduced into the data by the scanner
(2) calibration information is simultaneously computed
(3) according to customer preference, results can take one or more of the following forms: computer printouts, punched cards, magnetic tapes, and computer-generated histogram plots.

B.2.1.3 Analysis to Determine Best Channels for Multispectral Recognition

In multispectral data-processing operations, particularly those in which recognition of scene objects is based upon their spectral signatures, it is often desirable to know which channels of a given set of data are most useful for discriminating terrain features. We have developed an analysis program to compute the best single channel, best pair of channels, best three channels, and so on. The performance measure is the average pairwise probability of misclassification of all signatures fed into the program. We chose this measure rather than a distance measure (which would have been computationally simpler) so we can obtain, at each step, a measure of the performance of a maximum likelihood pattern classifier. Required as program inputs are the signatures of the objects to be separated and weights denoting the relative importance of various parts of objects. The program output is a rank ordering of channels, with a performance measure at each step.

* The Target Signature Analysis Center (TSAC) at ERIM, operated under sponsorship of the Air Force Avionics Laboratory, collects optical properties-of-materials data, provides analytical programs, and publishes data compilations.

B.2.1.4 Angle Effects: Analysis and Correction

Because of peculiarities in data collection (particularly flightline orientation with respect to the sun), a pronounced variation of average scene radiance with scan angle is often present in multispectral data. This angle effect seriously degrades multispectral recognition in classification of data sets because the voltage signature representing a scene object varies with that object's position in the field of view.

The presence of angle effects is not always easy to determine by examination of imagery. Even if the signals are examined on an oscilloscope and found to have angle effects, a quantitative measure is needed. Analysis programs are available to determine whether the angle effects are sizable enough to affect recognition processing; we recommend their use on data to be processed.

Any angle effects can usually be corrected by selectively applying special preprocessing steps, the efficacy of which can be explored without actually making a recognition map. After a reasonable preprocessing approach is formulated, processing of the data continues on either the digital or special-purpose analog computer.

B.2.2 MULTISPECTRAL RECOGNITION OPERATIONS

Here, basically, we attempt to recognize scene objects using spectral signature information only. Recognition processing begins with the selection of training sets representing verified signatures of objects of interest. The computer is given this signature information; then it is asked to classify an unknown scene based on the similarity of scene spectral signatures to those in the training sets. The measure of such similarity—a likelihood ratio—is computed for each scene point for each object to be recognized. A threshold circuit then decides which of the training set objects is most likely present in the scene.

Likelihood ratio processing is implemented in two ways at ERIM. In one, the CDC-1604B digital computer may be used to generate recognition maps from digitized data. These maps may be printed out either in black and white (with different objects represented by various typewriter symbols), or in color (with different objects represented by symbols of different color —red, green, blue, and black are available).

In the other implementation of likelihood ratio processing, a special-purpose analog computer, SPARC, is used to generate recognition maps. SPARC works with taped data from the aircraft at real-time rates and produces recognition maps directly comparable with imagery. Recognition maps of this type consist of black areas on a clear film background; by means of the same false-color ozalid process described in Section B.1.2, they may be color-coded to form a color composite recognition map.

User representatives will often find it constructive to discuss proposed processing work with ERIM data processing and analysis personnel who from wide experience can offer many helpful suggestions. When multispectral data is to be processed at ERIM, a number of essential inputs are required from the customer (i.e., user organization) to ensure optimum results:

(1) Designation of area to be processed. This can often be done initially through imagery inspection, but the final decision as to the most suitable area should rest on an oscilloscope examination of the data or other close analysis.

(2) Assembly of training sets. Such sets may be identified on either aerial photography or scanner imagery. Their size (in linear dimensions) will vary with flight altitude. A good rule of thumb in selecting a training set is that it should include at least 20 resolution elements. (A resolution element is approximately 3h ft square, where h is the scanner altitude in thousands of feet.) For very small objects, training sets can be smaller, but then the specification of what comprises each set must be carefully made to ensure good results.

(3) Availability of adequate ground truth. In order to establish training sets and make interim assessments of processing success, data-processing personnel must be provided with ground truth information that they can correlate with the imagery obtained.
NOTE: The recognition operation tends to be repetitious and often tedious. If the user does not plan to be present during processing, he should arrange to leave ground truth information with ERIM personnel.

(4) Display parameters and purposes. The user should give some thought to how he intends to display the results. Various options include recognition maps in combination with imagery, recognition maps with color photography, and lantern or 35 mm slides. ERIM's capable photographic laboratory and technical illustration department are skilled in all aspects of display preparation to suit the user's need.

(5) Realistic scheduling. Because of advance scheduling on the SPARC computer, we recommend that processing plans be made well ahead. Special requests for specific time periods will receive careful consideration, but it should be remembered that the SPARC is usable only on a non-interference basis with Air Force work (the Air Force sponsored SPARC's original construction). Normally, however, there is no interference problem.

(6) Constructive comment. The customer is encouraged to communicate to ERIM any helpful comments concerning data collection procedures or, after data processing, relative to the results achieved.

When processing has been completed, ERIM supplies the customer with a data package that includes a report which documents SPARC operations. This report usually contains imagery samples, discusses processing theory and its application to the problem at hand, mentions any pertinent data anomalies, and reviews SPARC's processing performance.

BIBLIOGRAPHY

This is a bibliography of reports issued by Willow Run Laboratories, its successor organization, ERIM, and others on the development of multispectral discrimination techniques. Those interested in making use of multispectral data generated by the M7 and other scanners may wish to obtain copies for study. For reader convenience in identifying recent publications, the listing is presented in reverse chronological order.

W. Malila, Discrimination Techniques Employing Both Reflective and Thermal Multispectral Signals, ERIM Report 31650-75-T, November 1973.

G. H. Suits, R. K. Vincent, H. W. Horwitz, and J. D. Erickson, Optical Modeling of Agricultural Fields and Rough-Textured Rock and Mineral Surfaces, ERIM Report 31650-78-T, 1973 (not yet published).

R. B. Crane, W. A. Malila, and W. Richardson, Suitability of the Normal Density Assumption For Processing Multispectral Scanner Data, (WRL Report 31650-70-J), Journal of Remote Sensing of Environment, October 1972.

R. Vincent, An Emission Polarization Study on Quartz and Calcite, WRL Report 31650-112-J, submitted to Applied Optics in September 1972.

R. Vincent, et al., Rock-Type Discrimination Ratio Images of the Pisgah Crater, California, Test Site, WRL Report 31650-77-T, June 1972.

W. Malila, et al., Information Extraction Techniques, WRL Report 31650-74-T, June 1972.

P. G. Hasell and S. R. Stewart, Maintenance and Operation of the Multispectral Data-Collection and Reproduction Facilities of the Willow Run Laboratories, WRL Report 25990-37-P, June 1972.

R. Vincent, F. Thomson and K. Watson, Recognition of Exposed Quartz Sand and Sandstone by 2-Channel Infrared Imagery, WRL Report 31650-111-J, Journal of Geophysical Research, pp. 2473-2477, Vol. 77, No. 14, May 10, 1972.

R. Vincent and F. Thomson, Spectral Compositional Imaging of Silicate Rocks, (WRL Report 31650-110-J), Journal of Geophysical Research, pp. 2465-2472, Vol. 77, No. 14, May 10, 1972.

R. Turner, Remote Sensing in Hazy Atmosphere, (WRL Report 31650-106-S/J), Presented to the ACSM/ASP Convention, Washington, D.C., March 1972. To be published in the Journal of Photogrammetric Engineering and in ACSM/ASP Proceedings.

D. Zuk and M. Gordon, Ground Measurements in Support of a Multispectral Data System Evaluation Flight, WRL Informal Technical Report 31650-113-T, March 1972.

R. Vincent and F. Thomson, Rock-Type Discrimination From Ratioed IR Scanner Images of Pisgah Crater, California, (WRL Report 31650-83-J), Science, March 1972.

R. Nalepka, et al., Estimating Proportions of Objects from Multispectral Data, WRL Report 31650-73-T, March 1972.

R. Crane and W. Richardson, Rapid Processing of Multispectral Scanner Data Using Linear Techniques, (WRL Report 31650-107-S/J), Remote Sensing of Earth Resources, Vol. I. Selected Papers from Earth Resources Observation and Information Analysis Systems Conference, 13-14 March, 1972.

W. A. Malila, Radiation Balance Mapping with Multispectral Scanner Data, (WRL Report 31650-92-S/J), Remote Sensing of Earth Resources, Vol. I, Selected Papers from Earth Resources Observation and Information Analysis Systems Conference, 13-14 March 1972.

G. H. Suits, Prediction of Directional Reflectance of a Corn Field Under Stress, (WRL Report 31650-95-S), Proceedings, 4th Annual Earth Resources Program Review, NASA/MSC, Houston, January 17, 1972.

R. F. Nalepka, J. P. Morgenstern, and W. L. Brown, Detailed Interpretation and Analysis of Selected Corn Blight Watch Data Sets, (WRL Report 31650-96-S), Proceedings, 4th Annual Earth Resources Program Review, NASA/MSC, Houston, January 17, 1972.

F. J. Thomson and R. F. Nalepka, Contribution to the Corn Blight Watch Final Report, WRL Report 31650-104-L, January 1972.

W. A. Malila, R. B. Crane, W. Richardson, and R. E. Turner, Information Extraction Techniques for Multispectral Scanner Data, (WRL Report 31650-97-S), Proceedings of 4th Annual Earth Resources Program Review, NASA/MSC, Houston, January 17, 1972.

R. K. Vincent, Experimental Methods for Geological Remote Sensing, (WRL Report 31650-101-S), Proceedings of 4th Annual Earth Resources Program Review, NASA/MSC, Houston, January 17, 1972.

J. D. Erickson, A Summary of Michigan Program for Earth Resources Information Systems, (WRL Report 31650-99-S), Proceedings of 4th Annual Earth Resources Program Review, NASA/MSC, Houston, January 17, 1972.

F. J. Thomson, User Oriented Multispectral Data Processing at The University of Michigan, (WRL Report 31650-100-S), Proceedings of 4th Annual Earth Resources Program Review, NASA/MSC, Houston, January 17, 1972.

P. G. Hasell, Jr., Michigan Experimental Multispectral Scanner System, (WRL Report 31650-102-S), Proceedings of 4th Annual Earth Resources Program Review, NASA/MSC, Houston, 17 January 1972.

L. J. Porcello and R. A. Rendleman, Multispectral Imaging Radar, (WRL Report 31650-103-S), Proceedings of 4th Annual Earth Resources Program Review, NASA/MSC, Houston, 17 January 1972.

R. F. Nalepka, H. M. Horwitz, P. D. Hyde, and J. P. Morgenstern, Classification of Spatially Unresolved Objects, (WRL Report 31650-98-S), Proceedings of 4th Annual Earth Resources Program Review, NASA/MSC, Houston, January 17, 1972.

G. H. Suits, The Calculation of the Directional Reflectance of a Vegetative Canopy, Remote Sensing of Environment 2, 1972, pp. 117-125.

V. Leeman, R. Vincent and S. Ladd, The NASA Earth Resources Spectral Information System: A Data Compilation, First Supplement, WRL Report 31650-69-T, 1972.

R. E. Marshall, F. J. Kriegler, and W. Richardson, Adaptive Multispectral Recognition of Wheat, WRL Report 31650-85-S, Presented at 1971 IEEE Decision and Control Conference, Miami, Florida, December 15-17, 1971.

R. E. Marshall, F. J. Kriegler, and W. Richardson, Adaptive Multispectral Recognition of Wheat Fields, WRL Report 31650-86-S, Presented at EAI Symposium on Automatic Photointerpretation, Washington, D.C., December 7-8, 1971.

R. Vincent, Iron Oxide Mapping from Ratioed Visible and Reflective IR Scanner Images of Pisgah Crater, WRL Report 31650-84-J, Submitted to Science, October 1971.

M. M. Spencer and F. J. Thomson, Experimental Study on Preprocessing of Multispectral Data of a Yellowstone National Park Site, WRL Report 31650-79-L, September 1971.

M. M. Spencer, Analysis and Recognition Processing of Multispectral Scanner Imagery of the Manitou Experimental Forest Site in Colorado, WRL Report 31650-81-L, September 1971.

J. Erickson and F. Thomson, Investigations Related to Multispectral Imaging Systems for Remote Sensing, WRL Report 31650-17-P, September 1971.

V. Leeman, NASA/MSC Earth Resources Spectral Information System Procedures Manual, Supplement, WRL Report 31650-72-T, September 1971.

F. Polcyn, et al., Investigation of Shallow Water Features, WRL Report 31650-31-T, August 1971.

L. Larsen, Detector Utilization in Line Scanners, WRL Report 31650-29-T, August 1971.

W. Malila, R. Turner, and R. Nalepka, Importance of Atmospheric Scattering in Remote Sensing, WRL Report 3165-44-S/SA/J, Journal of Atmospheric Sciences, Submitted July 1971.

R. E. Marshall and F. J. Kriegler, Data Display Requirements for a Multispectral Scanner Processor with High Throughput Capability, WRL Report 31650-28-L, July 1971.

F. J. Kriegler, Implicit Determination of Multispectral Scanner Data Variation Over Extended Areas, WRL Report 3165-43-S/S/Sa, Proceedings of 7th International Symposium on Remote Sensing of Environment, Ann Arbor, June 1971, pp. 759-778.

R. Turner, W. Malila, and R. Nalepka, Importance of Atmospheric Scattering in Remote Sensing, or Everything You've Always Wanted to Know About Atmospheric Scattering but Been Afraid to Ask, (WRL Report 3165-44-S/Sa/J), Proceedings of 7th International Symposium on Remote Sensing of Environment, Ann Arbor, June 1971, pp. 1651-1698.

R. B. Crane, Preprocessing Techniques to Reduce Atmospheric and Sensor Variability in Multispectral Scanner Data, (WRL Report 3165-45-S/Sa), Proceedings of 7th International Symposium on Remote Sensing of Environment, Ann Arbor, June 1971, pp. 1345-1356.

F. J. Kriegler and R. Marshall, An Operational Multispectral Survey System, WRL Report 3165-46-S/Sa, Proceedings of 7th International Symposium on Remote Sensing of Environment, Ann Arbor, June 1971, pp. 2169-2192.

R. K. Vincent and F. J. Thomson, Discrimination of Basic Silicate Rocks by Recognition Maps Processed from Aerial Infrared Data, WRL Report 3165-47-S/Sa, Proceedings 7th International Symposium on Remote Sensing of Environment, Ann Arbor, June 1971, pp. 247-252.

W. L. Brown, F. C. Polcyn, and S. R. Stewart, A Method for Calculating Water Depth, Attenuation Coefficients and Bottom Reflectance Characteristics, (WRL Report 10259-1-X), Proceedings of 7th International Symposium on Remote Sensing of Environment, Ann Arbor, June 1971, pp. 663-682.

H. M. Horwitz, R. F. Nalepka, P. D. Hyde, and J. P. Morgenstern, Estimating the Proportions of Objects Within a Single Resolution Element of a Multispectral Scanner, (WRL Report 31650-42-S/Sa), Proceedings of 7th International Symposium on Remote Sensing of Environment, June 1971, pp. 1307-1320.

W. G. Burge and W. L. Brown, Pond Censusing in Waterfowl Habitats by Automatic Processing of 1.5 to 1.8 Micrometer Data, (WRL Report 10259-1-X), Proceedings of 7th International Symposium on Remote Sensing of Environment, Ann Arbor, June 1971, p. 2229.

V. L. Larrowe, A Moving Window Display for Infrared Imagery, (WRL Report 10259-1-X), Proceedings of 7th International Symposium on Remote Sensing of Environment, June 1971, Ann Arbor, pp. 1497-1507.

A. L. Higer, M. C. Kolipinski, N. S. Thomson, and L. Purkerson, Use of Processed Multispectral Scanner Data with a Digital Simulation Model for Forecasting Thermally Induced Changes in Benthic Vegetation in Biscayne Bay, Florida, (WRL Report 10259-1-X), Proceedings of 7th International Symposium on Remote Sensing of Environment, Ann Arbor, June 1971, pp. 2055-2056.

H. W. Smedes, M. Spencer, and F. J. Thomson, Preprocessing of Multispectral Data and Simulation of ERTS Data Channels to Make Computer Terrain Maps of a Yellowstone National Park Test Site, (WRL Report 10259-1-X), Proceedings of 7th International Symposium on Remote Sensing of Environment, June 1971, pp. 2073-2094.

V. Leeman, et al., The NASA Earth Resources Spectral Information System: A Data Compilation, WRL Report 31650-24-T, May 1971.

R. Nalepka, et al., Investigations of Multispectral Sensing of Crops, WRL Report 31650-30-T, May 1971.

W. A. Malila, et al., Studies of Spectral Discrimination, WRL Report 31650-22-T, May 1971.

R. Vincent, et al., Remote Sensing Data Analysis Projects Associated with the NASA Earth Resources Spectral Information System, WRL Report 31650-26-T, April 1971.

R. Vincent, Data Gaps in the NASA Earth Resources Spectral Information System, WRL Report 31650-25-T, March 1971.

F. Kriegler and R. Marshall, A Prototype Hybrid Multispectral Processor (SPARC/H) With High Throughput Capability, WRL Report 31650-23-T, March 1971.

J. Braithwaite and E. Work, Optical Transfer Techniques for Orbital Scanners, WRL Report 31650-21-T, March 1971.

V. Leeman, et al., NASA/MSC Earth Resources Spectral Information System Procedures Manual, WRL Report 31650-32-T, 1971.

L. Larsen and P. Lambeck, Performance of MSDS as of 18 August 1971, WRL Informal Report 31650-82-T, 1971.

R. E. Marshall and F. J. Kriegler, Multispectral Recognition Techniques: Present Status and a Planned Hybrid Recognition System, Proceedings of 1970 IEEE Symposium on Adaptive Processes (9th) Decision and Control, December 1970, pp. XI.2.1 to XI.2.9.

J. Braithwaite, Calibration of Multispectral Scanners, WRL Report 31650-27-L, September 1970.

T. Wagner, Automatic Processing and Analysis of Soils and Soil Conditions, WRL Report 2760-2-F, July 1970.

W. G. Burge and W. L. Brown, A Study of Waterfowl Habitat in North Dakota Using Remote Sensing Techniques, WRL Report No. 2771-7-F, July 1970.

N. Thomson, Multispectral Studies of Vegetation and Hydrologic Conditions in South Florida, (WRL Report 3398-2-J), Proceedings Series No. 8, of Hydrobiology "Bioresearches of Shallow Water Environments," Sponsored by American Water Resources Association, June 1970, pp. 329-349.

F. Thomson, Investigations of Multispectral Discrimination of the Earth Surface Features, WRL Report No. 2528-10-F, April 1970.

J. E. Colwell, Multispectral Remote Sensing of Urban Features, WRL Report 2772-6-F, March 1970.

P. G. Hasell, Maintenance and Operation of the Multispectral Data Collection and Reproduction Facilities of The University of Michigan, WRL Report 2599-11-P, March 1970.

R. Nalepka, Investigation of Multispectral Discrimination Techniques, WRL Report 2264-12-F, January 1970.

F. C. Polcyn, N. A. Spansail, and W. A. Malila, How Multispectral Sensing Can Help the Ecologist, Remote Sensing in Ecology, ed. by Philip Johnson, Athens, University of Georgia Press, 1969.

F. C. Polcyn and I. J. Sattinger, Water Depth Determinations Using Remote Sensing Techniques, (WRL Report 31062-2-X), Proceedings of the Sixth International Symposium on Remote Sensing of Environment, October 1969, p. 1017.

W. G. Pearcy and J. L. Mueller, Upwelling, Columbia River Plume and Albacore Tuna, (WRL Report 31062-2-X), Proceedings of the Sixth International Symposium on Remote Sensing of Environment, October 1969, p. 1101.

M. G. Tanguay, R. M. Hoffer, and R. D. Miles, Multispectral Imagery and Automatic Classification of Spectral Response for Detailed Engineering Soils Mapping, (WRL Report 31062-2-X), Proceedings of the Sixth International Symposium on Remote Sensing of Environment, Ann Arbor, October 1969, p. 33.

D. L. Earing, A Spectral Discrimination Technique for Agricultural Applications, (WRL Report 31062-2-X), Proceedings of the Sixth International Symposium on Remote Sensing of Environment, Ann Arbor, October 1969, p. 21.

A. E. Coker, R. Marshall, and N. S. Thomson, Application of Computer Processed Multispectral Data to the Discrimination of Land Collapse (Sinkhole) Prone Areas in Florida, (WRL Report 31062-2-X), Proceedings of the Sixth International Symposium on Remote Sensing of Environment, Ann Arbor, October 1969, p. 65.

M. C. Kolipinski and A. L. Higer, Inventory of Hydrobiological Features Using Automatically Processed Multispectral Data, (WRL Report 31062-2-X), Proceedings of the Sixth International Symposium on Remote Sensing of Environment, Ann Arbor, October 1969, p. 79.

R. E. Marshall, N. Thomson, F. Thomson, and F. Kriegler, Use of Multispectral Recognition Techniques for Conducting Rapid, Wide-Area Wheat Surveys, (WRL Report 31062-2-X), Proceedings of the Sixth Symposium on Remote Sensing of Environment, Ann Arbor, October 1969, p. 3.

K. S. Fu, D. A. Landgrebe, and T. L. Phillips, Information Processing of Remotely Sensed Agricultural Data, Proceedings IEEE, Vol. 57, April 1969, p. 639.

R. A. Holmes and R. B. MacDonald, The Physical Basis of System Design for Remote Sensing in Agriculture, Proceedings IEEE, Vol. 57, April 1969, p. 629.

R. E. Marshall, Applications of Multispectral Techniques for Water Resource Investigations in Florida, Purdue Centennial on Information Processing, Vol. 2, April 1969, pp. 719-731.

D. S. Lowe, et al., Investigations of Spectrum Matching Techniques for Remote Sensing in Agriculture, WRL Report 1674-10-F, December 1968.

P. G. Hasell and L. M. Larsen, Calibration of an Airborne Multispectral Optical Sensor, WRL Report 6400-137-T, September 1968, ECOM-00013-137.

P. G. Hasell, Investigations of Spectrum Matching Techniques for Remote Sensing in Agriculture, WRL Report 8725-13-P, September 1968.

F. J. Kriegler and M. M. Spencer, Statistical Spectral Analyzer and Target Recognition Computer (SPARC), WRL Report 8640-17-F, September 1968, AD-392-774.

P. G. Thomas, Associate Editor, Earth-Resource Survey From Space, Space/Aeronautics, Vol. 50, July 1968, p. 46.

W. A. Malila, Multispectral Techniques for Contrast Enhancement and Discrimination, Photogrammetric Eng., Vol. 34, June 1968, p. 556.

R. J. Kauth, Preliminary Analysis of TVA Multispectral Data, WRL Report 1195-2-L, June 1968.

R. Horvath and D. S. Lowe, Multispectral Survey in the Alaskan Arctic, (WRL Report 4864-18-X), Proceedings, Fifth Symposium on Remote Sensing of Environment, Ann Arbor, April 1968, p. 483.

A. H. Muir and I. J. Sattinger, Methods of Feasibility and Economic Analysis of Remote Sensing Applications, WRL Report 4864-18-X, Proceedings of the Fifth Symposium on Remote Sensing of Environment, Ann Arbor, April 1968, p. 927.

D. S. Lowe, Line Scan Devices and Why Use Them, (WRL Report 4864-18-X), Proceedings of the Fifth Symposium on Remote Sensing of Environment, Ann Arbor, April 1968, p. 77.

R. C. Heller, Pre-Visual Detection of Ponderosa Pine Trees Dying from Bark Attack, (WRL Report 4864-18-X), Fifth Symposium on Remote Sensing of Environment, April 1968, p. 387.

R. Horvath, Multispectral Survey of Arctic Regions, WRL Report 1248-1-L, January 1968.

F. J. Thomson, Multispectral Discrimination of Small Targets, WRL Report 6400-135-T, December 1967, (ECOM-00013-135).

F. C. Polcyn, Investigations of Spectrum-Matching Sensing in Agriculture, WRL Report 6590-7-P, September 1967.

D. S. Lowe, J. G. Braithwaite, and V. L. Larrowe, An Investigative Study of a Spectrum-Matching Imaging System, WRL Report 8201-1-F, October 1966.

D. S. Lowe and J. G. Braithwaite, Spectrum-Matching Techniques for Enhancing Image Contrast, Appl. Opt., Vol. 5, June 1966, pp. 893-898.

M. R. Holter and W. L. Wolfe, Optical-Mechanical Scanning Techniques, Proceedings IRE, Vol. 47, 1959, p. 1546.